CZECH UNIVERSITY OF LIFE SCIENCES PRAGUE

Faculty of Environmental Sciences

Department of Landscape and Urban Planning

Master's Thesis

Cities require urban heat island knowledge in order to transform them into urban health islands

Author: Baraa Khalil Mohamad

2023 CZU Prague

CZECH UNIVERSITY OF LIFE SCIENCES PRAGUE

Faculty of Environmental Sciences

DIPLOMA THESIS ASSIGNMENT

Baraa Khalil Mohamad

Landscape Engineering

Landscape Planning

Thesis title:

Cities require more urban heat island knowledge in order to transform them into urban health islands

---

Objectives of thesis:

Objectives: The aim is to analyze the urban heat island (UHI) in the city of Prague to assist urban planners and decision-makers with urban greening issues and the means to mitigate urban hotspots. The study attempts, through the analysis of land use and land cover, to explain relationships between land use, land cover, urbanization, and seasonal characteristics of the Prague urban heat island. Remote sensing data

(Thermal imagery from Landsat and ASTER satellites) will be analyzed to detect to describe hotspots in the study area. The study will attempt to find out:

• What are the image and thermal characteristics of Heat Islands?

• What are the causes of UHI?

• What are seasonal variations of UHI?

• What data is useful for its detection?

• Which open-source image analysis software is useful for digital image processing?

• Why do we need Natural Landscapes in Urban Areas?

• What would be the best mitigation strategy to reduce urban heat islands?

Methodology:

For the purpose of assessing the relationship between land surface temperature, as well as the impact of urban areas on UHI, remotely sensed multi-temporal images (different spectral bands of Landsat data obtained from public sources, with different resolutions of 30m and 100 m) were analyzed. Hotspots have been outlined and described based on the assumption that patterns in the Landscape coincide with patterns of air temperatures. Split Window Algorithm techniques were used to convert TIRS (Thermal Infrared Sensor) data to the top of atmospheric brightness temperature to obtain surface temperature values. The contribution of several factors to UHI, including NDVI (Normalized Difference Vegetation Index), landscape emissivity, surface water, and building footprints, have been studied and assessed.

The proposed extent of the thesis

65 pages

Keywords

Urban heat island, urbanization, Thermal infrared remote sensing, mitigation of urban heat.

Recommended information sources:

- Beranová R, Huth R. (2005) 113–118. Long-term changes in the heat island of Prague under different synoptic conditions. Retrieved from hΣps://link.springer.com/arϴcle/10.1007/s00704-004-0115-y

- Dennis C. Reter, Cathleen M. Richardson, Fernando A. Pellerano, James R. Irons, Richard G. Alen Martha Anderson, Murzy D. Jhabval, Allen W. Lunsford, MaΣhew Montanaro Ramsey L. Smit, Zlalem Tesfaye, and Kurtis J. Thome. 2015, 7, 1135-1153. The Thermal Infrared Sensor (TIRS) on Landsat 8: Design Overview and Pre-Launch Characterization. Retrieved from https://www.researchgate.net/publication/264858961_The_Thermal_Infrared_Sensor_TIRS_on_Landsat_8_Design_Overview_and_Pre-Launch_Characterizattion

- Cheval S, Dumitrescu A, Kveton V. (2007). Modis-based investigations on the urban heat islands of Bucharest Romania and Prague (Czech Republic). Retrieved from https://www.researchgate.net/publicaϴon/252645903_MODIS based_investigations_on_the_urban_heat_islands_of_bucharest_romania_and_prague_czech_republic

- Lin L, Zhang Y. 2011, 3(7), 1535-1552. Urban Heat Island Analysis Using the Landsat TM Data and ASTER Data: A Case Study in Hong Kong. Retrieved from hΣps://www.mdpi.com/2072-292/3/7/1535/htm
- Ulpiani G. 2021, 141727. On the linkage between urban heat island and urban pollution island: Three-decade literature review towards a conceptual framework. Retrieved from https://www.sciencedirect.com/science/article/abs/pii/S0048969720352566.

Expected date of thesis defence

2022/23 SS – FES

The Diploma Thesis Supervisor

Doc. Peter Kumble, Ph.D.

Supervising department

Department of Landscape and Urban Planning

Advisor of thesis

Michal Lodin

Electronic approval: Electronic approval:

prof. Ing. Petr Sklenička, CSc.   prof. RNDr. Vladimír Bejček, CSc.

 Head of department   Dean

Prague on 22. 03. 2023

Declaration:

I hereby declare that the work presented in this thesis entitled "Cities require urban heat island knowledge in order to transform them into urban health islands" is original and done by me independently, under the direction of doc. Peter Kumble.

I have listed all literature and publications from which I acquired information in the attached list of references at the end of the thesis.
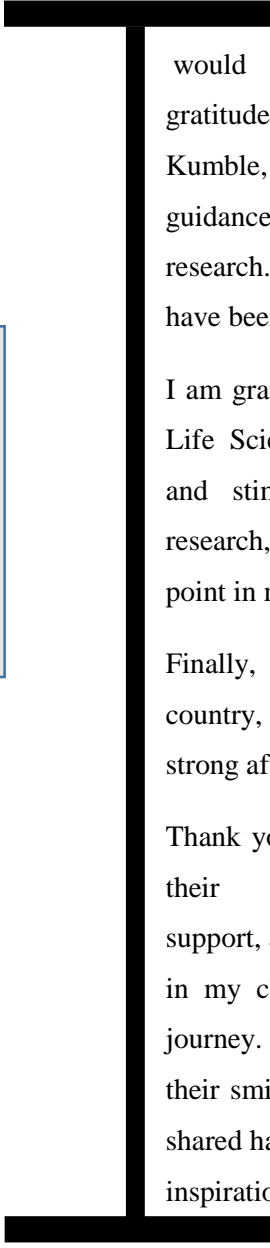
Date: _____   Signature: _____
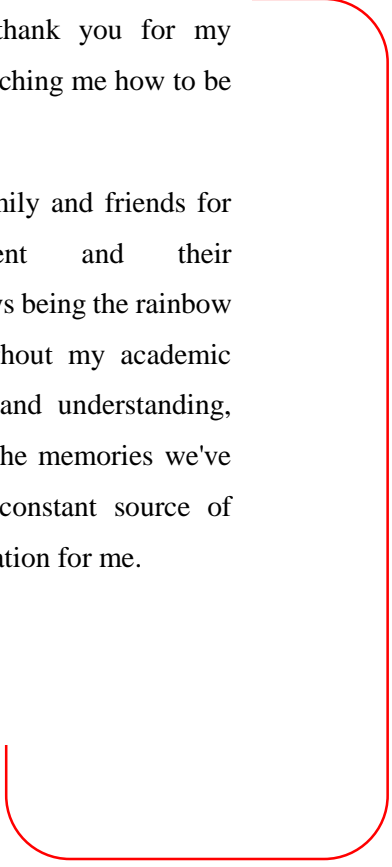
Baraa Khalil Mohamad

ACKNOWLEDGEMENTS

I would like to express my deepest gratitude to my supervisor, doc. Peter Kumble, and Mgr. Michal Lodin, for their guidance and support throughout my research. Their knowledge and insights have been a valuable asset to my work.

I am grateful to the Czech University of Life Sciences for creating a supportive and stimulating environment for my research, as well as for marking a turning point in my life.

Finally, I want to thank you for my country, Syria, for teaching me how to be strong after falling.

Thank you to my family and friends for their encouragement and their support, and for always being the rainbow in my clouds throughout my academic journey. Their love and understanding, their smiles, and all the memories we've shared have been a constant source of inspiration and motivation for me.

Abstract:

In this study, we examine the urban heat island phenomenon in Suchdol-Prague to investigate the relationship between land surface temperature and land use/land cover.

Mapping of land surface temperature was performed using satellite image data, including thermal infrared (TIR) data from Landsat 8 (Band 10), acquired on June 27, 2018, and Landsat 5 (Thematic Mapper (TM) Band 6) acquired on June 30, 2002. The ArcMap GIS software was utilized to extract land surface temperature information from the satellite data. The findings of this study reveal a remarkable disparity in temperature among various land cover types, including arable land, built-up areas, and forests. Our analysis underscores the strong connection between land use/land cover and land surface temperature, providing insights into the complex dynamics of urban climates. Arable land and green space, had the lowest LST, with a difference of around 12 °C, compared to built-up areas. The second part of this thesis includes using an infrared camera to measure surface temperature to investigate the thermal behavior of various materials such as concrete, asphalt, stone, paving stone, and others, which have a significant impact on the urban heat island. Our study shows that texture, roughness, and color of surfaces play a crucial role in determining their surface temperatures. For instance, we found that light-colored paving tiles, such as gray, had lower surface temperatures compared to dark gray tiles with a difference of approximately 7°C. On the other hand, the dark and rough asphalt had a surface temperature of 60°C, while white-painted asphalt showed a difference of at least 15°C. The results highlight the effectiveness of using light-colored materials in urban settings for reducing surface temperatures and the surrounding air temperature. Therefore, understanding the thermal behavior of various objects in our cities can also assist urban designers in achieving thermal comfort in urban areas.

Key Words:

Abstrakt

V této studii zkoumáme fenomén městských tepelných ostrovů v Praze, Suchdol a zjišťujeme vztah mezi povrchovou teplotou, typu zemského pokryvu a jeho využitím.

Mapování teploty povrchu země bylo provedeno s využitím satelitních snímků, včetně termálních infračervených (TIR) dat z Landsatu 8 (pásmo 10), získaných 27. června 2018, a Landsatu 5 (Thematic Mapper (TM) pásmo 6) získaných 30. června 2002. Software ArcMap GIS byl využit k extrakci informací o teplotě povrchu země ze satelitních dat. Výsledky této studie poukazují na pozoruhodný teplotní rozdíl mezi různými typy půdního pokryvu, včetně orné půdy, zastavěných ploch a lesů. Naše analýza podtrhuje silnou souvislost mezi využíváním půdy / pokryvem půdy a teplotou povrchu země, – a porozumění komplexní dynamiky městského klimatu. Orná půda a zeleň měly nejnižší LST s rozdílem kolem 12 °C oproti zastavěným plochám. Druhá část této diplomové práce zahrnuje využití infračervené kamery k měření povrchové teploty pro zkoumání tepelného chování různých materiálů jako je beton, asfalt, kámen, dlažba a další, které mají významný vliv na tvorbu městského tepelného ostrova. Naše studie ukazuje, že textura, drsnost a barva povrchů hrají zásadní roli při určování povrchových teplot. Zjistili jsme například, že světlé dlaždice, jako je šedá, měly nižší povrchové teploty ve srovnání s tmavě šedými dlaždicemi s rozdílem přibližně 7 °C. Naproti tomu tmavý a hrubý asfalt měl povrchovou teplotu 60°C, zatímco bíle natřený asfalt vykazoval rozdíl minimálně 15°C. Výsledky zdůrazňují účinnost použití světlých materiálů v městském prostředí pro snížení povrchových teplot a teploty okolního vzduchu. Pochopení tepelného režimu různých objektů v našich městech proto může pomoci městským projektantům k dosažení tepelné pohody v městských oblastech.

Klíčová slova:

Městský tepelný ostrov, urbanizace, tepelné infračervené záření, dálkový průzkum Země, využívání půdy, krajinný pokryv, termografie, Normalizovaný rozdílový vegetační index (NDVI), povrchová teplota země, městské materiály, Albedo.

Table of Contents

Introduction 1

1. Introduction

The urban heat island (UHI) is a phenomenon in which temperatures in cities are higher than in surrounding rural areas (Leal Filho et al. 2018). And according to (Stewart & Oke 2012), rural landscapes are defined by lower population densities and fewer built structures, allowing for more natural space for agricultural use. In contrast, urban landscapes have significantly higher population densities and a greater number of built structures.

Urban heat islands are a growing source of concern because they can harm communities by exacerbating air pollution and greenhouse gas emissions (due to increased use of air conditioning) and increasing the occurrence of heat-related illness, as well as leading to higher levels of mortality (Leal Filho et al. 2018). This helps to explain why the global stock of heat island studies has increased so dramatically in recent decades, the study of urban heat islands involves two of the most important environmental issues of the 20th century, namely population increase and climate change. Moreover, heat islands can be found in almost any urban area, large or small, in warm or cold climates (Stewart & Oke 2012).

According to, Akbari et al.(2001) the urban heat island effect is a result of the relative lack of greenery and the predominance of dark surfaces in urban areas, which causes these places to experience higher temperatures than the areas around them, Thus the, using high-albedo urban surfaces and planting trees in urban areas are effective ways to lower the urban heat island effect and consequently, summertime temperatures, and these are inexpensive measures. in the same research, the author proposed solutions for mitigating the urban heat island effect, some measures could be inexpensive, and very effective, such as using high-albedo urban surfaces (like roofs), this method offers an appealing solution for reducing overall radiative heat gains associated with a building's roof, thereby reducing the amount of energy required to cool the building. Planting trees in urban areas is another way to reduce urban heat islands. In this context, the benefits of trees can be divided into two categories: direct and indirect: The former refers to building shading, whereas the latter refers to the ambient cooling provided by the urban forest via evapotranspiration. Shade trees, for example, intercept sunlight before they can warm a building, whereas the urban forest cools the surrounding air by releasing moisture through plant transpiration. The incorporation of urban shade trees can thus provide significant benefits, such as reduced building air conditioning needs, lower air temperatures, and improved urban air quality through smog mitigation. Therefore, both cool surfaces (cool roofs and cool pavements) and urban trees are effective ways to lower the urban heat island.

2

Objectives of the study

2. Objectives of the study

The primary goal of this research is to determine the extent and intensity of the urban heat island phenomenon in Suchdol, Prague, and to investigate the relationship between land use/land cover and land surface temperature. We conducted a thorough review of literature and research projects related to the urban heat island, including key factors such as albedo and building footprint, in the first phase of our research. We also studied technical topics like thermography, emissivity, reflectivity, and black bodies to gain a better understanding of the underlying physics behind taking thermos pictures.

The second phase of this research involves a thorough analysis of the development and changes in the study area over time, using aerial images and maps to create a comprehensive overview of the study area's characteristics. Furthermore, Landsat data will be retrieved using the mono-window algorithm method, and the land surface temperature will be mapped using ArcMap GIS software. Furthermore, building footprints, digital elevation models, imperviousness, and the normalized difference vegetation index (NDVI) will be mapped, allowing us to identify the relationship between land surface temperature and land use/cover, providing insights into the factors that contribute to the formation of the urban heat island.

We will use a thermal camera to gain a better understanding of the thermal behavior of various materials, such as concrete, asphalt, stone, and paving stone, which have a significant impact on the urban heat island. This investigation will provide insights into the study area's characteristics and will assist us in better understanding our urban environment and how we can mitigate the effects of the urban heat island. Using this knowledge, we hope to identify the most significant land use/land cover factors that contribute to the formation of the urban heat island in Suchdol and to suggest effective strategies for mitigating its impact.

The findings of this study are important for urban planners and designers who want to create healthier urban environments by considering the urban heat island effect. Furthermore, greater public awareness is required to promote a more positive relationship with our urban areas and their sustainable development.

Literature Review 3

3.1 Factors influencing urban heat islands

3.1.1   Land use- Land cover
3.1.2   Topography
3.1.3   Albedo
3.1.4   Building footprint /height of the building

3.2   Understanding Thermography:

3.2.1   What is infrared thermography?

3.2.2   Principles of Thermal Radiation and Understanding the science of infrared.

3.2.3   How does thermal imaging camera work?

3.2.4   The thermal behaviour of urban materials.

3. Literature review

3.1 Factors influencing urban heat island:

3.1.1 Land use- Land cover:

The occurrence of urban heat islands is expected to increase as a result of global climate change, for instance, the air temperatures in cities have increased disproportionately to urban areas and have a locally acute, detrimental impact on human health, as well as on the economy, society, and environment, land use/cover has a connection to LST that can aid in land use planning, has influenced climate change globally, and has affected the intensity of UHI (Kaplan et al. 2018). Since temperatures have risen over time and there is a significant relationship between temperature and land use and land cover, it is likely that any future change in land use or land cover, no matter how small, will have a negative impact on the environment (Makinde & Agbor 2019). (Mohan et al. 2013) also emphasized that the three categories of UHI intensities—high, medium, and low—coordinated well with the LULC overall, therefore, researchers have used temperature as a function of how urban morphology, land use, and anthropogenic activities. And according to a study by (Ulpiani 2021), land use was one of 19 influencing factors that provided spatial predictors of hot and polluted spot areas. In a study conducted in Delhi to investigate UHI based on dominant land use-land cover (LULC) classification, high UHI was observed primarily in dense and commercial built-up areas, medium UHI was observed in medium and low dense built-up areas, and low UHI was observed in open and green areas (Mohan et al. 2013). That has been emphasized by (Kaplan et al. 2018), that lower land surface temperatures (LST) are typically found in areas with a lot of greenery. The amount of green areas determines LST using the latent heat flux from the surface to the atmosphere via evapotranspiration; this negative correlation between NDVI and LST is useful for urban climate studies (Kaplan et al. 2018). However, urbanization has resulted in significant changes in agricultural land, particularly on the outskirts of cities, causing the loss of green space and, as a result, numerous negative environmental effects (Zhou & Wang 2011). Figure 1 illustrates that temperatures in the core of densely populated cities with little vegetation and water may, in some cases, be up to 10°C warmer than in the nearby countryside (ESA 2008).
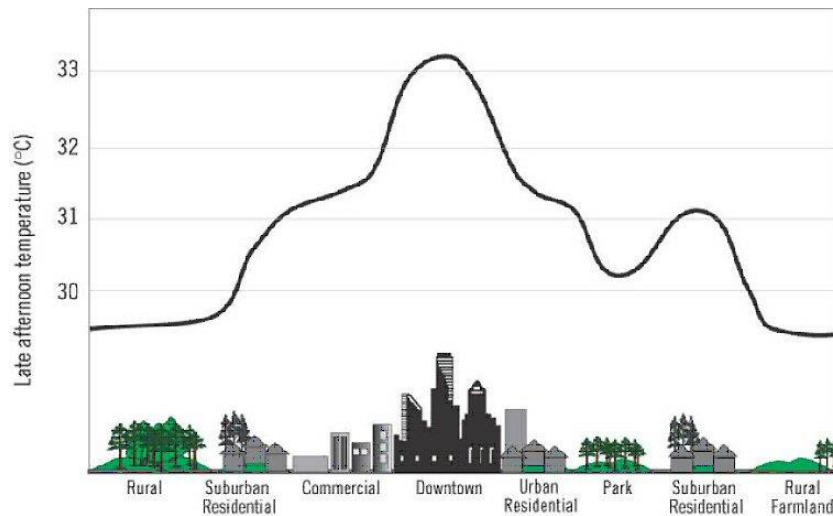
Figure 1. Profile of Urban Heat Island (ESA 2008).

54% of the world's population currently resides in urban areas, and by 2050, that number is predicted to increase to 66%, according to the World Urbanization Prospects report published by the UN in 2014. According to projections, the population of cities could increase by 2.5 billion people by 2050 as a result of urbanization and global population growth, as a result, the United Nations issued a report emphasizing the significance of successful urban planning (United Nations 2014). Therefore, designers should develop new towns to disperse urban overflow, improve fuel combustion efficiency, advocate for public transportation, and facilitate mass and energy exchange between urban areas and their surroundings, to construct more ecological corridors, because there is a strong positive correlation between UHI and energy consumption in urban areas, hence we can reduce UHI through scientific urban planning (Du et al. 2016). Besides that, as previously stated, there is a strong relationship between LST and land use/cover, and this relationship can aid in land use planning, therefore the amount of green space in densely populated urban areas should be increased by local governments (Kaplan et al. 2018).

This current study focuses on the urban heat island in Prague, considering the negative impact of urbanization over time and its effect on rising temperature trends, using Landsat data to determine how the impact of land use land cover change, and anthropogenic sources influence the spatial distribution of land surface temperature. I'll estimate the land surface temperature (LST) using the Mono-window algorithm method, as well as analyze the land-use change map and assess vegetation cover using the Normalized Difference Vegetation Index (NDVI), and use the thermal camera to investigate the thermal behavior of various elements in an urban environment

3.1.1.1 Case Study: Bucharest – Prague:

Prague is the Czech Republic's capital. As the country's largest city by area (496 km2) and population (1.2 million inhabitants), Prague is located on the Vltava River and its tributaries, it faces the same environmental challenges as other large cities around the world (Michal et al., 2016).

Urban heat island has already occurred and is getting worse in the case of Prague, the UHI project's results (http://eu-uhi.eu/) show that its annual average intensity from 1961 to 2012 was 2.2°C, with a peak in June and July (2.4°C), moreover, the heat island's intensity has been rising over the past few years, especially during the summer, by almost 0.5°C (Eliška et al. 2014).

The magnitude of the UHIs of Bucharest (Romania) and Prague (Czech Republic), were calculated in another research by (Cheval et al. 2007), as the difference between the highest temperature inside each city and the lowest temperature in the surrounding it, according to the research results, the local topography has a significant impact on the characteristics of the urban heat island because Bucharest is located in a much flatter area than Prague and lacks an influent watercourse, its urban heat island is larger and more intense than Prague's, furthermore, there is a real correlation between land cover and urban heat island, with high urban heat island found in areas with the dense urban fabric, as well as in industrial, traffic, and other urban sites.
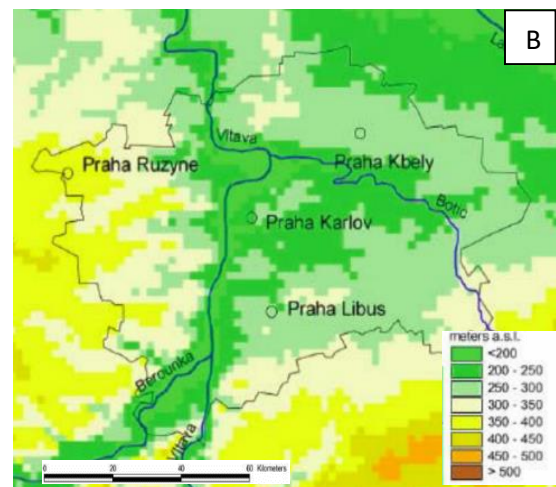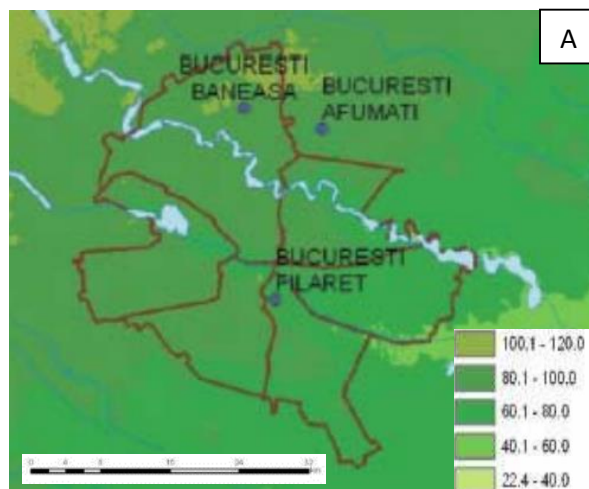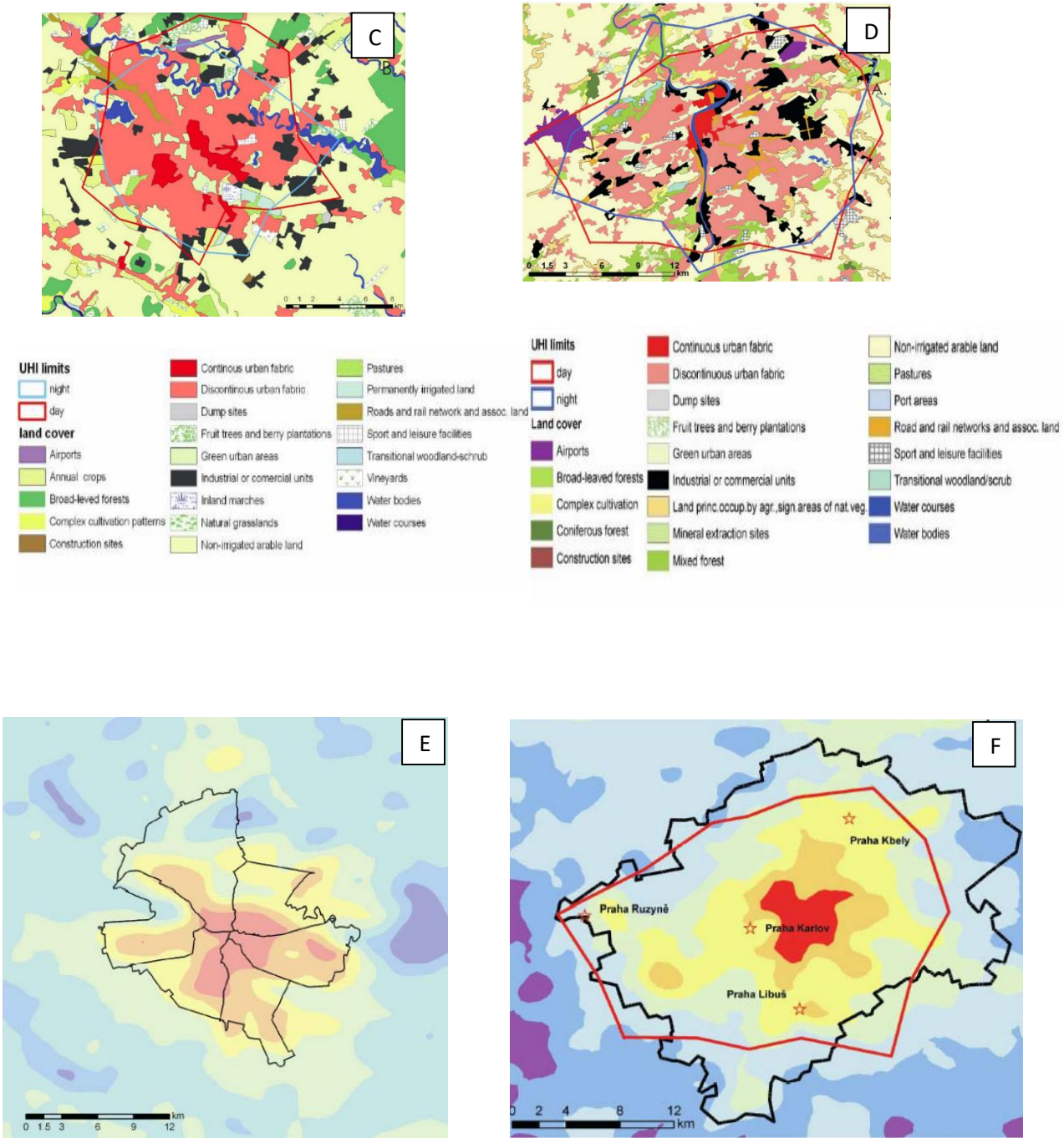
Figure 2. Digital elevation model -Bucharest (A), Prague(B), Land cover (2000) and July UHIs in Bucharest (c), Prague(D), Day LST in Bucharest (E), Prague (F), derived from July MODIS images (2000-2006) (Cheval et al. 2007).

3.1.1.2 Case study- India:

Rising land surface temperature as a result of the change and transformation of naturally vegetated and open areas into impervious surfaces is one of the most serious issues in urban areas, and this problem is more common in unplanned cities (Singh et al. 2017).
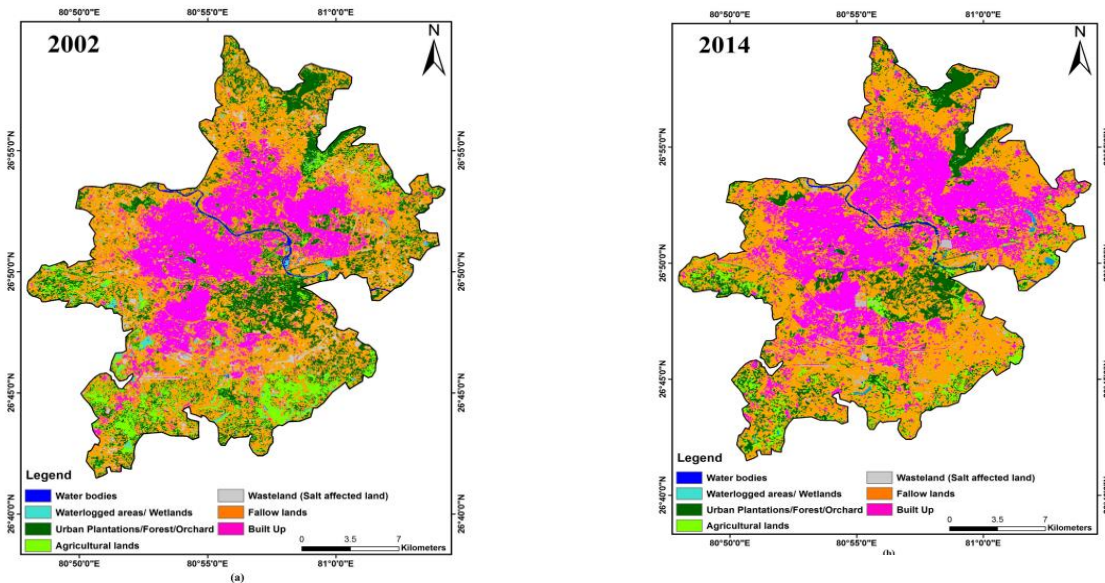
Figure 3. Land use/land cover map of Lucknow city for 2002 and 2014 (Singh et al. 2017).

Singh et al. (2017) conducted research in Lucknow, India, which is one of the most populated cities in central India, with one of the fastest-growing economies and industries. The study investigated the negative impact of urbanization and its effect on increasing the temperature in the city; thus, land surface temperatures in Lucknow were estimated in 2002 and 2014. In addition, the authors of the study used the Normalized Difference Vegetation Index (NDVI) and an ecological evaluation of the city with the Urban Thermal Field Variance Index (UTFV) to assess vegetation cover and its relationship with the UHI because changes in land use patterns affect all aspects of the urban and sub-urban environment, including land surface temperature, evaporation rates, and urban hydrology, the researchers state that there is a strong positive correlation between the land use-land cover and UHI.

In this case, the authors used multi-temporal Landsat satellite images to create the LULC map for Lucknow city in 2002 and 2014 (Fig 3), showing significant changes in the city over the last two decades (Singh et al. 2017). The built-up area (urban and semi-urban), increased from 93.97 sq. km to 130. 33 sq. km in 2014, was found to be the most vulnerable land use change, while agricultural land was found to have decreased

from 32. 37 sq. km in 2002 to 25. 03 sq. km in 2014, In addition, it was discovered that the area covered by urban plantations and forests had Urban plantations from 75.97 sq. km. in 2002 to 50.27 sq. km. in 2014, (Table 1). Furthermore, a stronger heat island phenomenon was found in 2014 as compared to 2002 (Fig 4), with a mean value of 36.75 C in 2002 and a temperature mean value of 37.8 C in 2014, which is due to the urbanization that occurred over the years and had a significant impact on the distribution of the land surface temperature, with a 0.75 C difference in the mean of the temperature between the two years (Singh et al. 2017).

Table 1 Land use/land cover of Lucknow city during 2002 and 2014 (Singh et al. 2017).

Lucknow temporal landuse (in sq.kms)		
LULC	30th September 2002	23rd September 2014
Built up area (urban and rural)	93.97	130.33
Waterlogged areas/wetlands	6.71	8.18
Wasteland (salt affected land)	14.68	12.11
Urban plantations and forest	75.97	50.27
Agricultural lands	32.37	25.03
Fallow lands	202.47	201.84
Water bodies	3.29	1.71
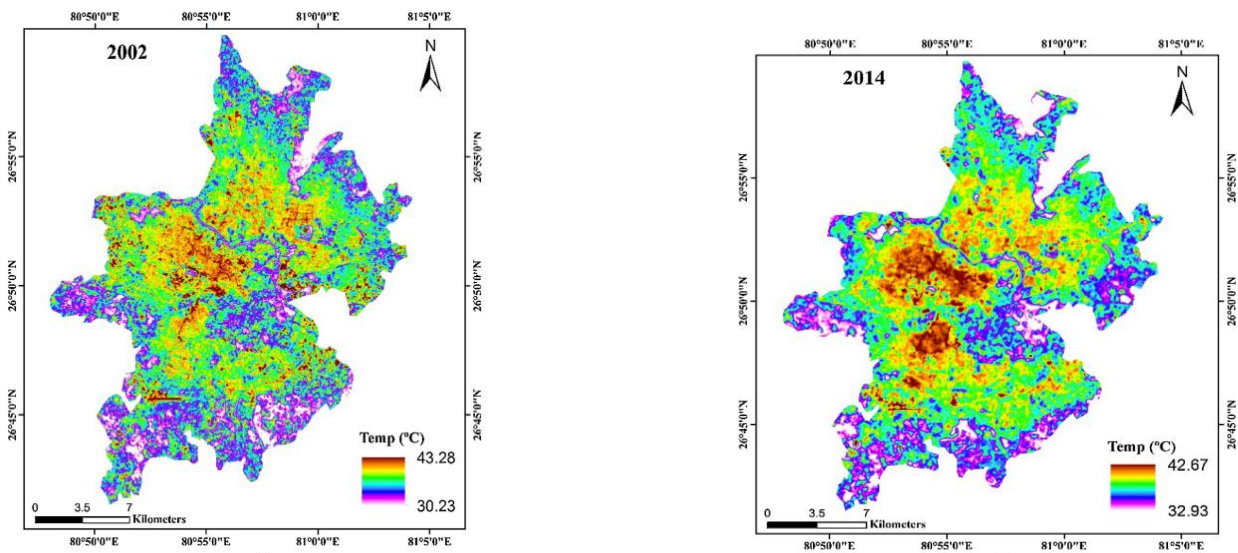
Figure 4. LST map of Lucknow city for 2002 and 2014 (Singh et al. 2017)

3.1.1.3 Case study- Prague:

According to Žák et al. (2016), Prague, particularly the city center, is one of the warmest places in the Czech Republic, with an annual average air temperature of around 10 °C (Fig. 5), this is due in part to the

urban heat island (UHI), which has increased significantly over the last 50 years due to increased transportation and urban growth, this intensification of UHI is shown in Fig. 6, which illustrates differences in daily air minimum temperatures between 2001-2010 and 1961-1970. The largest increase in temperature and intensification of UHI can be seen in the city center, near the Vltava river, in the city's densely built-up area.

Furthermore, the authors Žák et al. (2016), described the UHI in Prague as follows:

- When we use the average daily temperatures, the intensity of UHI is about 1.6 °C.
- The intensity is at its peak in June and at its lowest in September.
- It should be noted that Prague's UHI intensity is noticeably higher when considering minimum temperatures (annual average is about 3 °C), whereas it is significantly lower when considering maximum temperatures (annual average is about 1 °C).

By studying Legerova Street in Prague, the research also addressed the issue of urban form and the built environment. Legerova Street is a 25-meter-wide corridor surrounded by buildings that are 21 meters high. About 45,000 cars pass through four lanes of traffic each day.
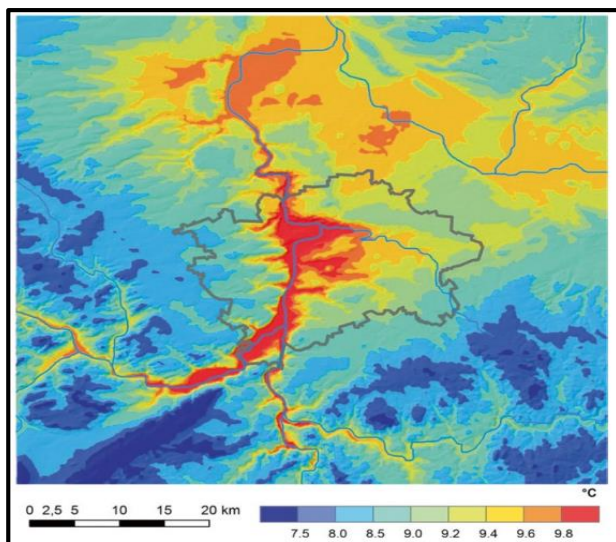
The street travels through a residential area from north to south. It is exposed to the sun in the summer, and the asphalt, concrete, and building facades absorb the majority of the solar energy that enters the area. Only a few patchy grass beds and no available shade are present.

The study used two models developed at CUNI Prague's Department of Meteorology and Environment to simulate thermal comfort as well as air pollution concentrations.

Figure 5. Annual average air temperature for Prague and surrounding, period 1961–2010 (Žák et al. 2016)

In the scenario, they have added to the model a small and large tree that is densely planted along the sidewalks to investigate the effect of shade on the UHI, and specifically, physiologically equivalent temperature (PET factor), which indicates the temperature a human standing outside and considers not only air temperature and wind but also humidity and radiation, including radiation from buildings in the streets.

Figure 6. The difference in daily air minimum temperature between the period 2001–2010 and 1961–1970 (Žák et al. 2016)

The simulation results showed that there is a possibility of reducing the PET by 2.3° in the shade. The shade lasts for a short period in the scenario with small trees positioned densely along the sidewalks, whereas the shade lasts for a longer afternoon period in the scenario with large trees positioned densely along the sidewalks due to a larger shade, where the large crowns have a significant impact on airflow.

**Figure 7. Legerova Street in Prague (Žák et al. 2016)**

However, all scenarios have a negative impact on the ventilation conditions for air pollutants in some way.

3.1.2 Topography:

Topography has a significant impact on the size and intensity of urban heat islands (Landsberg 1981). For instance, the location of cities in sink-like basins, combined with complex topography, can exacerbate urban climate issues, primarily through worsening air quality, decreased ventilation, and a further reduction in total turbulent heat transport (Landsberg 1981; Ketterer & Matzarakis 2014). Nonetheless, the topography allows for the formation of numerous local climates over a short distance. As a result of changing elevation and land use, city dwellers can visit and experience diverse micro-climates in a small area, However, distinguishing between topographic and urban effects is challenging (Ketterer & Matzarakis 2014). When researchers investigate UHI, they often attempt to eliminate elevation differences by using a correction based on an assumed average lapse rate. (Landsberg 1981). For example, the relationship between local climate zone and the land surface temperature has been extensively studied, but mostly in flat terrain, although there have been some studies on UHI in mountainous regions, the majority of them concentrated on the interaction between topography, land use/land cover, and temperature (Badaro-Saliba et al. 2021).

(Badaro-Saliba et al. 2021) conducted a study to assess the impact of urban structure on UHI in Beirut, a coastal city with diverse urban morphology and complex topography. According to the author, no research has been conducted on the relationship between land surface temperature and local climate zone in cities with complex topography, where LST variability may be significantly influenced by topography at a local scale. By means of using a topographic normalization method, the study sought to comprehend how 3D urban morphology and its underlying surface cover influence UHI. Two models that show the LST variation after and before removing the effect of topography were created, Fig.8. Result clearly shows a better understanding of the UHI because topographic normalization can reduce LST variability, and thus there is a clear effect of topography on the spatial distribution of the LST and thus on the UHI (Badaro-Saliba et al. 2021). Nitis & Klai (2005), state, that local topography, particularly in cities with complex topography, played a significant role in the formation and evolution of the UHI.
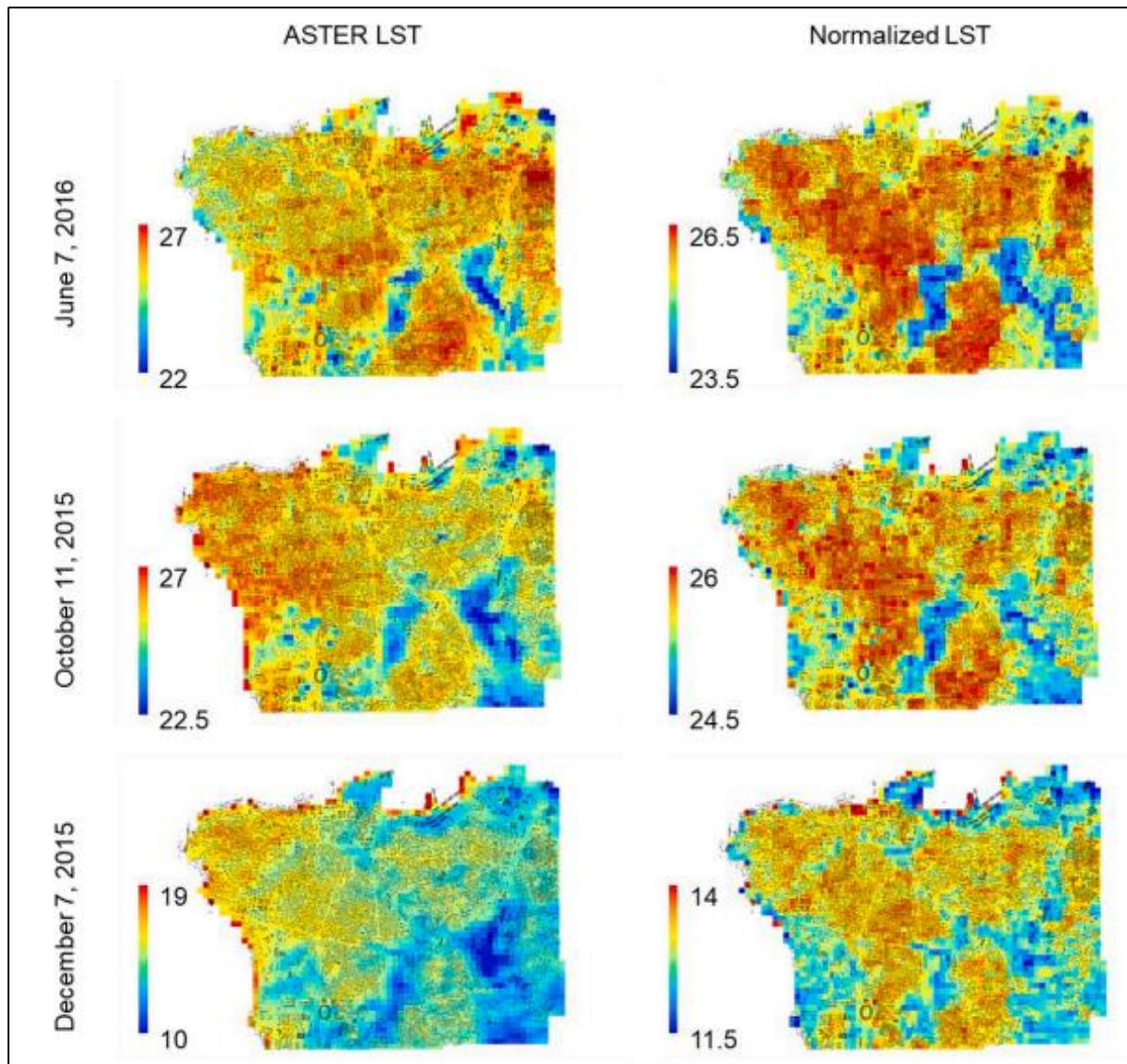
Figure 8. LST maps before (left) removing the effect of topography and after (right); grey polygons represent buildings (Badaro-Saliba et al. 2021)

3.1.3 Albedo:

Albedo' is a Latin term that means "whiteness." The albedo of a surface is the fraction of the incident sunlight that the surface reflects (Coakley 2003). The processes that control the magnitude, distribution, and variability of this reflected energy are fundamental to the Earth's energy balance and have a significant impact on both climate and climate change (Stephens et al. 2015). Unreflected radiation is absorbed by the surface, which raises the surface temperature, evaporates water, and melts and sublimates snow and ice. The albedos of various surfaces vary. Oceans, lakes, and forests have low albedos and reflect only a small fraction of incident sunlight.

Table.2 albedo values of a different kind of surfaces (Kotak et al. 2015).

Surface	Albedo
Corrugated roof	0.1 - 0.15
Colored paint	0.15 - 0.35
Trees	0.15 - 0.18
Asphalt	0.05 - 0.2
Concrete	0.25 - 0.7
Grass	0.25 - 0.3
Ice	0.3 - 0.5
Red/Brown roof tiles	0.1 - 0.35
Brick/Stone	0.2 - 0.4
Oceans	0.05 - 0.1
Old snow	0.65 - 0.81
White paint	0.5 - 0.9
Fresh Snow	0.81 - 0.88

Deserts, sea ice, and snow all have high albedos and reflect significant amounts of incident sunlight (Coakley 2003). Here are some different albedo values shown in table 2. for various materials.

Nevertheless, it should be acknowledged that an albedo is not an intrinsic characteristic of a surface. Instead, the albedo of any surface is dependent on the spectral and angular distributions of the incident light, which in turn are determined by the composition of the atmosphere and the direction and incidence of the sun's light beam (Coakley 2003).

The use of high-albedo materials reduces the amount of solar radiation absorbed by building envelopes and urban structures, keeping their surfaces cooler reducing the intensity of long-wave radiation. Moreover Because of smaller convective heat fluxes from cooler surfaces, local and downwind ambient air temperatures would be lower. Such temperature drops can have a significant impact on cooling energy consumption in cities, which is especially important in hot climate cities. As a result, those studying the effects of urban heat islands have been interested in the sensitivity of air temperature to albedo change (Taha 1997).

Mohammed et al. (2021), conducted a study to investigate and analyze the climatic processes caused by a potential increase in albedo at the city scale (Dubai, UAE) and its impact on urban cooling. by implementing

reflective and super-reflective materials. During the summer months, the average daily surface temperature over Dubai city is around 41 degrees Celsius, with some hotspot regions reaching 45 degrees Celsius. The average surface temperature during the summer peak hour (14:00 LT) ranges between 46 and 50 degrees Celsius. In the research, three scenarios are designed and evaluated, using low, average, and high albedo modifications. And as a result, when urban albedo is improved by 0.20, 0.45, and 0.60 respectively, it is shown that the reduction in ambient temperature during the peak of a summer day (14:00 LT) is 0.6, 1.4, and 2.6 degrees Celsius respectively.

Nevertheless, surfaces have different geometric structures, textures, and complex mixtures, where for example any combination of soil, vegetation, twigs, branches, rocks, snow, ice, water, and so on can be found.

3.1.4 Building footprint /height of the building:

Building heights are becoming more varied as urbanization progresses quickly. As a result, cities are dealing with the problem of non-uniform distribution of urban climate parameters (e.g., temperature, wind velocity), which may lead to urban heat islands (UHI) and increased building energy consumption, among other things (Xi et al. 2021).

The urban building has a significant impact on the urban thermal environment by altering heat exchange. The difference in the average temperature on the same day across weather stations located within the same region would be caused by the specific environment around each station, and the buildings are one of the primary causes of these differences (Lan & Zhan 2017). According to the research by (Lan & Zhan 2017; Middel et al. 2012), warming impacts remain longer on hotter days because urban buildings absorb and retain a significant amount of heat throughout the day. a longer period will be needed to release this heat. This may be due to the relatively large heat storage capacity of urban buildings. According to a case study of Nanjing, China (144 km2 containing 140 thousand buildings), to investigate the relationship between urban environments and building height, the UHI intensity of high-rise buildings is more (0-0.7) C higher than that of middle-rise and low-rise buildings. which is due to the buildings' windward obstruction and the heat accumulated nearby the buildings. Therefore, that will impact the thermal comfort of the area. Due to UHI, high-rise buildings have the highest energy consumption, at 1.2% to 4.5% (Xi et al. 2021).

One of the most helpful urban spatial indicators for assessing radiation and thermal environments is the Sky View Factor (SVF) (Zeng et al. 2018). The Sky View Factor is the ratio of radiation received from the sky by a planar surface to that received from the entire hemispheric radiating environment (Watson & Johnson

1987). Simply, the SVF is the percentage of visible sky that is important for determining surface radiation balance (Dirksen et al. 2019; Theeuwes et al. 2017; Zeng et al. 2018). The sky-view factor indicates street geometry, as well as building density and location within the city, on the edge of the city, or in the center, because building density is generally higher in the center of a large city (Theeuwes et al. 2017).

Sky View Factor has values between zero and one (OKE 1981). A value of one indicates that the sky is completely visible and unobstructed from a specific point on the Earth's surface. This means that short-wave radiation from the sun can reach the surface without being blocked by obstacles like buildings or trees. When the Sky View Factor is less than one, it indicates that the terrain is more complex and that there are obstacles that can block some of the radiation. In this case, the terrain's surface will either absorb or reflect the long-wave radiation emitted from the Earth's surface.(Dirksen et al. 2019). Due to this, the sky-view factor and street surface temperature have a clear relationship, the street surface temperature decreases as building height increases, but Building height is not always uniform in the real world, and the varying height distribution affects the urban surface energy balance. (Yang & Li 2015).

3.2 Understanding Thermography:
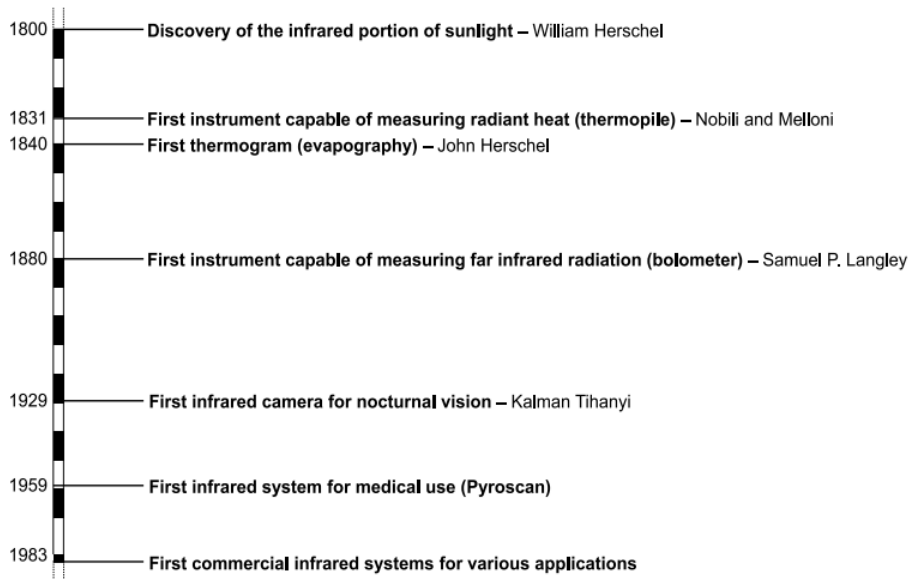
3.2.1 What is infrared thermography?

Over two centuries have passed since the beginning of infrared thermography research, the history of significant contributions between the 19th and 20th centuries is shown in Fig. 9, Although infrared thermography originated in the 19th century, considerable technical advances were made throughout the twentieth century (Martin et al. 2022).

Sir William Herschel (1738-1822), Royal Astronomer to King George III of England and best known for discovering the planet Uranus, was testing various samples of colored glass that produced similar reductions in brightness by passing sunlight through a glass prism when he discovered that some of the samples passed very little of the Sun's heat while others passed so much heat, Herschel proved that the heat continued to increase in the dark region beyond the red end of the spectrum and that he had finally identified the maximum point, which lay much beyond the red end in what is now known as the "infrared wavelengths.", Herschel named this new portion of the electromagnetic spectrum the "thermometric spectrum" when he revealed his discovery. The radiation itself was sometimes referred to as "dark heat" or simply "the invisible rays," however Herschel did not create the term "infrared"(McKenna & Gromicko 2006).

Infrared (IR) thermography as a term is the science of collecting and analyzing thermal data using non-contact thermal imaging devices (Williams 2014). And the outcome is an image produced based on the heat signature of the object, Thermal Imaging is also called "Forward Looking Infrared Technology" due to the usage of thermal Infrared Sensors (Nayak 2018).

Johnson et al. (2011), mentioned in a more detailed definition, that Infrared thermography uses a specialized camera that detects thermal radiation or surface temperature radiated by an object and presents the various temperatures observed as an image, with different colors or shades of the image indicating the different temperatures. Therefore, the properties that make infrared detection useful to military forces around the world make it useful to other sectors. Thermal imaging is now widely used in law enforcement, commercial and industrial applications, security, transportation, and many other industries (McKenna & Gromicko 2006).

Furthermore, infrared thermography has grown strongly within the scientific community throughout the years, the reason for this is that infrared thermography can provide images of the surface temperatures of various items (Martin et al. 2022).

```
1800 ──── Discovery of the infrared portion of sunlight – William Herschel

1831 ──── First instrument capable of measuring radiant heat (thermopile) – Nobili and Melloni
1840 ──── First thermogram (evapography) – John Herschel

1880 ──── First instrument capable of measuring far infrared radiation (bolometer) – Samuel P. Langley

1929 ──── First infrared camera for nocturnal vision – Kalman Tihanyi

1959 ──── First infrared system for medical use (Pyroscan)

1983 ──── First commercial infrared systems for various applications
```

Figure 9. History of infrared thermography between the nineteenth and twentieth centuries (Martin et al. 2022)

# 3.2.2 Principles of thermal Radiation and Understanding the science of infrared:

Thermal radiation covers a range of wavelengths in the electromagnetic spectrum, primarily in the infrared region.

3.2.2.1 electromagnetic radiation:

Because electromagnetic radiation can be characterized as a stream of photons, each carrying energy and flowing at the speed of light, the electromagnetic (EM) spectrum is the range of all types of EM radiation and can be defined in terms of energy, wavelength, or frequency, the relationships between energy, wavelength, and frequency can be expressed mathematically as wavelength equals the speed of light divided by the frequency: $\lambda = c / v$

● λ is the wavelength

● **V** is the frequency

● **C** is the speed of light

The human retina is sensitive to electromagnetic waves with frequencies ranging from 4.3 x 10^{14} cycles per second to 7.5 x 10^{14} cycles per second; this range of frequencies is referred to as the visible part of the electromagnetic spectrum; the eye does not respond to electromagnetic waves with frequencies greater than 7.5 x 10^{14} cycles per second (Liou 2002).
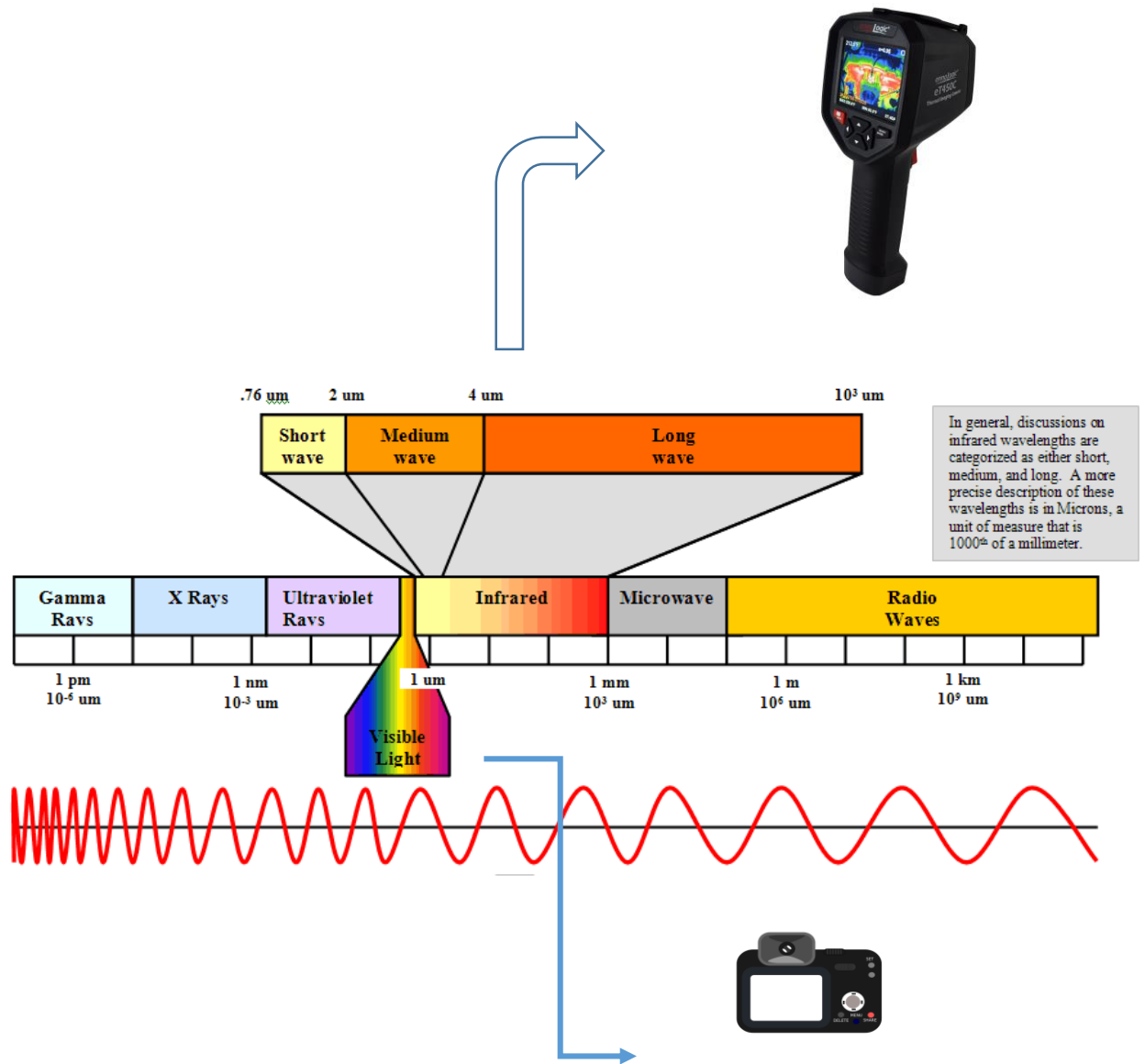
Figure 10. Electromagnetic spectrum _ various types of electromagnetic radiation as defined by wavelength Sizes (Protherm 2013).
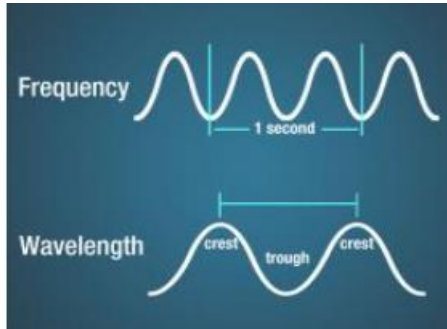
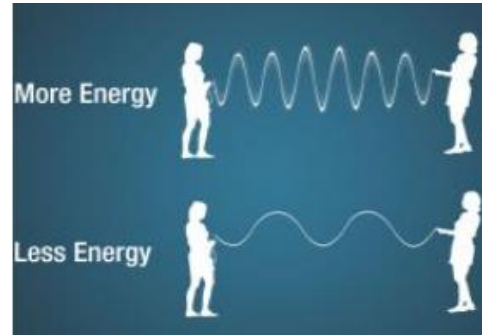**Figure 11. Electromagnetic waves (Butcher 2016) .**

Figure 12. The relationship between the energy and the wavelength (Butcher 2016).

Therefore frequency and wavelength are both forms of electromagnetic energy (Mattson & Newman 2013). (Ward & John 1998), also, underline how the wavelength and intensity of this radiation serve as distinguishing features. The number of crests that pass across a given point is referred to as its frequency. A Hertz is defined as one wave or cycle per second (Hz), the wavelength is the distance between crests and ranges in size from very tiny, measured in billions of meters or nanometers, to extremely long waves measured in meters, as shown in the illustration below (Campbell 2018). Lower wavelengths emit at higher temperatures, whereas larger wavelengths emit at lower temperatures, in other words, the lower the frequency, the longer the wavelength, and the higher the frequency, the shorter the wavelength, it's like pulling the ends of a jump rope up and down. Larger energy is required to create more waves in the rope (NASA 2010). To clarify, the temperature of an object affects the wavelength of the electromagnetic waves it emits, and how frequency and wavelength are related, for example: heating a metal, at higher temperatures, the metal will begin to emit light, starting with red, orange, then, yellow (long waves), and eventually blue (short waves). This is due to the increased temperature causing the atoms in the metal to vibrate faster and release more energy, resulting in the emission of shorter wavelength electromagnetic radiation (light).

Quantitative analysis of atmospheric radiation by (Liou 2002), underlines that the amount of radiant intensity is a function of temperature and wavelength. Where the amount of radiation emitted increases with temperature (Iznita Izhar & Petrou 2012).

3.2.2.2 visible light:

The only wavelengths of the electromagnetic spectrum that humans can see are visible light waves (0.4-0.7 µm) (National Geographic 2022). The three primary colors of the visible area are (blue, green, and red) (Jain & Singh 2003). More precisely the visible light is divided by color: blue/violet (0.4-0.5 µm), green

(0.55-0.56 μm), yellow (0.56-0.59 μm), orange (0.59-0.62 μm), or red (0.62-0.70 μm) (Austin et al. 2021). while The different wavelengths of visible light are seen as the colors of the rainbow: red, orange, yellow, green, blue, indigo, and violet, the longest wavelengths (around 0.7 μm) are red and the shortest wavelengths (0.38 μm) are violet, the human eye and brain collaborate to convert visible light energy into an electrical impulse that can be translated into an image (National Geographic 2022). Visible light refers to the portion of the spectrum that depends on reflectance properties, for instance, Chlorophyll in healthy vegetation absorbs blue and red light and reflects green light from the visible spectrum (Jain & Singh 2003).

3.2.2.3 infrared light:

The infrared section of the electromagnetic spectrum is typically split into three regions: near-, mid-, and far-infrared, which are called for their relationship to the visible spectrum. The higher-energy (frequency) near-IR, with a wavelength of 14000-4000 cm^{-1} (0.8-2.5 μm), can excite overtone or harmonic vibrations. The mid-infrared range, 4000-400 cm^{-1} (2.5-25 μm), can be utilized to investigate basic vibrations and related rotational-vibrational structure, then the far-infrared, measuring around 400–10 cm^{-1} (25–1000 μm), which is nearby to the microwave area (Nayak 2018). Some infrared radiation can be sensed as heat. Some objects, such as fire, are so hot that they emit visible light. Humans, for example, are not as hot and only emit infrared radiation, these infrared waves are invisible to our eyes, but tools that can detect infrared energy, such as night-vision goggles or infrared cameras, allow us to "see" the infrared waves emitted by warm things, such as humans and animals (Science Mission Directorate 2010).

(Martin et al. 2022) discovered that the majority of researchers used images that had been collected by an infrared camera to evaluate the thermal performance of buildings, in other words, thermal imaging allows us to assess how cold or hot certain elements in the built environment are in comparison to others. Furthermore, earth scientists indicated that the thermal infrared (long-wave infrared) range of 8 to 15 μm is best for studying the longwave thermal energy radiating from our planet, further to that, scientists can measure how near-infrared radiation reflects off the surface to identify changes in land cover such as cite growth, vegetation changes, or even the health of a forest (Science Mission Directorate 2010).
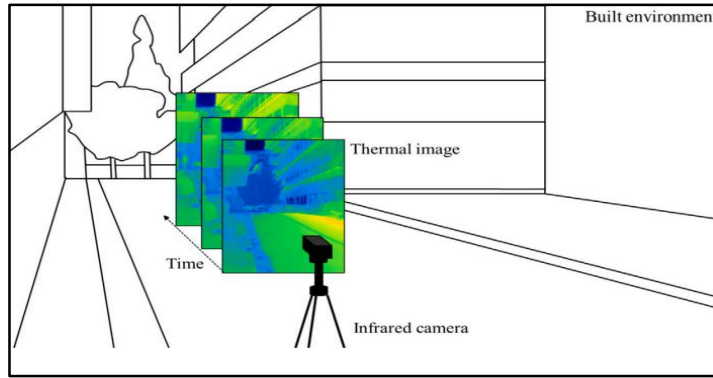
Figure 13. Thermal images using an infrared camera in the built environment (Martin et al. 2022).

The near-infrared band is best for determining the biomass index at the earth's surface, while the middle-infrared region is more sensitive to plant leaf moisture levels. Longwave radiation, also known as thermal infrared radiation, has been used in vegetation stress monitoring and thermal pollution research (Huete 2004).

Band	Wavelength	Useful for mapping
Band 1 - blue	0.45-0.52	Bathymetric mapping, distinguishing soil from vegetation and deciduous from coniferous vegetation
Band 2 - green	0.52-0.60	Emphasizes peak vegetation, which is useful for assessing plant vigor
Band 3 - red	0.63-0.69	Discriminates vegetation slopes
Band 4 - Near Infrared	0.77-0.90	Emphasizes biomass content and shorelines
Band 5 - Short-wave Infrared	1.55-1.75	Discriminates moisture content of soil and vegetation; penetrates thin clouds
Band 6 - Thermal Infrared	10.40-12.50	Thermal mapping and estimated soil moisture
Band 7 - Short-wave Infrared	2.09-2.35	Hydrothermally altered rocks associated with mineral deposits
Band 8 - Panchromatic (Landsat 7 only)	.52-.90	15 meter resolution, sharper image definition

Figure 14. Landsat 4-5 TM and Landsat 7 ETM+ and their uses (USGS 2016).

On the other hand, Infrared sensors, for instance, can provide clear infrared images in which the temperature and emitted heat define the target intensity. As a result, infrared pictures are not affected by solar, lighting, and infrared sensors can be used in low visibility circumstances such as darkness, smoke, fog, and haze (Ding et al. 2018). However, unlike the visible light image, the infrared image is limited by the infrared detector, which makes it challenging to obtain a high-resolution (HR) image (Wu et al. 2022).

Therefore and according to the research of (Wu et al. 2022), they suggested that Dual-camera imaging using infrared and visible light can efficiently combine the observation capabilities of infrared images and the detailed texture of visible light images.

3.2.2.4 Black bodies, Emissivity, and Reflectivity:

We cannot discuss thermal radiation without mentioning one of the most important terms in thermography, the concept of the black body and, Emissivity and Reflectivity.

Reflectivity is the total amount of incident energy that bounces off the surface. It is a surface phenomenon. Reflectivity depends on the wavelength of light, direction of the incident and reflected light, polarization of light, type of the material (metal, plastic, etc.), chemical composition and structure of the material, and state of the material and its surface (temperature, surface roughness, degree of oxidation and contamination). For emissivity, the incident energy is first absorbed and then radiated. Emissivity is defined as the ratio of the energy radiated from a material's surface to that radiated from a blackbody (a perfect emitter) at the same temperature and wavelength and under the same viewing conditions. It is a dimensionless number between 0 (for a perfect reflector) and 1 (for a perfect emitter). The emissivity of a surface depends not only on the material but also on the nature of the surface. For example, a clean and polished metal surface will have a low emissivity, whereas a roughened and oxidized metal surface will have a high emissivity. The emissivity also depends on the temperature of the surface as well as wavelength and angle.

Measurements of the electromagnetic spectrum are used in remote sensing to determine the properties of various earth features and vegetation. The basic idea is that each object reflects, emits, and absorbs varying intensities of radiation at different electromagnetic (EM) spectrum wavelength ranges depending on its physical characteristics (Jain & Singh 2003).

A blackbody is an ideal surface that absorbs all incident radiation at all wavelengths and in all directions, therefore, it is the ideal absorber. As a result of this definition, the blackbody has three properties: (a) it is the surface that emits the most for a given temperature and wavelength, (b) blackbody radiation is diffuse and does not depend on direction, and (c) total blackbody radiation in a vacuum depends only on temperature (Meseguer et al. 2012).

Since a blackbody is an ideal emitter at all wavelengths, there are also imperfect emitters that, at the same temperature, emit less radiation than a blackbody, to describe the level of imperfection in an emitter, a value is provided to the material that indicates its ability to emit radiation as a proportion of that possible by a black body at the same wavelength; this value is known as the emissivity (Ward & John 1998). Emissivity

is a term used to describe the optical properties of materials in terms of the amount of energy emitted when compared to an ideal black body (Avdelidis & Moropoulou 2003; Moropoulou et al. 2021).

Determining the emissivity of metals (or other materials) entails determining the ratio of the radiant intensity of the metal's surface at T temperature to that of a blackbody at the same temperature (De Vos 1954). In other words, Clair, 1978 highlighted that the Emissivity of a surface is a function of wavelength, temperature, and direction.

The emissivity of a blackbody in thermal equilibrium is 1.0. Real objects don't heat up as much as an ideal black body would. They are referred to as gray bodies because they emit less heat than a black body therefore the Stefan-Boltzmann law must include emissivity to account for the fact that actual objects are gray bodies (Connor 2019).

Emissivity, in other words, is a relationship between two similar energies, According to (Parente & Pepe 2019). so, the main issue with infrared thermographic readings is the material's emissivity. Given that an infrared camera detects radiation emitted by a material under investigation and converts this energy to a temperature—thermal image, the feature that describes the relationship between the emitted radiation and the temperature of the material is referred to as emissivity, again the emissivity is a surface property that describes the ability of a material to emit energy (Avdelidis & Moropoulou 2003).

Therefore, it is a dimensional magnitude with values ranging from 0 to 1 (theoretically). A material with an emissivity of one can absorb all incoming energy and then emit it as if the object was a black body (Parente & Pepe 2019).

The emissivity of most natural Earth surfaces is a unit-less parameter that ranges between 0.6 and 1.0, however, emissivity less than 0.85 are generally limited to deserts and semi-arid environments. In the thermal infrared wavelength range, vegetation, water, and ice have high emissivity exceeding 0.95 (NASA 2014).

Dr. Zhengming Wan's Group at ICESS (Institute for Computational Earth System Science), University of California, Santa Barbara, has measured the emissivity of natural and man-made materials and created a library of that data for instance Water, ice, snow, soils, and minerals, plant (leaf, bark, and grass), and anthropogenic materials are among the items measured in the Library (brick, stone, lumber, masonry, pavement, tile, and painted sandpaper)(Wang et al. 2005).

For example, water, ice, and snow generally have a high emissivity, 0.94 to 0.99, across the thermal infrared region (ICESS 1999). And, as we know, water has low reflectivity (Yang et al. 2020). To clarify, we must understand both terms emissivity and reflectivity, which I have already explained previously. Emissivity is

the ability of a surface to emit thermal radiation (Jeanette 2013). whereas reflectance is the percentage of energy reflected in total energy incident on a body. As an example, an object appears green because it reflects only wavelengths in the visible spectrum that correspond to the color green. Thus, blue-colored objects absorb all light waves except those that are blue, and so on (Jain & Singh 2003). And the greater the reflectivity, the lower the emissivity, and thus the greater the chance of 'seeing' a thermal reflection (Jeanette 2013). As a result, and because water has a high emissivity, it has a low reflectivity and thus is a good absorber, and according to Butcher (2016), water absorbs the majority of the Earth's emitted longwave infrared radiation. As shown in fig.17, Clearwater has a low reflectance in the visible range and almost completely absorbs radiation in the Near-infrared (NIR) range. The reflectance of the electromagnetic spectrum by impure water is affected by several variables, including suspended particles, floating materials, and the depth of the water body. In general, turbid water reflects more than clear water in the visible and near-infrared bands, with the difference depending on the properties of the suspended material (Jain & Singh 2003).

The signature of the Soil and Minerals in the 3 to 5 µm region depends strongly on the water and organic content, and the dryer, purer soils have lower emissivity in this region (ICESS 1999). And based on a study by (An et al. 2017), the value of soil emissivity varies in a narrow range, from 0.9 to 0.98. According to (Li et al. 2013), the soil composition is generally dominated by quartz, which is both a common mineral and resistant to weathering; therefore, the soil spectral behaviors at 3−5 µm and 8−14 µm are both impacted by quartz. Not just by the quartz concentration, but also by the water content. Emissivity will increases when water content increases in the soil, thus the importance of an accurate determination of emissivity variation with soil water content is important to get suitable temperature retrievals (Mira et al. 2007). The Vegetation, green vegetation typically has a very high emissivity because it contains water, on the contrary, Man-made materials such as refined, polished metals have among the lowest emissivity values while Rough dielectric materials such as asphalt and brick are in the same range as natural materials, approximately 0.90 to 0.98 (ICESS 1999). Therefore Acknowledging emissivity is essential for taking accurate surface temperature measurements (Monchau et al. 2013). (Teledyne FLIR 2021) mentioned that when the emissivity decreases, what we are measuring (and see thermally) comes from the surfaces of surrounding objects rather than the item we are studying, As a result, we must set the emissivity in the thermal camera according to the emissivity of the object that we are measuring and that in general for objects with an emissivity less than 0.5. While the objects with higher emissivity reflected temperature has less influence.

3.2.3 How does a thermal imaging camera work?

Thermal cameras are passive sensors that capture the infrared radiation emitted by all objects with a temperature above absolute zero (Gade & Moeslund 2014). The thermal imaging cameras used today are based on technologies developed by the military, infrared technology because it allows us to see and target opposing forces in the dark or across a smoke-filled battlefield (McKenna & Gromicko 2006). An infrared (IR) camera is versatile, and lightweight, it can read heat as color and then display that information in a way that's easily understood. it captures the light that exists just outside the visible spectrum. IR goes beyond the apparent. The IR image provides precise proof of a problem that the digital camera is unable to fully capture. As an illustration, a digital image can show a dried water stain where a wall meets a ceiling while an IR image displays a black spot in the same area (Gromicko & Ward 2006). A thermographic camera converts infrared radiation (IR) into a visual image that depicts temperature variations across an object or scene. The basic parts consist of an IR-focusing lens, electronics, and software for handling and displaying the signals and images (FLIR 2008). Because glass has a very low thermal radiation transmittance percentage, the lenses must be made of a different material. Germanium is the most commonly used element. This is a grey-white metalloid that is nearly transparent to infrared light while reflecting visible light. Because germanium is relatively expensive, the size of the lens is essential (Gade & Moeslund 2014).

3.2.4 The thermal behavior of urban materials :

The sensor measures the reflected, and/or emitted radiation from an object. The strength of the electrical signal is determined by the radiation received by the sensor, and this strength is converted and stored as digital numbers. The remotely sensed measured signal as a function of wavelength is often referred to as the target's spectral signature because its analysis provides useful information about the target's properties. Spectral reflectance is the ratio of reflected energy to incident radiation as a function of the wavelength. Therefore, the spectral reflectance characteristics of most targets depend upon the illuminating region of the EM spectrum (Jain & Singh 2003).

Thermal behavior of diverse urban surfaces and landscape components is an effective instrument for planners and designers because it is connected to the phenomenon of Urban Heat Island (UHI), therefore it can help climatic rehabilitation in urban areas as well as an improvement in the outdoor thermal environment (Xiaoshan & Lihua, 2016). Because the thermal environment has a variety of effects on people who use outdoor spaces, particularly on university campuses where the thermal environments of educational living spaces are critical (Srivanit & Hokao 2013).

(Huang et al. 2008), emphasized that the distribution of UHI in a region is a result of climatic circumstances; consequently, various aspects should be considered for urban planning, for instance, urban characteristics such as land use, greenery, the density of buildings, traffic loads, and anthropogenic heat sources and construction materials, even the amount of shade can plays a significant role in affecting the air temperature, moreover, uneven shadowing could be a key contributor to the fluctuating cooling of regions with green areas, In other words, different levels of shading will create different levels of cooling.

As previously mentioned, emissivity is a significant aspect when studying thermography. And that's what has been emphasized in a study by Jose et al (2005) the land surface emissivity (LSE), as an important property of natural materials, is frequently used to predict material composition.

3.2.4.1 Trees/vegetation:

Green trees in cities have already been investigated as a possible contributor to reducing UHI and enhancing building and residential air quality (Huang et al. 2008).

Trees' canopies (the part made up of branches and leaves) prevent heat from reaching these surfaces. Tree canopies can block up to 90% of the sun's rays, and the heat that comes with them. Some tree species have wider canopies, wider leaves, and more leaves than others. Beeches, for example, can block up to 97% of the light that falls on them (SAURAB 2020). Radiation is intercepted more effectively by dense canopies than by sparse canopies. Radiation intercepted is absorbed, transmitted, or reflected (Amthor 2010). In addition, trees transfer water from their roots to the leaves, where photosynthesis takes place, through their trunks. However, up to 99% of the water that reaches the leaves evaporates (transpiration) When water evaporates as vapor, more energy leaves the system than was drawn to convert water to water vapor. If the amount of energy entering the system is less than the amount of energy leaving the system, the system cools to maintain equilibrium, according to the law of conservation of energy (SAURAB 2020).

The spectral reflectance curve has been used to explain the vegetation's reflectance characteristics. Understanding the spectral plant reflectance (spectral signature) in the context of the electromagnetic spectrum is critical for environmental research (Roman & Ursu 2016). A leaf is composed of structural fibrous organic matter layers. There are pigmented water-filled cells and air spaces in this. The reflectance, absorptance, and transmittance properties of a leaf are affected by its pigment properties, physiological structure, and water content (Jain & Singh 2003). Light absorption by leaf pigments dominates the reflectance spectrum in the visible region (0.4-0.7 µm) of vegetation, while chlorophyll pigments absorb blue (0.4-0.5 µm) and red (0.6-0.7 µm) wavelengths for photosynthesis. In the red/infrared boundary near

0.7, absorption decreases and reflection increases. Reflectance is nearly constant from 0.7-1.3 μm and then decreases for longer wavelengths (Huete 2004).
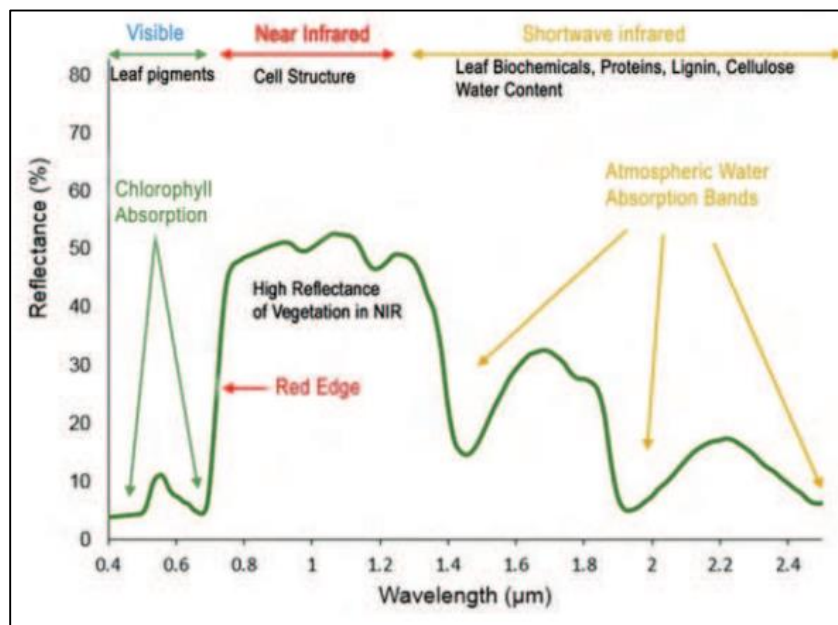
Figure 15. Spectral Reflectance Curve for vegetation (Roman & Ursu 2016).

The vegetation and its water content have an important impact on the thermal variations in an urban area, besides the relationship between the sky view factors (SVF) and the vegetation area for instance, if the SVF is high, thermal energy can efficiently radiate into the open sky; contrarily, if the SVF is low in the vegetation area, the amount of radiation emitted into the open sky is reduced (Huang et al. 2008). Research conducted by Shashua-Bar & Hoffman (2000) on the cooling impact of small urban green woodland sites of various geometric configurations in summer, to anticipate the cooling effect inside the wooded areas, discovered that on average, 80% of the cooling effect was linked to tree shade, even a moderate tree shade coverage of 60% can significantly reduce the thermal effect of heavy traffic. That is also highlighted in a study by Huang et al. (2008), which found that even a single tree can decrease the air temperature in the surrounding region by 0.5-3 degrees Celsius. In the same study, they observed that during the hot season, the city's commercial core was warmer than the surrounding areas by 1–4.2 C and warmer than other areas included in the study, such as the rural region, lake, and mountain area, which was the coolest. In addition to the greenery at the street level (Yang & Zhao 2016). Green roofs have an important role, in research on the effects of community-scale green-roof installation on air temperature, the study underlined the environmental benefits of green roofs, such as lowering energy consumption and improving microclimate and air quality (Peng & Jim 2013). Therefore, vegetation in big green spaces can affect the air temperature above it, which enhances the urban area's thermal environment (Shashua-Bar & Hoffman 2000).

3.2.4.2 Soil:

Is the temperature of the soil higher in the urban area than in the rural area? A study conducted by Shi et al. (2012) revealed that after consistently measuring the temperature of underground soil (0-300 cm depth) for one year, the soil temperature in the rural area was lower than in the urban area. Another study by (Ferguson & Woodbury (2007), found that there is a strong link between subsurface temperatures and land use, and to understand that link, they examined the subsurface temperatures in an urban environment and the surrounding rural area, the result was that in the urban area that is full of high buildings and a small amount of vegetation has the highest temperature, while the urban green space was cooler, and even the agriculture land has the lowest temperature, indicating that the land use has a strong link to the differentiation in the soil temperature. Moreover, lower surface temperatures were recorded in greening regions during the daytime in the urban environment, but higher temperatures were reported on the soil and buildings (Huang et al. 2008).

Soil, bare ground, and built-up areas have a greater impact on UHI than vegetated land because each of them shows a different type of thermal behavior, as previously stated, urbanization is a major cause of UHI because it is the result of replacing bare land or vegetative land cover with built-ups, where bare land and built-up land covers have higher land surface temperature (LST) values than other land covers such as vegetation, and converting land from bare land to urban can result in a small decrease in land surface temperature, whereas converting land from vegetation to urban can have a large effect on the LST, thus, replacing vegetation with urban land cover has a significant impact on raising the intensity of the UHI effect, and keeping the land as just soil or barren field or converting bare land to buildable space also has an impact on the UHI (Bala et al. 2021). The UHI significantly impacts the soil because it increases soil water evaporation, which can lead to compaction, shrinkage, and consolidation of the soil (Shi et al. 2012). For example, if the environmental temperature rises by 1 degree Celsius, evaporation and volume shrinkage rates will increase by around 15% (Chaosheng et al. 2011; Shi et al. 2012). And several variables can affect heat transmission in soil, including particle size, density, water content, composition, ground temperature, and organic matter, making it difficult to estimate thermal behavior (Di Sipio & Bertermann 2018).

Regarding reflectivity, the chemical and physical properties of soil components, organic matter, texture, moisture, surface roughness, and sun angle all influence its reflectance. In the visible bands, soils typically have a higher reflectance than plants. The typical curve in fig.17 shows increasing reflectivity as the wavelength increases. Organic matter and moisture affect reflectivity in the visible band. Plants have a

higher reflectance in the NIR band than soils. In general, a reduction in soil grain size results in increases in reflectance. The reflectance properties of rocks are heavily influenced by their type, chemical composition, weathering, rock outcrop, and so on (Jain & Singh 2003).

3.2.4.3 Pavements/concrete/ asphalt:

Urban heat islands are caused by several factors, but one of the biggest contributors is artificial impermeable surfaces because conventional absorptive pavements can heat the air surrounding them as they get hotter due to higher absorption or lower albedo (Shimazaki et al. 2021). In other words, the thermal balance of these materials can be determined based on their reflectivity to solar radiation and emissivity to long-wave radiation during the day (Doulos et al. 2004a). In general, lower surface temperatures can contribute to a decrease in ambient air temperature, which can have a significant impact on cooling energy usage in urban environments, but materials such as asphalt, concrete, stone, pebble, and so on which it stored the heat, can has a significant influence on urban temperature. Several factors, such as color, surface texture, and construction material, can affect the thermal properties or albedo of this type of material, for instance, rough and dark-colored surfaces absorb more solar radiation than smooth, light-colored, and flat surfaces, so dark colored surfaces are warmer than light-colored surfaces; additionally, tiles with smooth and flat surfaces are cooler than tiles with rough and anaglyph surfaces, such as asphalt (Doulos et al. 2004a). For example, in comparing the heat of asphalt, pavement, concrete, and grass covers, the asphalt was the warmest (Chudnovsky et al. 2004; Shi et al. 2012). Fig.16 illustrates smooth and light-colored surfaces as "cold" materials, whereas rough and dark-colored surfaces, as well as building materials consisting of pebble, pave stone, and asphalt, are "warm" materials (Doulos et al. 2004a).
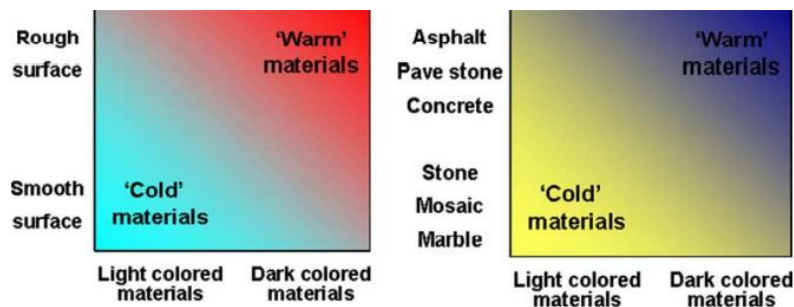
Figure 16. differences between 'cold' and 'warm' materials (Doulos et al. 2004a).

As a result, we can understand how much the thermal behavior of pavement materials contributes to the urban heat island, as well as how people behave when they sprinkle water on the street to create a cooling

effect through evaporation on hot summer days, A similar environmentally friendly technique utilizes regular natural rainfall is water-retaining pavement technology (Shimazaki et al. 2021).

Which is a technique where the pavement is made of a porous asphalt mixture, allowing rainwater or other water that falls on the paver block's top side to enter and be retained there, On hot sunny days, the held water in the block evaporates, keeping it cold and ready to hold rainfall for the next precipitation event (Qin et al. 2018). The thermal environment on a water-retaining pavement and a normal asphalt pavement was tested with Japanese volunteers to evaluate the effectiveness and application of evaporative pavements, In other words, the physiological and psychological reactions of the human body were measured based on the type of pavement (Shimazaki et al. 2021). The conclusion indicated that the reflected solar radiation   (The solar radiation and infrared radiation in upward and downward directions were measured at a height of 1.5 m using a net radiometer), from water-retaining-pavement, was significantly bigger, and the infrared radiation of water-retaining-pavement significantly lesser than that of asphalt pavement. Thus water-retaining-pavement greatly decreases human thermal load, which can be considered as an indicator and assessment tool for UHI (Shimazaki et al. 2021).

Furthermore, the water-retaining (WR) paver block can be 2-10 degrees Celsius colder for 6 cm-thick paver blocks and can hold around 9.5 L/m2 of water, which can be evaporated during a hot, sunny day or stored and reduce urban runoff on a rainy day (Qin et al. 2018). Another strategy for mitigating urban heat islands is the application of "cool" coatings, which give a high reflection of solar radiation on pavement materials and are estimated to be capable of decreasing the surface temperature by up to 7-8 C on ground level, leading to a drop in ambient temperature (Georgakis et al. 2014).

3.2.4.4 Water bodies:

It's an important question how different sorts of water, and grassland corridors, generate cooling and influence the urban heat island in a city (Huang et al. 2008). When designing urban morphology, we must consider wind direction. For example, when groves of trees are placed next to blue space (blue space is defined as all forms of natural and manmade surface water (Smith et al. 2021), humid air may become trapped beneath the canopy in the wind-sheltered zone, and that can lead to reducing evapotranspiration from both the greenspace and blue space, resulting in uncomfortable environmental conditions, However, blue spaces contribute significantly less to cooling than green spaces (Gunawardena et al. 2017). Yet, land use planners and urban designers have used the evaporative power of water bodies as a strategy to mitigate the urban heat island effect (Steeneveld et al. 2014). Waterbodies in the urban area contributed to lower LST values as compared to bare land and built-up land covers (Bala et al. 2021).

The water heat exchange process has 3 types: radiant heat transmission to the surroundings, evaporative heat dissipation, and convective heat transfer with the air. In terms of physical characteristics, water has low reflectivity, so it receives more solar radiation; In other words, when solar radiation reaches a body of water, it is absorbed rather than reflected back into the atmosphere. Water receives more solar radiation as a result of its low reflectivity, which means that it absorbs more solar energy. This increased absorption of solar radiation can cause an increase in water temperature, particularly in shallow bodies of water exposed to direct sunlight for extended periods of time. Additionally, Due to its high thermal capacity, the temperature of the water body will gradually and slowly rise, in addition to evaporation, which can improve air humidity; and finally, the temperature difference between land and water forms and speed up the airflow (Yang et al. 2020). The absorption in the NIR and beyond is the most distinguishing feature of water (Fig.17). Water bodies exhibit a variety of conditions that manifest themselves in visible wavelengths. At these wavelengths, there are complex energy-matter interactions that are affected by a variety of factors. These factors include interactions with the water's surface and material suspended in the water. Clearwater reflects the most at 0.6 μm. Moreover, the transmittance of the water is significantly influenced by the presence of organic and inorganic elements, and as a result, the reflectance is dramatically impacted. A body of water with a high concentration of suspended sediments, for example, will reflect better than 'clear' water. A rise in chlorophyll levels reduces reflectance in blue wavelengths while increasing it in green, Fig.17. This can be used to detect algae in water using remote sensing (Govender et al. 2007; Lillesand et al. 2015).
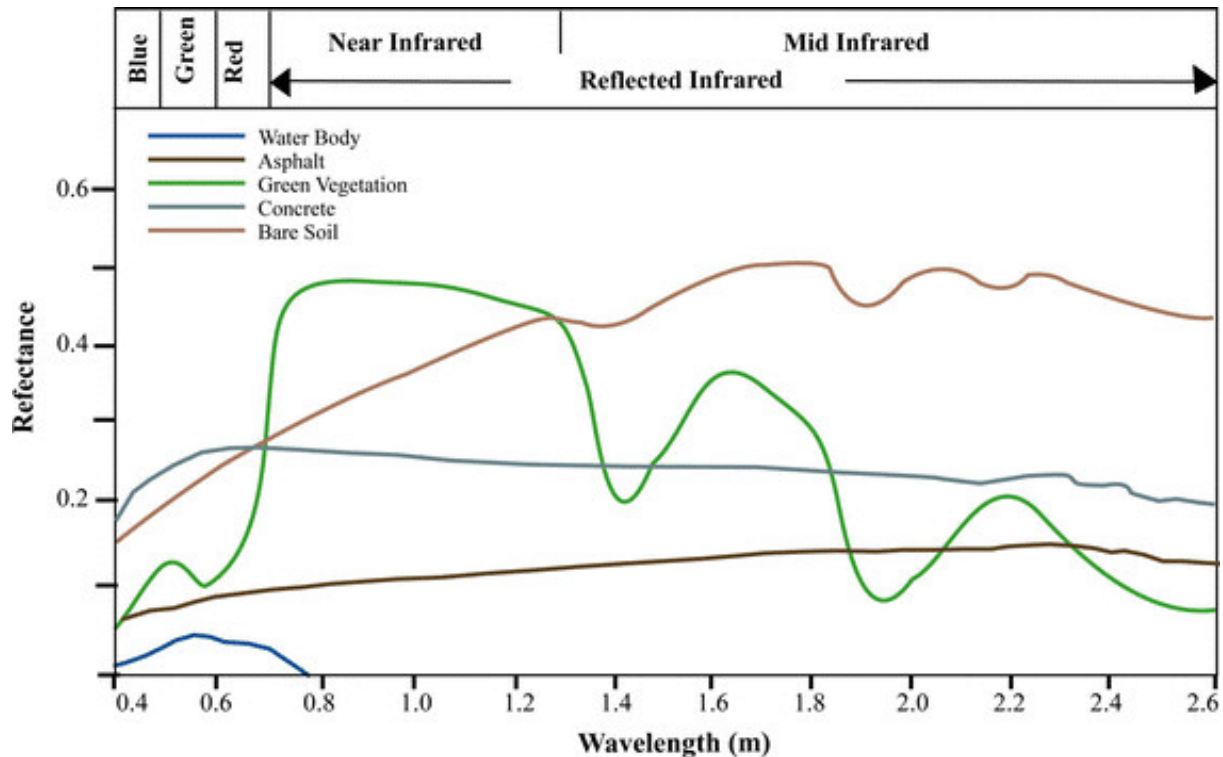
Figure 17. Spectral signatures for dry bare soil, green vegetation, Clearwater, and asphalt.

(coops et al. 2002; Govender et al. 2007)

(Hathway & Sharples 2012) carried out a study to investigate the effect of small urban rivers on UHI mitigation in the UK, and they found that the cooling was stronger during the daytime in May than in June because the water temperature in June was 2 degrees Celsius higher than in May, therefore the river's water temperature had a large impact on the cooling potential, thus the cooling would be limited as the water temperature rose. Moreover, Hathway & Sharples (2012), highlighted that if the location receives significant sun radiation and there are dark, engineering elements (such as buildings or bridges with dark surfaces) in the river's surroundings, cooling will be limited, which means that the presence of vegetation next to the river plays an important role in increasing cooling on the bank, and thus the design of the local urban form has a large impact on river cooling. Thus, water bodies are capable of providing cooling; in the spring, when the water is cold, the river will contribute to cooling the air temperature; however, a variety of factors, including the urban shape along the riverbank, sun radiation, wind speed, and relative humidity, can affect the river's ability to cool the temperature. Overall, the surrounding environment can affect air temperatures more significantly than the presence of the river (Hathway & Sharples 2012). Similarly, a study that examined the impact of small rivers (5.8 km) on urban cooling found an important correlation between urban shape and river cooling intensity, and the writer means by urban shape, the morphology of the urban area, the height of the buildings, and the width of the street, because the height and density of

buildings, as well as the width of streets, have a significant impact on the amount of solar radiation that is absorbed or reflected. Understanding the role of these factors in shaping urban microclimates is therefore critical for developing effective strategies to mitigate the heat island effect and improve the livability of our cities. In addition, the research also found that even though the river is small, it can cool a surrounding region at a distance of 30 m (Park et al. 2019).

Another study by (Yang et al. 2020), emphasized the importance of the location of the water bodies during the planning process because organizing the water bodies in the proper locations can fully enhance the surrounding thermal environment, for instance, based on the research, adding a wetland, artificial lake or pond in the residential area, it should be in the central position. Another important factor to consider is the thermal impact of water on wind velocity. In the absence of water bodies in an urban area, wind velocity will be low due to the blockage effect of the buildings, resulting in high temperatures in the residential area. Conversely, Wind speed will increase in urban areas with water bodies. This is due to the temperature difference between the land and the water body, which efficiently promotes airflow (Yang et al. 2020).
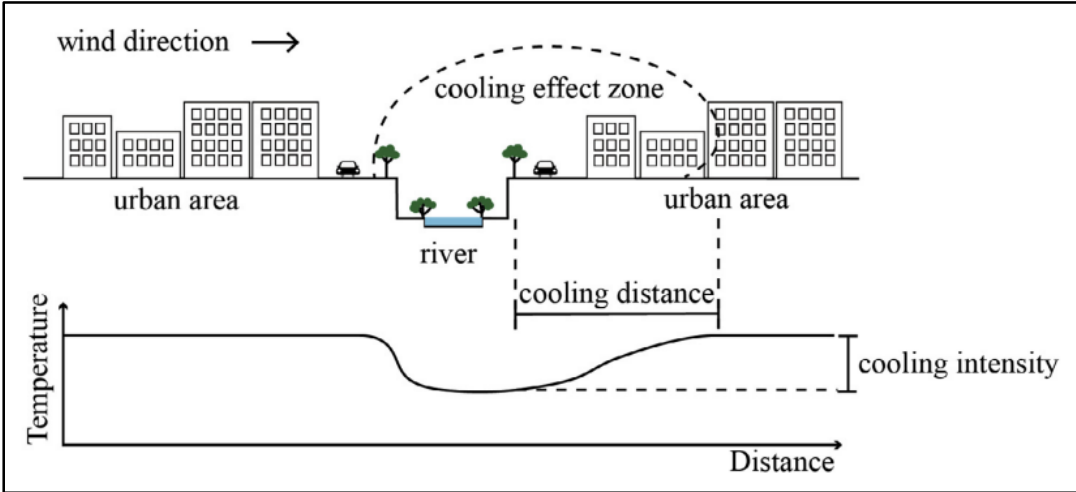
Figure 18. Illustration of the cooling impact of urban river

Methodology

4

4.1 Retrieving land surface temperature from Landsat data:

4.1.1 Mapping of Surface Temperature.

4.1.2 Normalized Difference Vegetation Index (NDVI).

4.1.3 Calculating the final land surface temperature from Landsat.

4.2 Study area:

4.2.1 Background of the study area.

4.2.2 The Climate in Suchdol.

4. Methodology

The methodology of this study is divided into two parts. Because land surface temperature (LST) is an essential factor in determining UHI, the first part of the methodology is to retrieve LST from satellite data, using ArcMap GIS as software.

According to (Zhao & Wentz 2016), thermal imagery is widely used to monitor the spatial extent and thermal intensity of the urban heat island (UHI) effect. Particularly LANDSAT 8 (2018) and LANDSAT 5 (2002), using the mono-window algorithm method. In addition to studying the development of land use/land cover over time, moreover, the building footprint, imperviousness, digital elevation model (DEM), and normalized difference vegetation index (NDVI) of the study area have been investigated to understand the character of the study area and investigate the relationship between land surface temperature and land cover/use. The second part includes using an infrared camera to measure surface temperatures to investigate the thermal behavior of various materials such as concrete, asphalt, stone, paving stone, and others, which have a significant impact on the urban heat island. Understanding the thermal behavior of various objects in our cities can also assist urban designers in achieving thermal comfort in urban areas. The methodology for the analysis will describe in the chapter below, but first, the data and the maps used in this study will be presented.

Figure 19. A Mind map depicts the data and maps that have been used to achieve the study's goal

4.1 Retrieving land surface temperature from Landsat data:
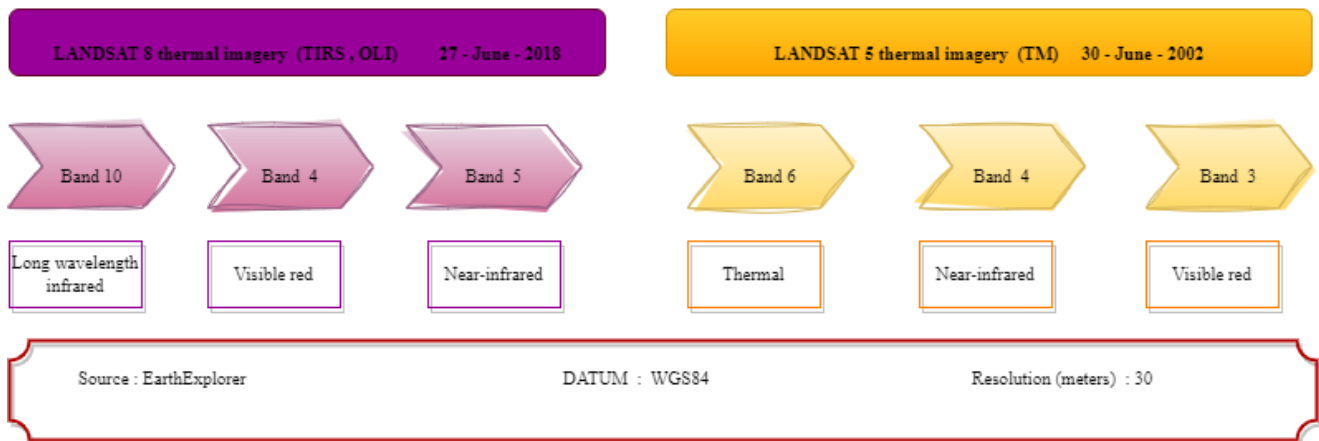
Figure 20. GIS datasets were used in the research to retrieve land surface temperature (LST).

4.1.1 Mapping of Surface Temperature:

Land surface temperature plays a significant role in a variety of processes, including hydrology, geophysics, biophysics, urban land use, and land cover (Avdan & Jovanovska 2016). The main goals of this research are to investigate the phenomenon of urban heat islands in Suchdol as a study area and to investigate the relationship between land surface temperature and land use/land cover. By using Landsat 8 data (Operational Land Imager (OLI) &Thermal Infrared Sensor (TIRS)) acquired on June 27, 2018, and Landsat 5 data (Thematic Mapper (TM)) acquired on June 30, 2002, from the USGS library of the Earth Explorer webpage to retrieve the LST.

The first step is to obtain a raw multi-spectral image from the US Geological Survey (USGS), including thermal IR band 10. Landsat 8 carries two sensors. The Operational Land Imager sensor is built by Ball Aerospace & Technologies Corporation. And the Thermal Infrared Sensor that is built by NASA Goddard Space Flight Center. Furthermore, the satellite sensors collect raw data at a depth of 12 bits, which improves the overall signal-to-noise ratio. This translates to 4096 potential grey levels, as compared to 256 grey levels in Landsat 1-7 8-bit instruments. Improved signal-to-noise performance allows for more accurate characterization of land cover state and condition. Moreover, 12-bit data are scaled to 16-bit integers and delivered in Level-1 data products (USGS 2013).

The Landsat 8 Thermal Infrared Sensor (TIRS) is the most recent thermal infrared sensor for the Landsat project, offering two adjacent thermal bands that are extremely useful for LST inversion (bands 10 and 11)

(Yu et al. 2014). In this study, band 10 has been used. And TIRS measures land surface temperature in two thermal bands 10 and 11, whereas the OLI measures in the visible, near-infrared, and shortwave infrared portions (VNIR, NIR, and SWIR) of the spectrum (bands 1 to 9) (USGS 2013). Band 4 and band 5 have been used to calculate the Normalized Difference Vegetation Index (NDVI).

Regarding Landsat 5 which carried two sensors: the Multispectral Scanner System (MSS) and the Thematic Mapper (TM) instruments (USGS 2013). Bands 3, 4, and 6 have been used.
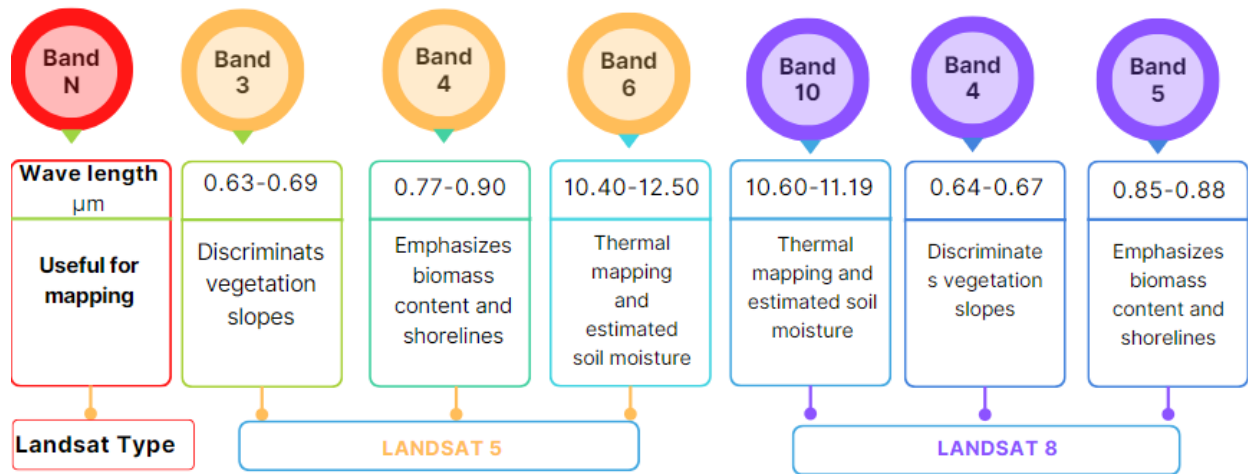
Figure 21. The Characteristics of the Landsat data (Credits: USGS 2013). Edited by the author.

The second step in retrieving LST from Landsat 8 is Converting the values of digital number (DN) to spectral radiance at the top of the atmosphere (TOA) radiance Lλ (W/m2 sr μm) (Zhao et al. 2017).

 Using the following equation (Avdan & Jovanovska 2016) :

Lλ = ML * Qcal + AL - Oi   (1)

DN is the digital number of the pixel image.

Lλ: TOA spectral radiance (W/m2 sr μm)

ML: Radiance multiplicative band 10

Qcal: Quantized and calibrated standard product value (DN)

AL: the re-scaled bias corresponding to a specific band, W/m2 sr μm

Oi: correction value for band 10 which is 0.29.

All of the values required for this equation were obtained from the image's metadata file.

In the step of Converting the values of digital number (DN) to spectral radiance (L), the equation for retrieving LST from Landsat 5 is (Grover & Singh 2015) :

$$L\lambda = LMIN + (LMAX - LMIN) \times DN/255 \qquad (2)$$

where $L\lambda$ = spectral radiance, LMIN = 1.238, LMAX = 15.600 and DN = digital number.

The third step in retrieving LST from Landsat 8 is reversing the at-sensor brightness temperature (Zhao et al. 2017). In another word, following the conversion of digital numbers (DNs) to reflection, the TIRS band data should be converted from spectral radiance to brightness temperature (BT) using the thermal constants provided in the metadata file (Avdan & Jovanovska 2016). And the equations for both Landsat were the same.

$$BT = K2 / (\ln [(K1/L\lambda)+1]) \qquad (3)$$

BT is the Top of atmosphere brightness temperature (K), where $K1$ and $K2$ stand for the band-specific thermal conversion constants from the metadata (Avdan & Jovanovska 2016). Then conversion of Kelvin to Celsius (Grover & Singh 2015).

$$TB = TB - 273.15 \qquad (4)$$

4.1.2 Normalized Difference Vegetation Index (NDVI):

This study also investigated the relationship between land cover irradiance and vegetation content using the Normalized Difference Vegetation Index (NDVI), which was produced from Landsat 5 Thematic Mapper (TM) using band 3 (Visible red with Wavelength 0.63 to 0.69 μm) and 4 (Near-infrared with Wavelength 0.76 to 0.90 μm), and from Landsat 8 Operational Land Imager (OLI), using band 4 (Visible red with Wavelength 0.630 to 0.680 μm) and 5 (Near-infrared with Wavelength 0.845 to 0.885 μm). It represents the vegetation coverage and health in the study area. The NDVI range runs from +1 to 1 (Grover & Singh 2015). The normalized difference vegetation index (NDVI) is a standardized index that allows to generate an image displaying greenness (relative biomass). Based on the difference in brightness of two bands in a multi-spectral raster dataset—the chlorophyll pigment absorptions in the red band and the high reflectivity of plant materials in the near-infrared band. NDVI can be used to analyze remote sensing measurements and determine the presence or absence of live green vegetation, vegetation types, and overall vegetation health (Esri).

Very low values of NDVI (0.1 and below) correspond to barren areas of rock, sand, or snow. Moderate values represent shrub and grassland (0.2 to 0.3), while high values indicate temperate and tropical rainforests (0.6 to 0.8) (NASA 2000).
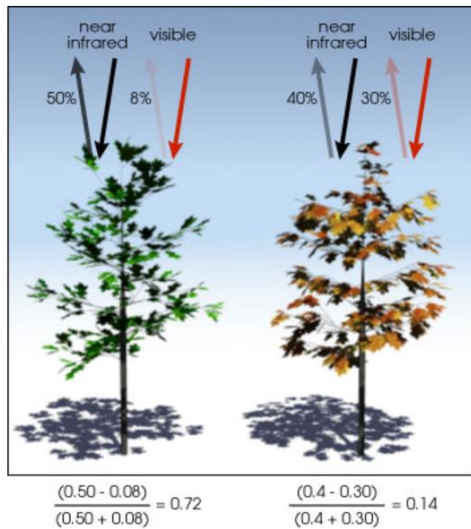
Figure 22. Normalized Difference Vegetation Index (NDVI) (Credits: NASA 2000).

Healthy vegetation (left) absorbs the majority of visible light and reflects the majority of near-infrared light. Vegetation that is unhealthy or sparse (right) reflects more visible light and less near-infrared light. The figures above represent actual values, but real vegetation is much more varied, (Illustration by Robert Simmon) (NASA 2000).

For Landsat 8 The NDVI is calculated using the following equation, where NIR is the near-infrared band (Band 5) and R is the red band (Band 4) (Avdan & Jovanovska 2016).

$$NDVI = NIR \text{ (band 5)} - R \text{ (band 4)} / NIR \text{ (band 5)} + R \text{ (band 4)} \tag{5}$$

Whereas, in Landsat 5 imagery, it is calculated from red and near-infrared bands (bands 4 and 3) from Thematic Mapper (TM) (Grover & Singh 2015).

$$NDVI = (Band4 - Band3) / (Band4 + Band3) \tag{6}$$

4.1.3 Calculating the Proportion of Vegetation and Land Surface Emissivity:

Emissivity (ε) is a proportionality factor that predicts emitted radiance by scaling blackbody radiance (Planck's law). Thus, must be known to accurately estimate land surface temperature (T). The NDVI method has been used to calculate Emissivity, therefore a proportion of vegetation should be calculated. (Jiménez-Muñoz et al. 2006). The equation has been used to calculate the vegetation proportion (Sobrino et al. 2004; Avdan & Jovanovska 2016).

$$P_v = ((NDVI - NDVI_{min}) / (NDVI_{max} - NDVI_{min}))^2 \tag{7}$$

The final equation for land surface emissivity is:

$$\varepsilon = 0.004\ P_v + 0.986 \tag{8}$$

And the explanation for why the emissivity equation has this shape has been given by (Sobrino et al. 2004). To apply this methodology, and calculate the Emissivity there is a need for soil and vegetation emissivity values. To achieve this, a typical emissivity value for plants of 0.99 has been chosen. Given that soil emissivity values vary more than those for vegetation, choosing a typical value for soil is a more important decision. The mean value for the emissivity of soils included in the ASTER spectral library (http://asterweb.jpl.nasa.gov) and filtered using the band TM6 filter function is one possible solution. Using this method and 49 soil spectra, a mean value of 0.973 (with a standard deviation of 0.004) is obtained. Using these data (TM6 emissivity of soil and vegetation of 0.97 and 0.99, respectively).

4.1.4 Calculating the final land surface temperature from Landsat 8:

The Brightness temperature derived from Eq. (4) is the temperature that a blackbody would obtain to produce the same radiance at the same wavelength (λ = 11.5 µm). Therefore, additional correction for spectral emissivity is required to account for the non-uniform emissivity of the land surface, and is computed as follows (Stathopoulou & Cartalis 2007) :

$$Ts = BT / \{1 + [(\lambda BT/\rho)\ \ln \varepsilon\lambda]\} \tag{9}$$

where Ts is the land surface temperature (∘C); BT is at-sensor brightness temperature (∘C); k is the wavelength of emitted radiance (11.5 µm); ρ = (h x c/r) = 1.438 · 10-2 m K; ε is the spectral surface emissivity (Stathopoulou & Cartalis 2007).

The following flowchart illustrates the process of obtaining land surface temperature from Landsat 8:
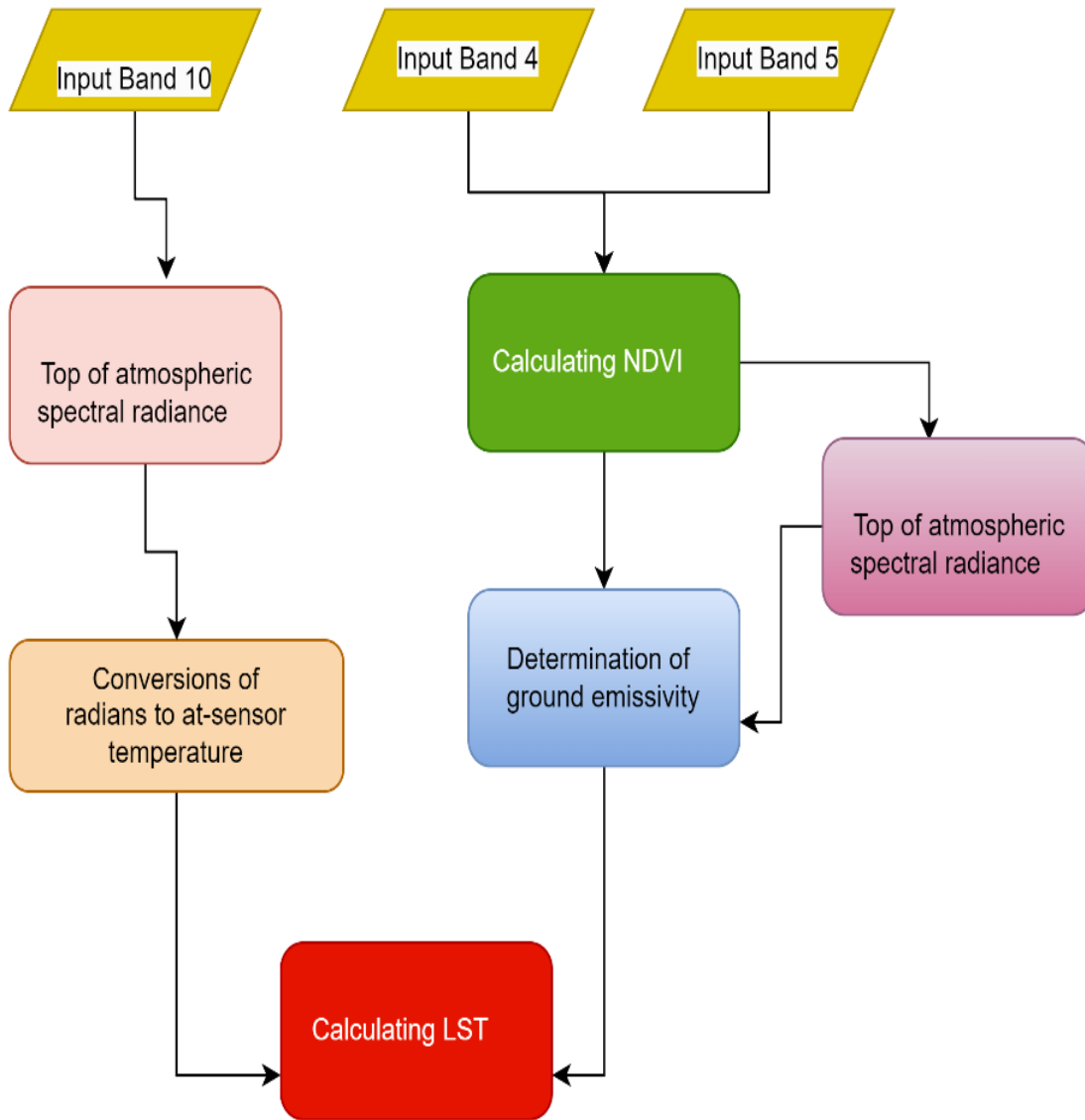
Figure 23. Flowchart for LST retrieval (Credits: Avdan & Jovanovska 2016). Edited by the author
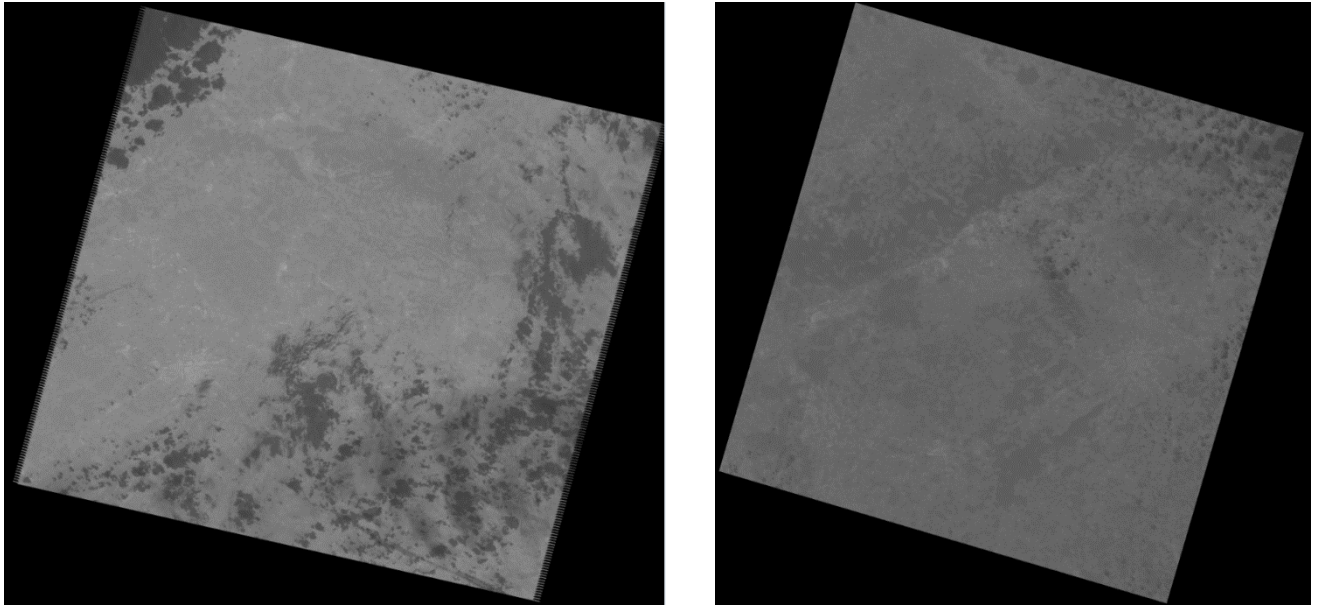
Figure. 24 Raw satellite data. Left, band 6, 8 bits (Landsat 5), and right, band 10, 16 bites (Landsat 8) (Earth Explorer).

4.2 The study area (Suchdol – Prague):

4.2.1 Background of the study area:

Suchdol is a district located on the northwestern outskirts of Prague, the administrative district is Prague 6, on the left bank of the Vltava River. The total area is 19.5 km2, with an urban area of 5.12 km2 and a population of 6.840 people. (the urban district).

The methodology used in determining the appropriate locations for this study entailed a thorough examination of several critical factors. The locations were chosen based on the presence of a heterogeneous landscape that includes a variety of land covers such as open spaces, forests, arable lands, pastures, and urban areas made up of both continuous and discontinuous urban fabrics. This diverse landscape provides an excellent opportunity to investigate the relationship between different land covers and land surface temperature, as well as to gain insights into the distribution of land surface temperature, thereby contributing to a better understanding of the subject.

Suchdol and Sedlec were founded in the 10th century by the Přemysl family, who then lived in nearby Levý Hradec (městská část). The territory of Suchdol was part of an extensive deciduous forest called Liboca,

according to the earliest documents from the 11th century AD. It was a hunting area full of game and wild animals. The road from Prague Castle led through the forest to Levý Hradec, which was the administrative, religious, and political center of Central Bohemia at the time. Levohradec hunters built a hunting hut, a log cabin, and a game storage room. The hut gradually changed into a hunting lodge. and later on, to the village of Suchdol,

According to the Suchdol website (https://historiesuchdola.cz), the development and growth of Suchdol over the centuries have been truly remarkable. The village began with a mere 11 buildings at the end of the 11th century, but by 1706 had expanded to 20 buildings with a population of 106. By 1878, the number of buildings had increased to 48 and the population had increased to 346. However, the twentieth century saw a significant increase in development. In 1900, there were 86 buildings and 747 people. The most significant growth occurs between the 1930s and the 1950s, when the population jumps from 2475 in 1930 to 4023 in 1956, with an incredible 860 buildings. The trend continued into the 1980s, with the number of buildings reaching an impressive 1050 in 1980, accommodating a population of 5012. Although the population fell slightly over the next 20 years, it had increased to an impressive 6699 by 2010. And, while the population hit its peak at 7151 in 2017, it fell slightly to 6840 in 2021, according to the Suchdol municipal documentary of 2022 (městská část).
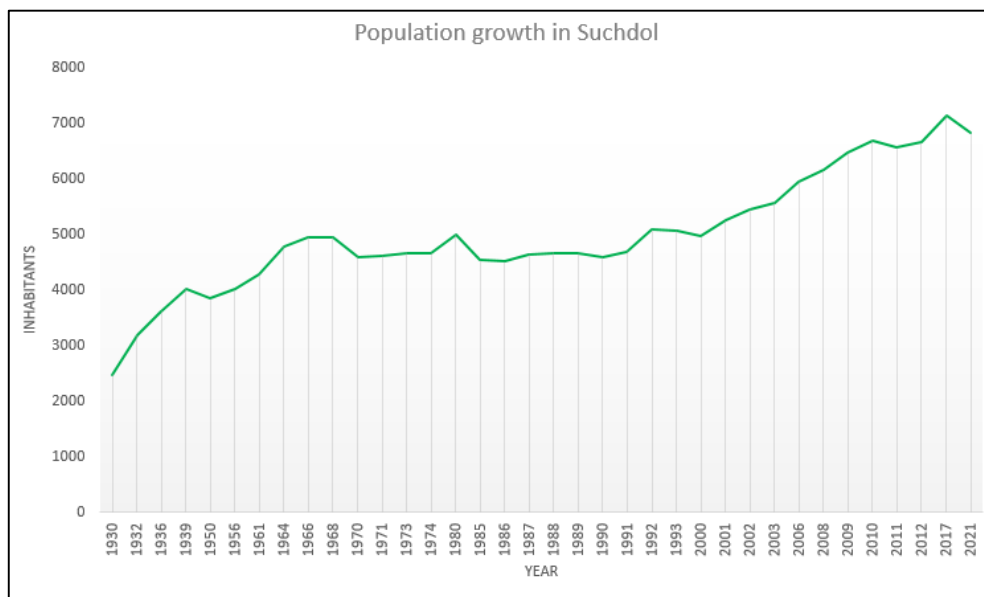
Figure 25. The population of Suchdol over time.

4.2.2 The Climate in Suchdol:

Suchdol (Longitude: 14.3768816, Latitude: 50.1331113) does not have a complex topography, with an elevations gradient ranging from 300 to 180 meters above the sea, Suchdol has, a warm summer climate,

and the district's yearly temperature is 10.64ºC (51.15ºF) and it is 0.57% higher than Czechia's averages. Suchdol typically receives about 44.48 millimeters (1.75 inches) of precipitation and has 117.16 rainy days (32.1% of the time) annually. and the Humidity is 76.2%. The annual maximum temperature is 13.26ºC (55.87ºF) whereas the annual minimum temperature is 5.52ºC (41.94ºF). The Warmest month in Suchdol is August (24.26ºC / 75.67ºF) and the coldest month is January (-2.96ºC / 26.67ºF). The wettest month is July (75.48mm / 2.97in) and the driest Month   November (24.59mm / 0.97in) (weather and climate 2022). Figures 26 and 27. depict the general climatic conditions for the Suchdol area based on this data.
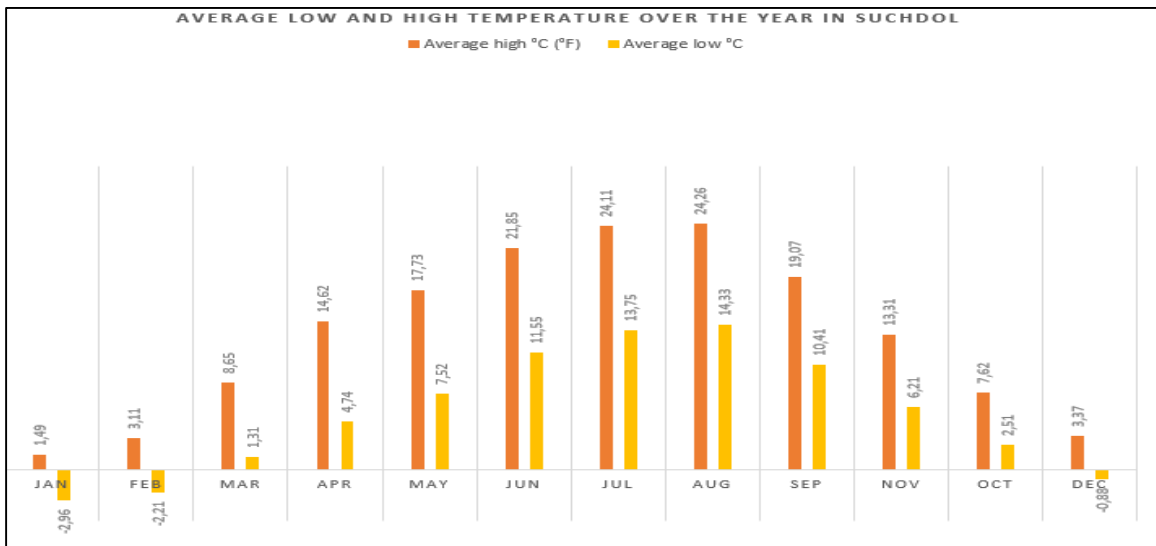
Figure 26. A. The average of low and high temperatures over the year in Suchdol.
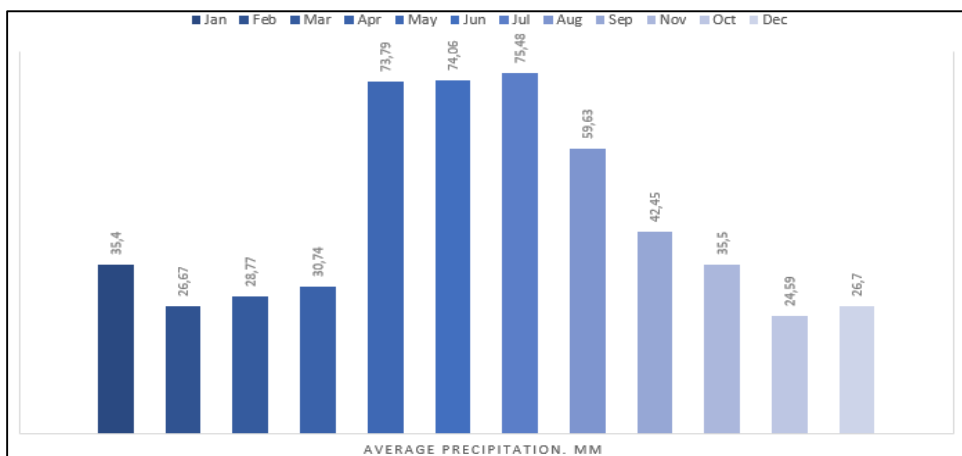
Figure 26. B. Annual precipitation in Suchdol.
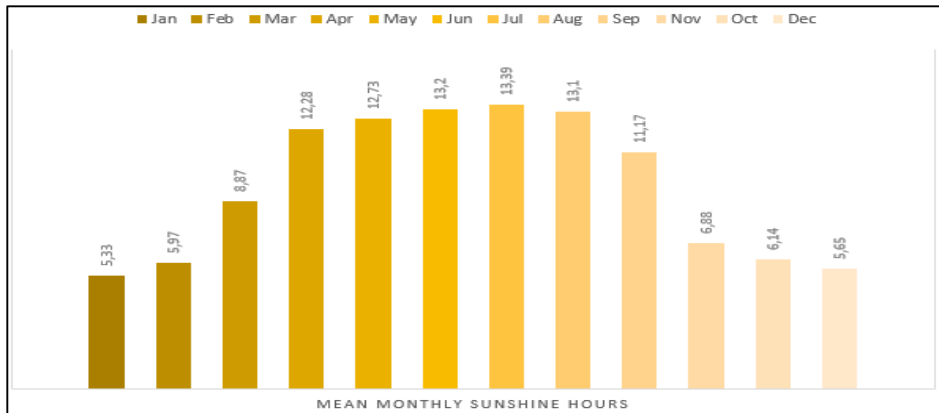
Figure 27. Annual mean monthly sunshine hours in Suchdol
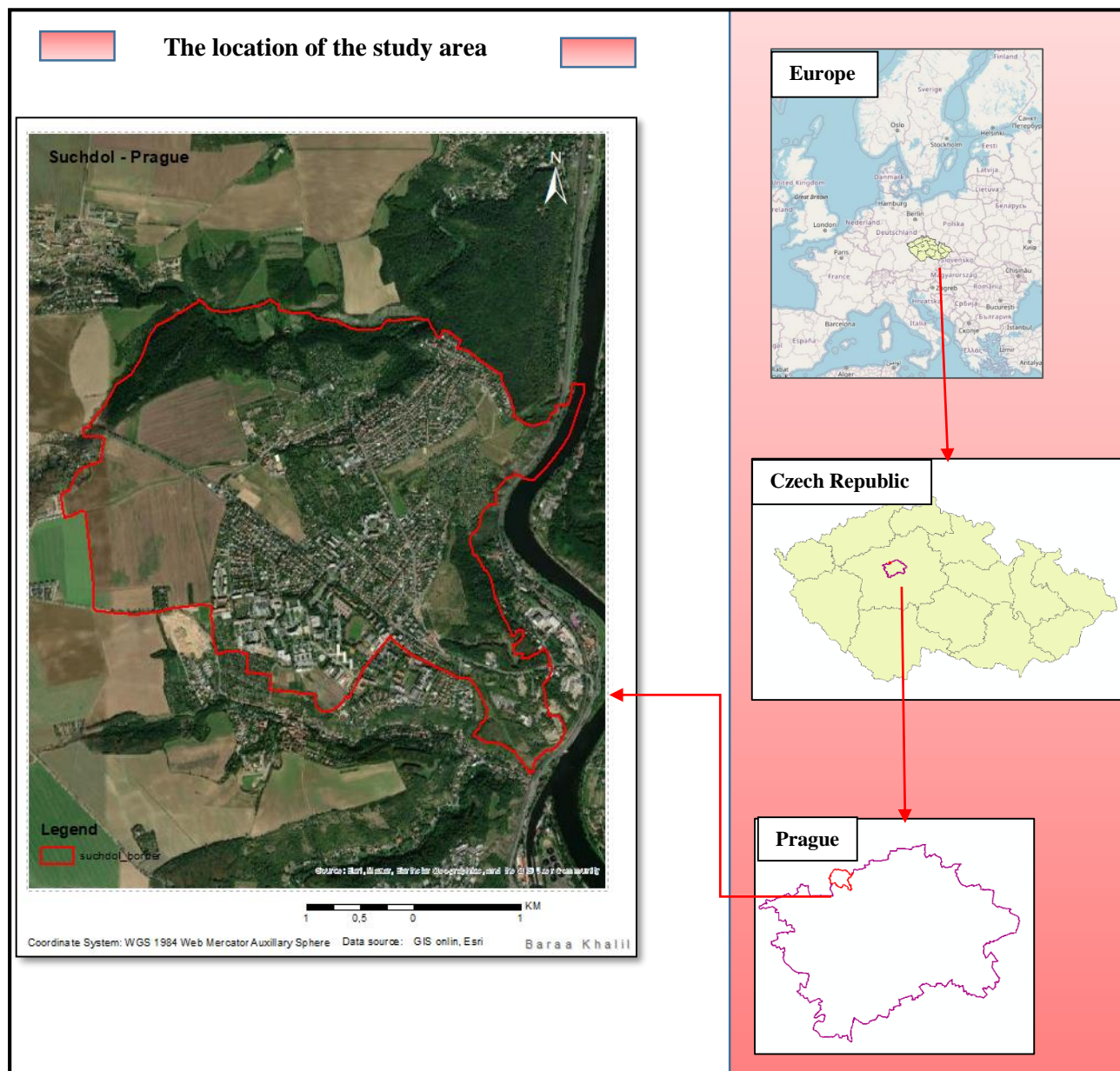
Figure 28. The location of the study area.

The following figures show the development of land cover/land use changes in Suchdol over time. The area has been divided into 2 parts, with the left side containing 5 residential zones (indicated by circular markings) and the right side primarily consisting of open spaces.
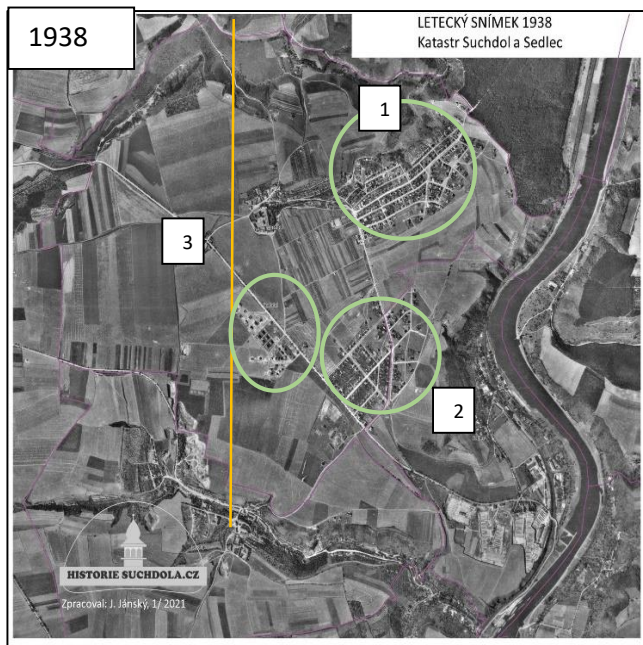
Figure 29. Suchdol 1938 (IPR Praha)
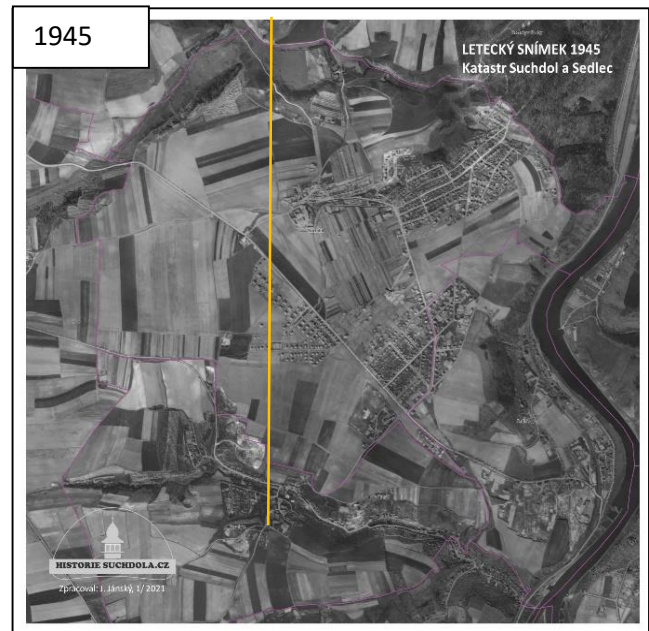
Figure 30. Suchdol 1938 (IPR Praha)
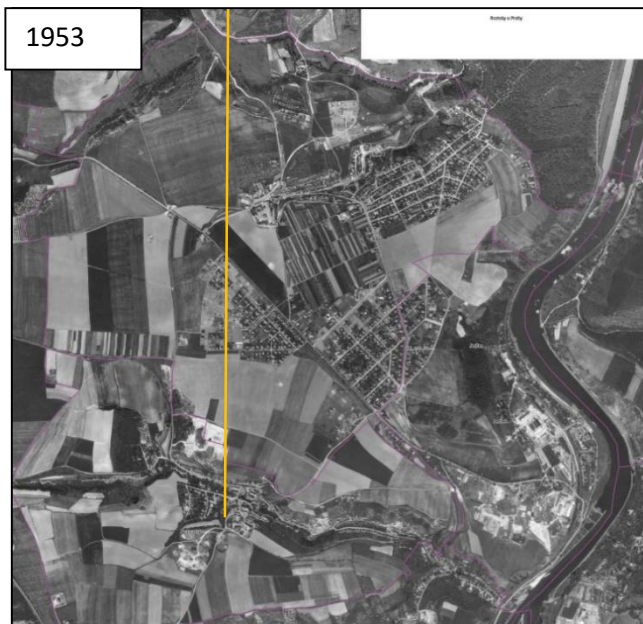
Figure 31. Suchdol 1953 (IPR Praha)
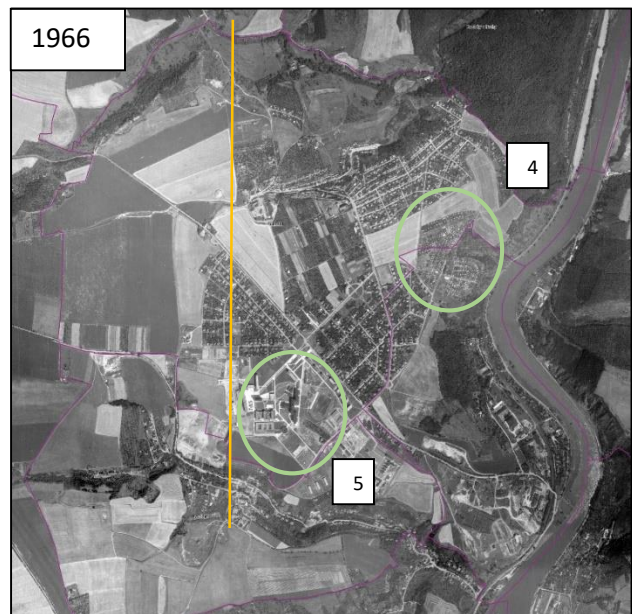
Figure 32. Suchdol 1966 (IPR Praha)
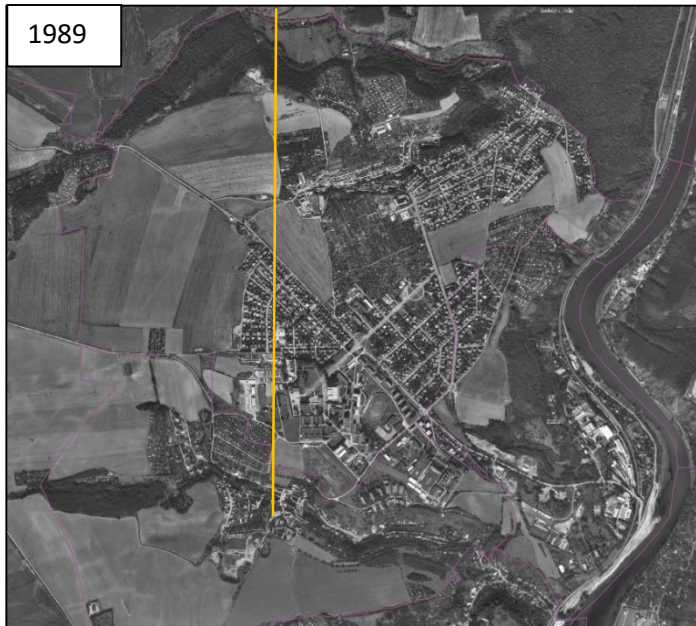
Figure 33. Suchdol 1989 (IPR Praha)
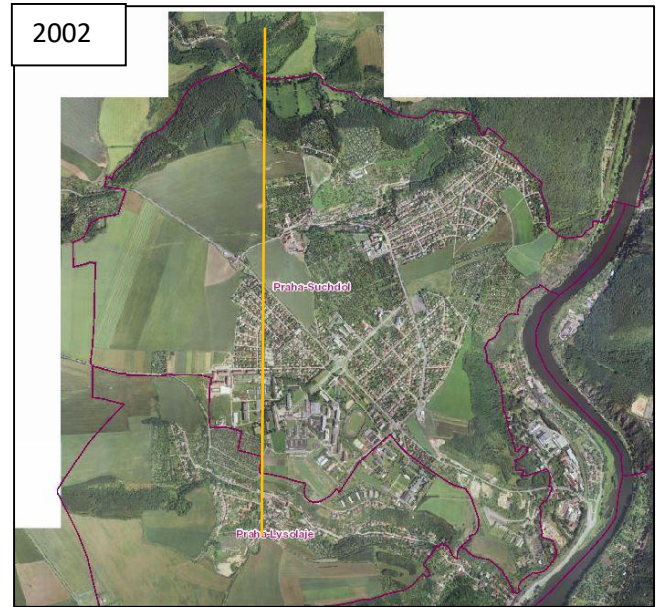
Figure 34. Suchdol 2002 (IPR Praha)
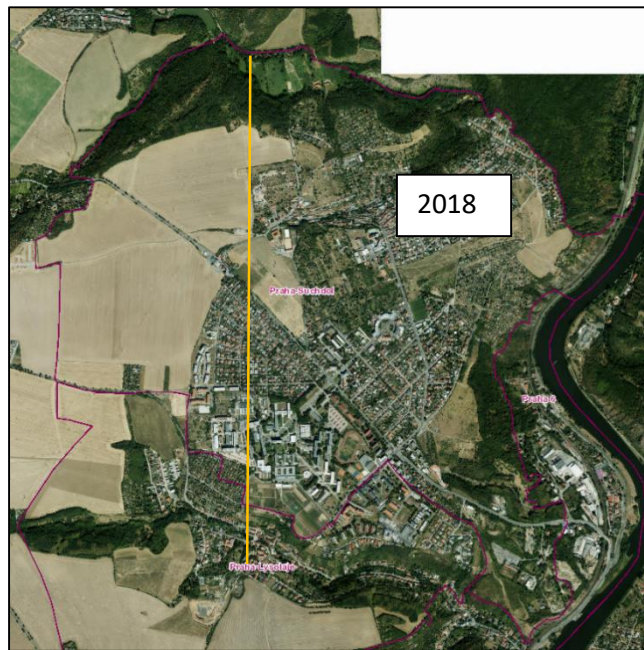
Figure 35. Suchdol 2018 (IPR Praha)

Results

5

5. Results

5.1 Land Use/Cover Changes Over Time:

The analyzed period of the development that happened in the study areas (1938-2018), using aerial photographs and maps, according to the aerial photograph from 1938, the region can be characterized as predominantly rural, with a sparse distribution of homes located in the eastern portion. Conversely, the western portion of the area is primarily comprised of open spaces. Based on this observation, the area was divided into two distinct segments, one with the residential areas being concentrated in the eastern and southeastern portions, and the second in the western portion with open areas. This division makes it easier to analyze the urban development that occurred in the study area.

In 1945, after a period of seven years, it was observed that the core of the eastern part of Suchdol remained devoid of housing, with only a limited number of homes constructed in the upper eastern region. Additionally, a few homes began to emerge and exceed the boundary line that we drew, and these houses are located to the left of Kamycka Road, which serves as the main road in Suchdol, connecting it to Dejvice in the south and extending towards the western part of the area.

In 1953, the growth of housing on the left side of the road (referred to as Zone 3) became more apparent, signifying the formation of a new residential area. At the same time, expansion was observed in Zone 2, characterized by the addition of new roads and buildings, in addition to the establishment of a construction site in the northern region of Suchdol. In contrast, there was also a noticeable increase in tree density in the area closest to the center. Thirteen years after, in 1966, additional roads were constructed to interconnect the entire area, resulting in a greater number of buildings in all three zones. Additionally, two previously open areas were transformed into built-up zones, thus two new zones were added to the map: Zone 4, a residential area, and Zone 5, which encompasses the Czech University of Life Sciences. The next available historical map in the Geoportal dates back to 1989, and despite some expansion in Zone 5 and the appearance of a limited number of buildings in the central area and Zone 2, the overall character of the landscape remained relatively unchanged. This trend continued until 2002, with minimal changes observed.

The study area appears to have developed its distinct character, as evidenced by the presence of five predominant residential zones, significant arable lands in the western sector, forests along the northern edge and in the eastern southern part, and a few scattered pastures. This scenario continued until 2006. and even the same landscape characteristics in 2018, as I will explain next.

5.2 Land Use/Cover Characterization in 2018:

The data for land cover in 2018, and changes in land cover in 2006_ 2012, and 2012_2018 from CORINE Land Cover (CLC). CORINE Land Cover (CLC) was designed to standardize data collection on land in Europe to aid in the development of environmental policies. Three iterations of this land cover inventory have been realized since the late 1980s (timed around 1990, 2000, and 2006). The fourth inventory has just begun as part of the GIO land (GMES Initial Operations Land) project. In the European context, CLC is widely used in indicator development, environmental modeling, and land use/land cover change analysis (Büttner 2014). Additional data sources from IPR Praha related to the development of the studied area over time were also used. Based on the Ariel photos from the IPR website, the changes in land use/ land cover were very limited between 2000 and 2018, and the changes began to show in 2006 (even though were very limited). Therefore, we decided to analyze the changes from 2006 to 2018, and use land cover 2018 to show the type of land in the study area.
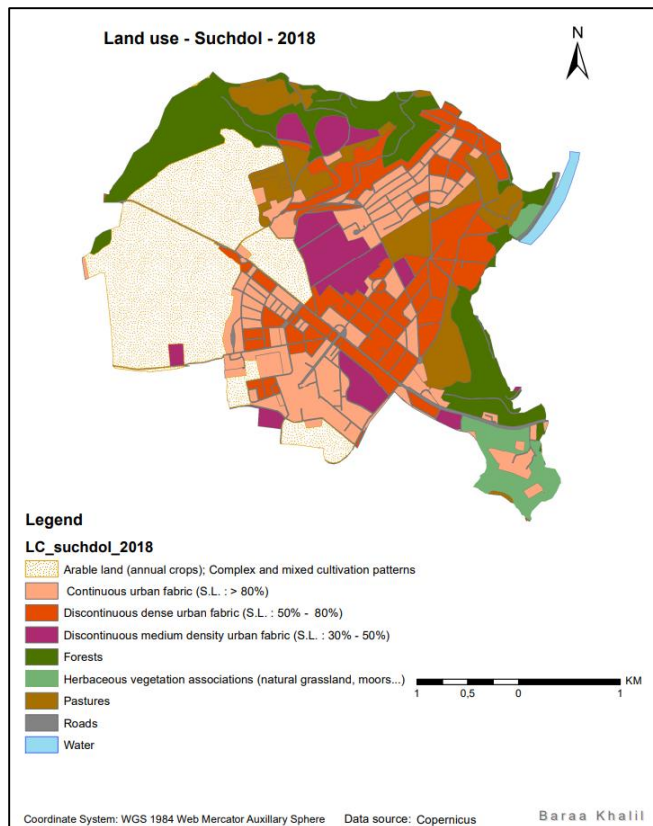
Agriculture occupies nearly half of the land cover in the Suchdol study area, with 25% arable land, 16% forest, 9% pasture, and 3% Herbaceous vegetation associations (natural grassland, moors...), Whereas the percentage of built-up area is around 40%, it varies between high-density and low-density built-up areas and is divided into 16% continuous urban fabric (> 80%), 16% discontinuous dense urban fabric (50% - 80%), and 8% discontinuous medium density urban fabric (30% - 50%) as shown in Figure 37.

Figure 36. Land use /land cover in Suchdol 2018
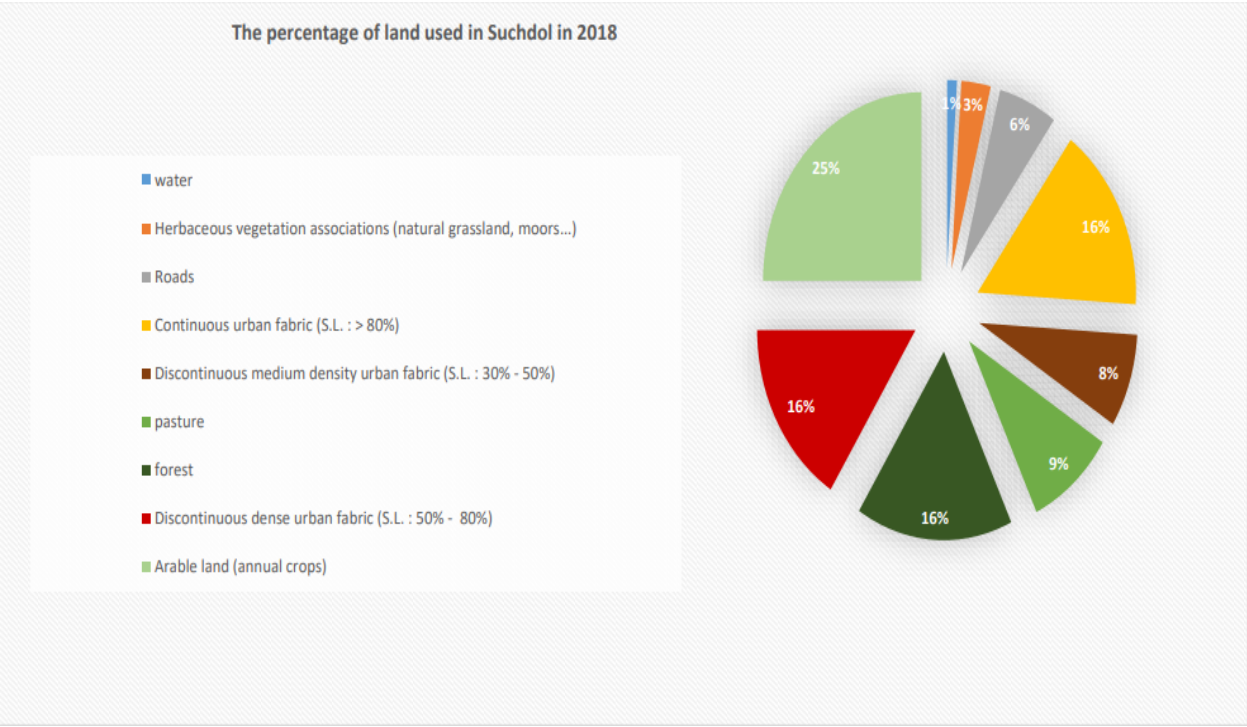
Figure 37. Land cover percentage in Suchdol 2018.
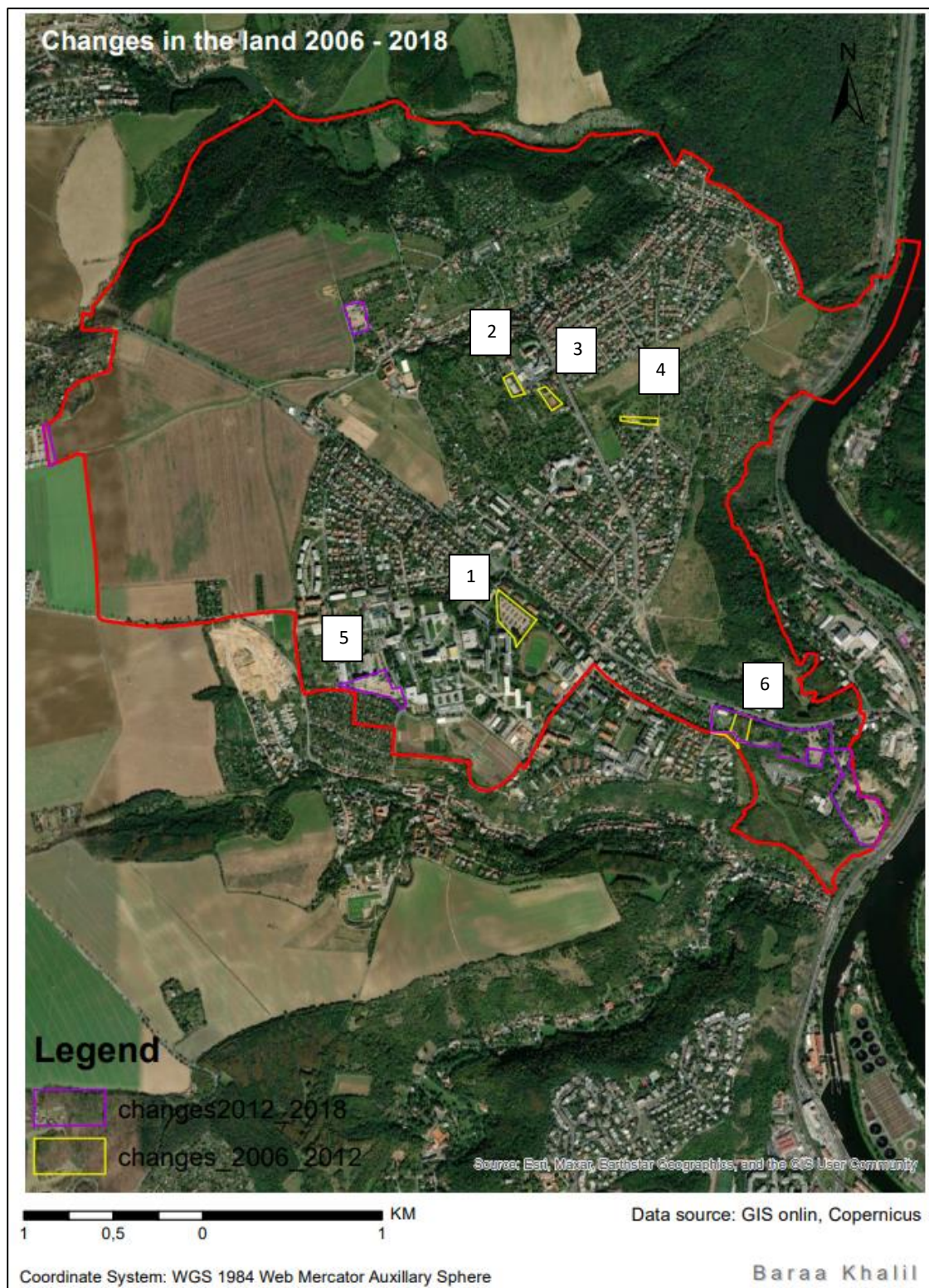
Figure 38. Land cover/land use changes in Suchdol between 2006 and 2018.

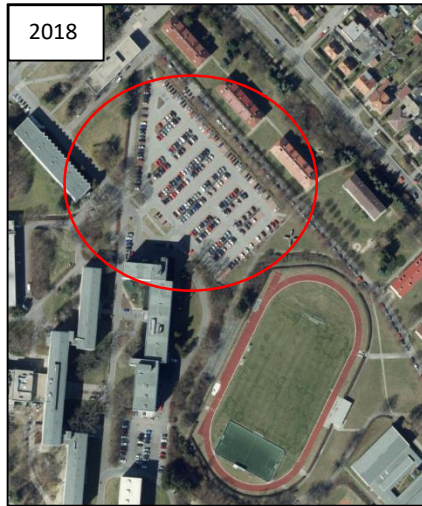In the following picture, I show the changes in the land between 2006 and 2018.

Figure 39, which depicts Area 1, clearly shows that the nearby football stadium's land has been changed from a green space to a parking lot.

Figure 40 shows a new building in the southeast corner of the image, close to the roundabout.

Figure 39. The changes in land use/cover in Area 1 (IPR Praha).

Figure 40. The changes in land use/cover in Area 2, and 3 (IPR Praha).
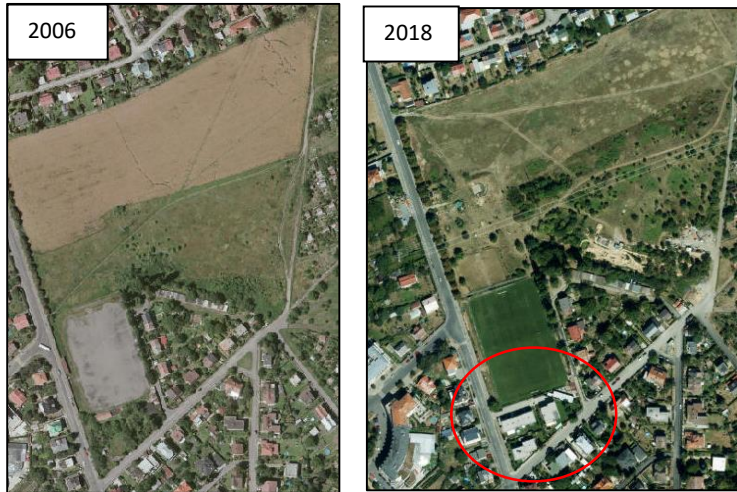
Figure 41. 42. depicts the changes in land use/cover in Areas 4, and 5 respectively where we can see new buildings have been built, but on the other hand, more greenery has been planted as well.

Figure 41. The changes in Area 4 (IPR Praha).
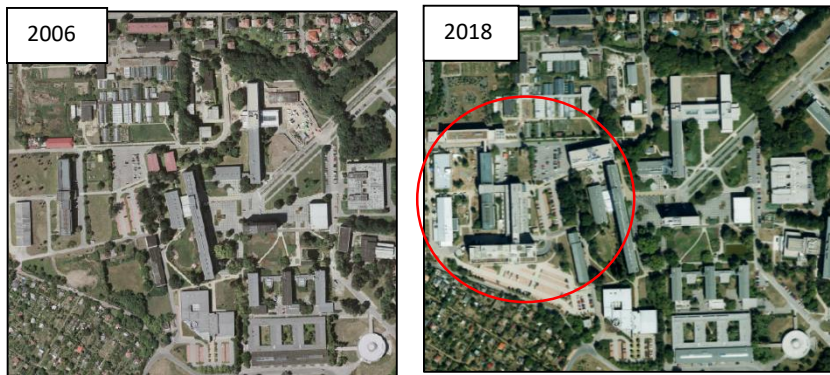
Figure 42. The changes in Area 5 (IPR Praha).

Figure 43 depicts more changes that occurred in Area No. 6, where green space was increased but a parking lot was constructed in the center of the greenery scene.

Figure 43. The changes in Area 6 (IPR Praha).

5.3 Land surface temperature:

In ArcMap GIS, the mono-window algorithm method was used to map the spatial distribution of land surface temperature in Suchdol figure 44. The satellite images were taken on June 27, 2002, and June 30, 2018. The mean land surface temperature for both years was calculated using a spatial analysis tool in ArcMap GIS and was 21.96 degrees Celsius in 2018, while the mean LST in 2002 was 24.73 degrees Celsius, demonstrating a significant 3 C difference. After adjusting the temperature classes of the two years to be as comparable as possible, in order to investigate the temperature distribution, we found that the temperature in 2002 was higher overall, and the temperature variability was wider.
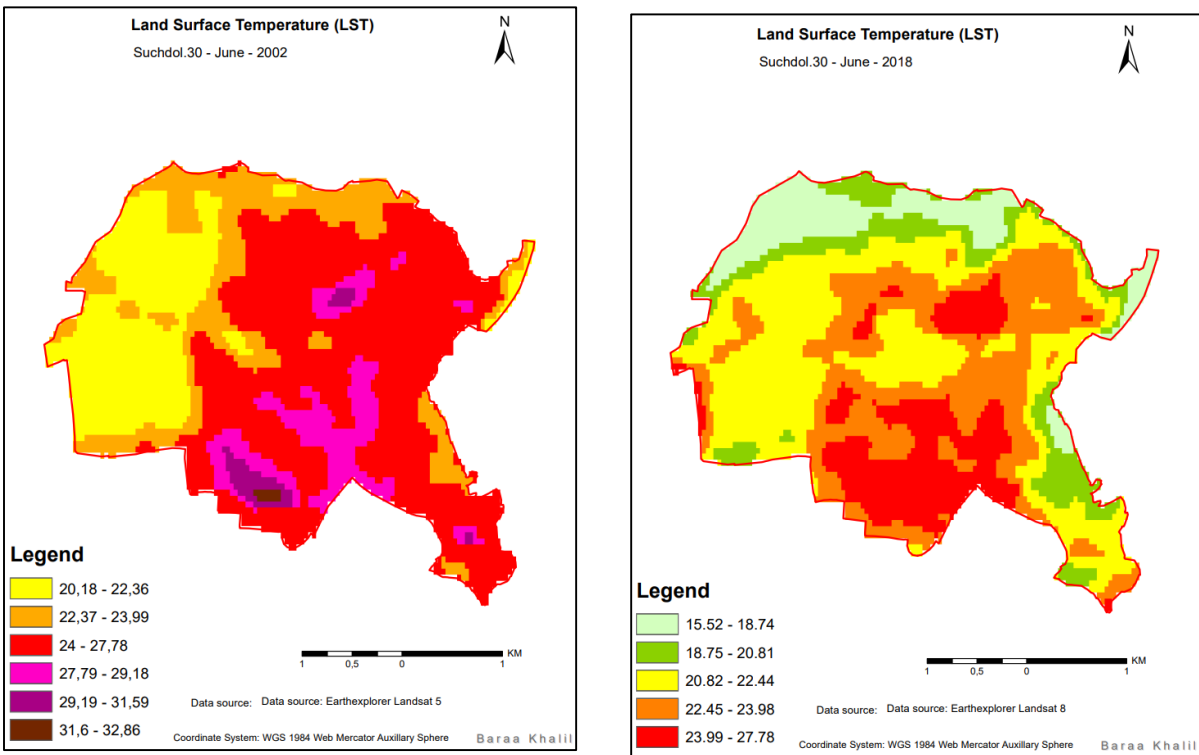
Figure 44. The land surface temperature of Suchdol (in degrees Celsius) in 2002 and 2018

5.4 Normalized difference vegetation index (NDVI):

The lighter-colored areas (yellow and green) depict healthy vegetation; the darker-colored areas depict less dense vegetation; or water, buildings, and other barren areas. Examining the changes in the images, especially the area in the western part of Suchdol that is classified as arable land (crop rotation), which was green in 2002 and dark in 2018, indicates a different crop, or was grass in 2002 and became a barren land in 2018.

In contrast, a part of the east that was dark in 2002 and became green in 2018, indicating healthy vegetation, appears in this area.
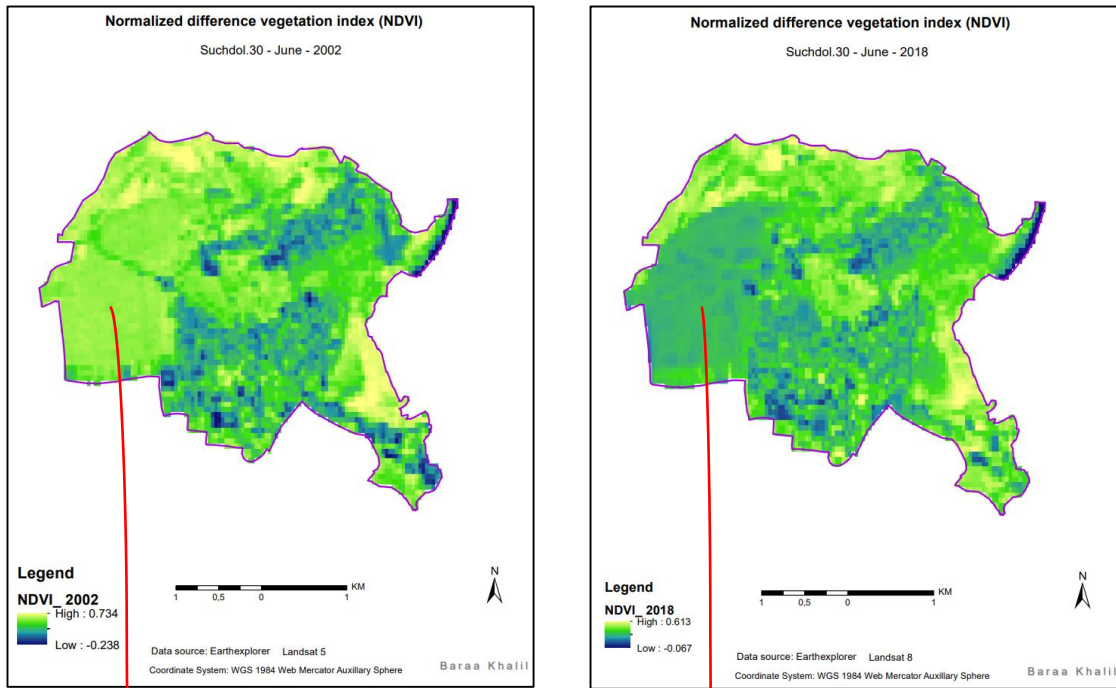
Figure 45. Normalized difference vegetation index (NDVI) of Suchdol in 2002 and 2018
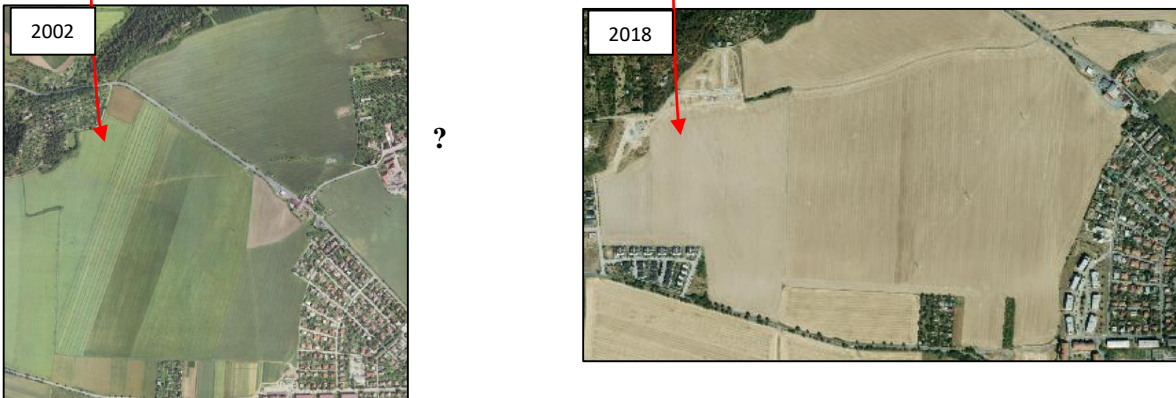
Figure 46. Different uses of the same land in different years

5.5 Building footprints, Elevation, and imperviousness:

Building footprints and imperviousness in urban areas can have a variety of environmental effects. In comparison to their rural surroundings, urban areas are distinguished by the dominance of impervious surfaces and the absence of vegetation. The resulting temperature rise is known to amplify global warming,

with negative health consequences and increased energy requirements for cooling. In cities, surfaces like concrete and asphalt that prevent water from seeping through can retain heat, increasing LST and exacerbating the effects of climate change. However, increasing vegetation coverage can help mitigate this and improve residents' summer comfort and health. (Alexander 2021). According to a study in Italy, the density and height of buildings in a city area influence potential temperature and mean radiant temperature; in the majority of cases studied found, higher density causes higher temperatures When it comes to the effects of vegetation in mitigating potential temperatures, the number of green areas, vegetation type (green roofs, green areas with trees, shrubs, and grass), atmospheric conditions, locations, building density, and height all make a difference (Perini & Magliocco 2014).

Moreover, building width and height can necessarily require wider roads and larger parking lots, increasing impervious surfaces. The impact of building coverage and height can also indicate an increase in impervious surfaces. Other factors, such as building design and materials, may also have an impact on Land Surface Temperature (LST) (Alexander 2021).

To investigate the effect of building density, we examined the distribution of buildings in the study area and how it relates to the land surface temperature derived from Landsat data. Fig. 47 depicts the potential temperature reduction in areas covered by forest, arable land, water, pasture, and Herbaceous vegetation associations (natural grassland, moors...), as well as areas covered by discontinuous medium-density urban fabric (30% - 50%). We can also see the higher temperatures present in the areas of building
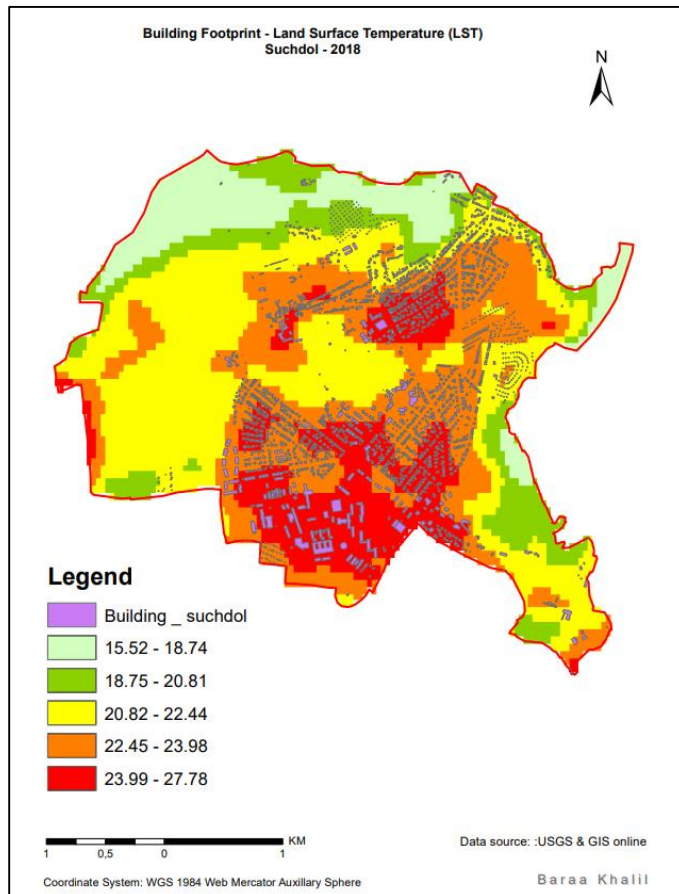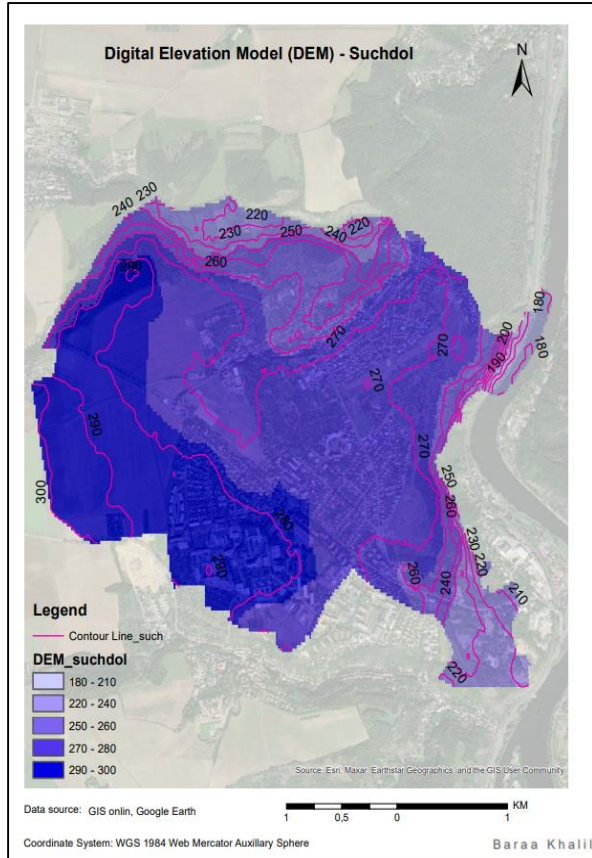

cluster**Figure 47. Buildings footprint and LST.**

This conclusion was reached after comparing the land use/ land cover map in figure 36, and LST 2018 with building footprints in figure 47. After overlapping land cover map, LST, and building footprint maps, the positive effect of temperature reduction can be seen in green areas where the temperature ranged between 15.52 and 20.8 degrees Celsius. In densely built-up areas the range was between 22.45 and 27.78 degrees

Celsius, which makes a difference in temperature around 6.93 and 6.97 or we can say approximately 7 degrees Celsius, between green areas and built up areas.
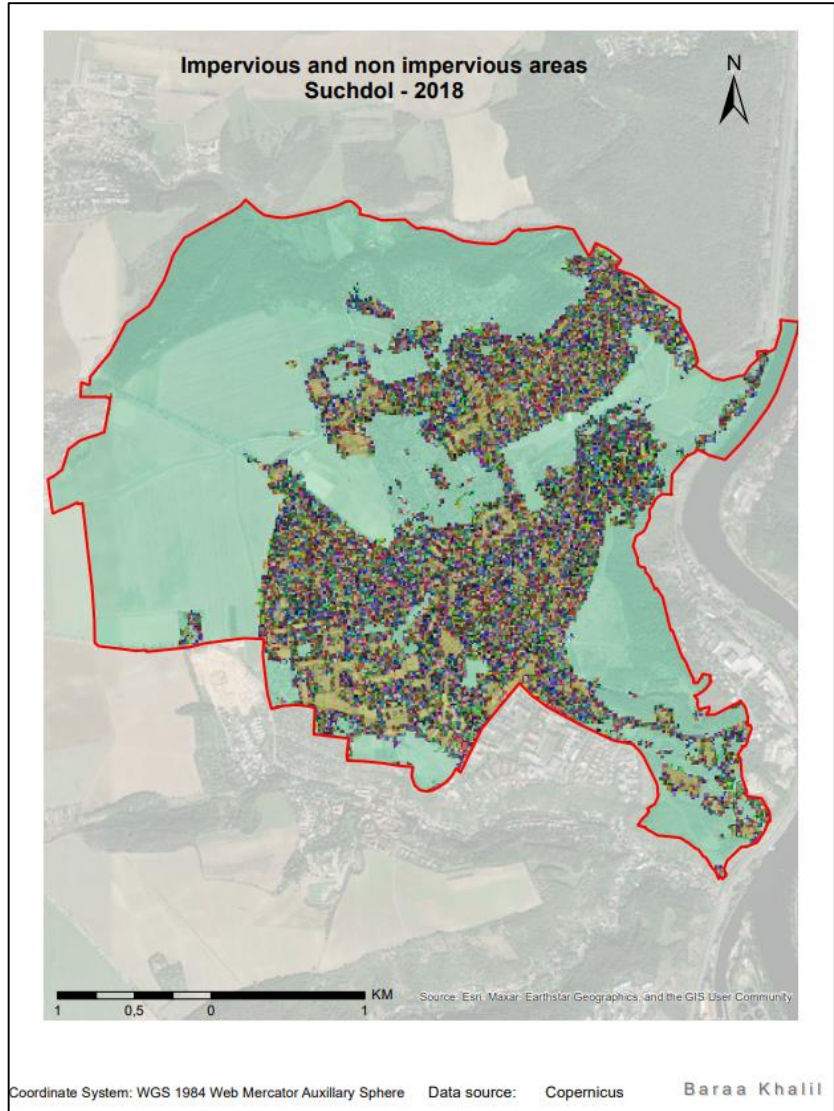
Elevation impacts LST dynamics and the spread of LST (Mathew et al. 2016). In the context of this study, the Digital Elevation Model (DEM) has been incorporated.. The contour lines obtained from Google Earth have been transformed into a Digital Elevation Model (DEM) using the ArcMap GIS software. DEM is a raster data set that represents a continuous elevation surface in which each cell represents the elevation at its location, and is typically used to represent bare-earth terrain devoid of vegetation and manmade features. Suchdol is considered flat land, as shown in Figure 48. The difference between the high and low elevation values is only 120 meters, which is not much considering the surface area is estimated at 19.5 km2 square kilometers.

Figure 48. The Digital Elevation Model (DEM) of Suchdol.

The imperviousness map, obtained from the Copernicus website, was demonstrated by the 100 categorizations shown in figure 49. which makes it difficult to distinguish the areas, so to simplify the analysis, we merged some categories, to get in the end 11 categories as shown in figure 50. Where we can see that non-impervious surfaces comparable with Arable land (annual crops), forest areas, and to the area that discontinuous medium-density urban fabric (30% - 50%), appear also as non-impervious surfaces, according to Lu & Weng (2006), impervious surfaces are commonly mixed with vegetation and soil in less-developed areas, such as medium- and low-intensity residential lands. Tree crowns can also contribute to the underestimation of impervious surfaces, retrieve from Landsat data. by covering portions of some impervious surfaces, such as roads. as a result, the map may not be completely accurate. In other words, complex landscapes with mixed pixels in GIS can present classification challenges due to the difficulty in distinguishing between similar objects. In urban areas, classification algorithms that rely solely

on spectral signatures are insufficient for distinguishing between water, dark surfaces, shadows from buildings, and forest canopy, or for distinguishing between dry soils, commercial/industrial/transportation lands, and dense residential areas, or for distinguishing forests from low-density residential areas (Lu & Weng 2006). That's why the discontinuous dense urban fabric ranging from 50% to 80% showed varying degrees of imperviousness, ranging from 10% to 40% (represented by the violet and blue hues in the figure). However, buildings and roundabouts were depicted with an imperviousness of 90% to 100% (represented by the brown hue in figure 50).

Impervious and non impervious areas Suchdol - 2018

Coordinate System: WGS 1984 Web Mercator Auxillary Sphere   Data source: Copernicus   Baraa Khalil

Legend

- all non-impervious areas
- 99% imperviousness value
- 98% imperviousness value
- 97% imperviousness value
- 96% imperviousness value
- 95% imperviousness value
- 94% imperviousness value
- 93% imperviousness value
- 92% imperviousness value
- 91% imperviousness value
- 90% imperviousness value
- 9% imperviousness value
- 89% imperviousness value
- 88% imperviousness value
- 87% imperviousness value
- 86% imperviousness value
- 85% imperviousness value
- 84% imperviousness value
- 83% imperviousness value
- 82% imperviousness value
- 81% imperviousness value
- 80% imperviousness value

- 8% imperviousness value
- 79% imperviousness value
- 78% imperviousness value
- 77% imperviousness value
- 76% imperviousness value
- 75% imperviousness value
- 74% imperviousness value
- 73% imperviousness value
- 72% imperviousness value
- 71% imperviousness value
- 70% imperviousness value
- 7% imperviousness value
- 69% imperviousness value
- 68% imperviousness value
- 67% imperviousness value
- 66% imperviousness value
- 65% imperviousness value
- 64% imperviousness value
- 63% imperviousness value
- 62% imperviousness value

- 23% imperviousness value
- 22% imperviousness value
- 21% imperviousness value
- 20% imperviousness value
- 2% imperviousness value
- 19% imperviousness value
- 18% imperviousness value
- 17% imperviousness value
- 16% imperviousness value
- 15% imperviousness value
- 14% imperviousness value
- 13% imperviousness value
- 12% imperviousness value
- 11% imperviousness value
- 100% imperviousness value
- 10% imperviousness value
- 1% imperviousness value

- 42% imperviousness value
- 41% imperviousness value
- 40% imperviousness value
- 4% imperviousness value
- 39% imperviousness value
- 38% imperviousness value
- 37% imperviousness value
- 36% imperviousness value
- 35% imperviousness value
- 34% imperviousness value
- 33% imperviousness value
- 32% imperviousness value
- 31% imperviousness value
- 30% imperviousness value
- 3% imperviousness value
- 29% imperviousness value
- 28% imperviousness value
- 27% imperviousness value
- 26% imperviousness value
- 25% imperviousness value
- 24% imperviousness value

- 61% imperviousness value
- 60% imperviousness value
- 6% imperviousness value
- 59% imperviousness value
- 58% imperviousness value
- 57% imperviousness value
- 56% imperviousness value
- 55% imperviousness value
- 54% imperviousness value
- 53% imperviousness value
- 52% imperviousness value
- 51% imperviousness value
- 50% imperviousness value
- 5% imperviousness value
- 49% imperviousness value
- 48% imperviousness value
- 47% imperviousness value
- 46% imperviousness value
- 45% imperviousness value
- 44% imperviousness value
- 43% imperviousness value

Figure 49. The imperviousness and non-imperviousness Surface with all the classifications.
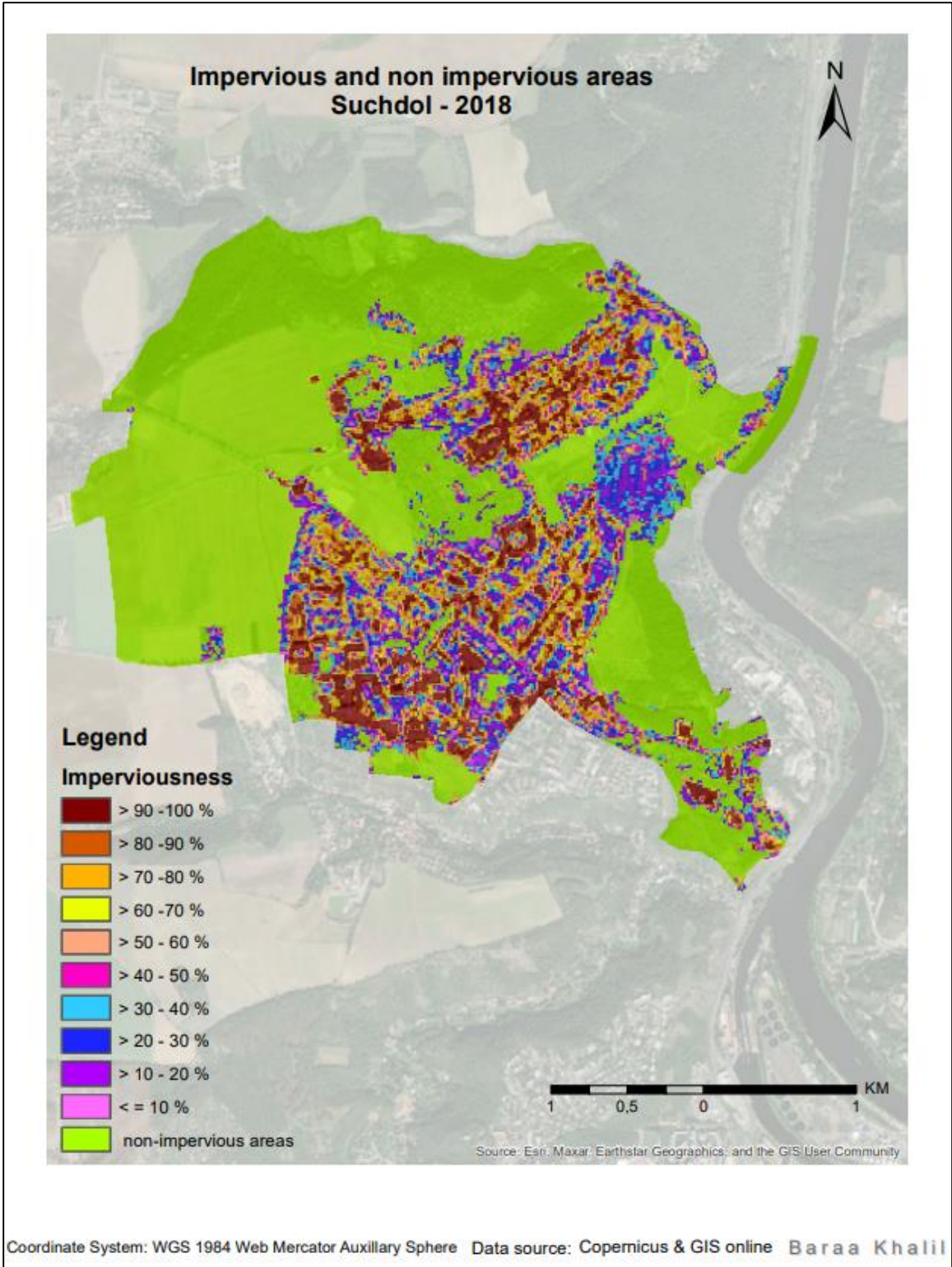
Figure 50. The imperviousness and non-imperviousness Surfaces with 11 categories.

5.6 Thermal Behavior of Urban Materials:

Over the past several years, the utilization of appropriate building materials has garnered increasing attention as a means of mitigating the heat island effect and enhancing the thermal properties of urban environments (Doulos et al. 2004b). Therefore, the latter section of the research focused on examining the thermal characteristics of diverse materials situated in outdoor urban environments. The study involved different materials like Concrete, Pebbles, Asphalt, Pave stone, Stone, vegetation, mulch, etc. This type of material is frequently used in exterior urban surfaces, such as pavements, streets, playgrounds, educational facilities, parking lots, green areas, and parks as well as building walls and roofs (Doulos et al. 2004b).

In this study, the primary experimental field-deployed device was the FLIR E60bx Infrared Camera, having serial number 64502133. This instrument was utilized to measure surface temperatures using high-resolution imaging capabilities, with a pixel resolution of 76,800 (320 x 240). Surface temperature measurements were conducted on the dates of 20th May 2022, and 19th June 2022. Most of the measurements were taken on the campus of the Czech University of Life Sciences, which is located in the southern part of Suchdol.

The following table shows the weather on the selected dates as recorded by the LKPR, a weather station at Václav Havel Airport Prague (50.10 Latitude, 14.27 Longitude), as we can see, the hottest day was 19 June, with a maximum temperature of 35 degrees Celsius, a wind speed of 31 kilometers per hour, and high humidity on all selected days.

Table.3 Weather data for the selected days:

|	Tem / °C		Humidity / %		Wind / (km/h)
Date	Max	Min	Max	Min	Average
20- May	28	15	94	45	44.4
19 - June	35	18	73	20	31.5

Figure 51. presents the temperature differences recorded within the same scene, on the same day, wherein the temperature of the following materials was measured: mulch, grass, vegetation, dark tile, light tile, and painted wood. The temperature on June 19, 2022, was recorded at a sweltering 35°C. An investigation of the various surfaces in the area revealed that the painted wood had reached a temperature of 70°C, the mulch exposed to the sun had a temperature of 50°C, and the mulch in the shade had a temperature of 30°C. A comparative analysis of the temperature of tiles with different colors was conducted and results showed that the dark-colored tile had a temperature of 60°C, while the white-colored tile was slightly cooler at 50°C.
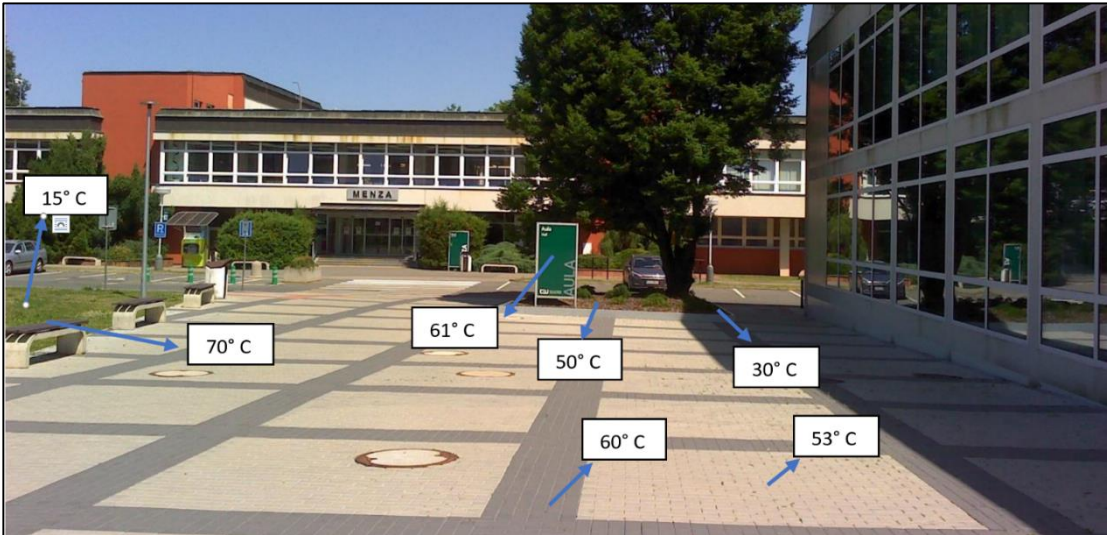
Figure 51. Temperature Differences Among Urban Environment Materials (19 June 2022, at 14.04).
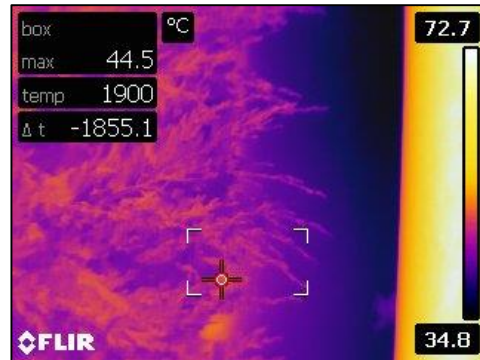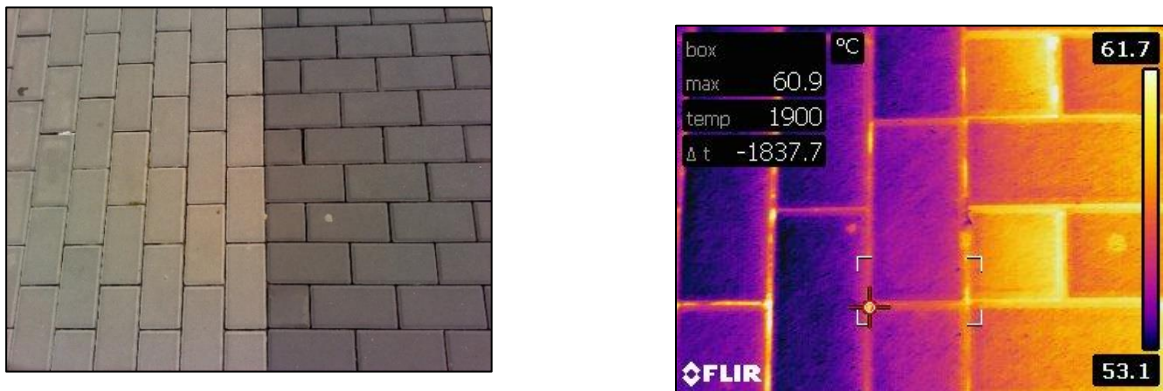

Figure 52. Visible and infrared image of painted wood and plant (19 June 2022, at 13.55).
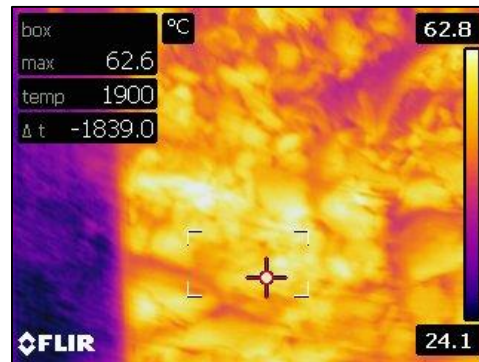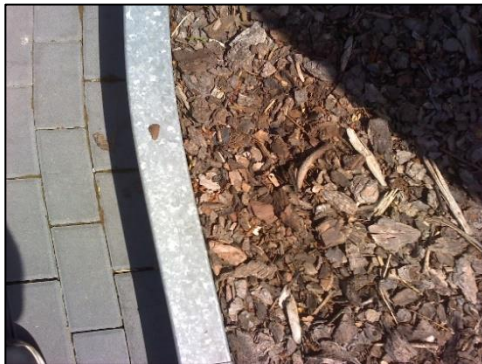
Figure 53. Visible and infrared image of mulch and a stone edge (19 June 2022, at 13.58)

Regarding the mulch material in figure 53. Mulch, a material spread over soil to aid in soil and water conservation and enhance soil productivity, is a crucial material for agriculture. Mulch can be either organic or inorganic in nature and plays a crucial role in modifying soil conditions for better plant growth. Studies have shown that mulch modifies the heat and water balance of soil, leading to a more favorable environment for plant growth. The use of different types of mulch influences the soil temperature, which is more significant for agriculture than the air temperature. The effects of mulch on soil hydrothermal regimes, such as the radiation balance, heat and water transfer, and soil heat capacity, have been extensively researched and proven to conserve soil moisture, suppress weed growth, and increase soil productivity. However, the effectiveness of mulch depends on factors such as the quality, quantity, and durability of the mulch material, soil type, and climate conditions. In the face of climate change, the use of mulch should be emphasized, especially in rainfed conditions, to conserve soil and moisture, moderate temperature, maintain soil health, and ultimately increase agricultural productivity. The economic and environmental impact should also be considered when choosing the appropriate mulch material (Pramanik et al. 2015). Hence, the inclusion of mulch was purpose-driven to protect and improve the health of the soil.

Moreover, (Doulos et al. 2004b) affirms that the primary reasons behind the uneven distribution of surface temperature of concrete tiles are the stark contrast in color, the textural variations of the surface, and the heat transfer dynamics of the tile. and that's what can be explained in Figures 54 and 55.
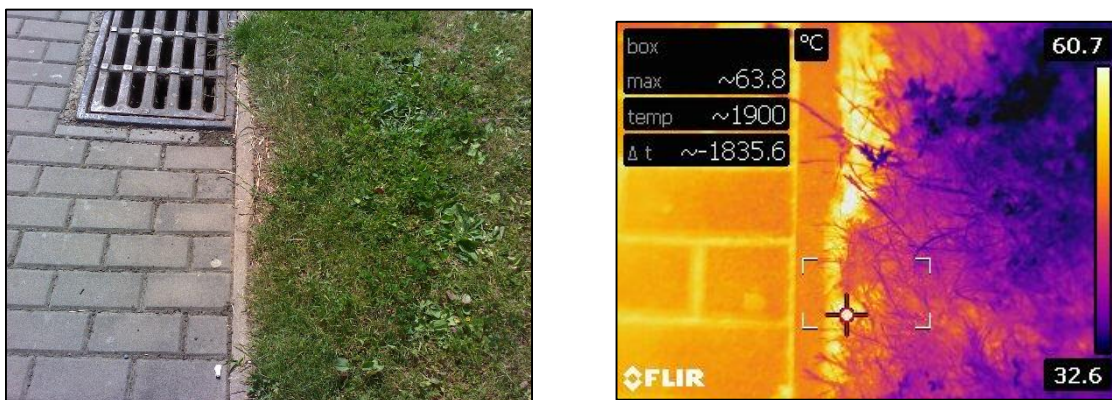

Figure 54. Visible and infrared image of dark and light paving tile (19 June 2022, at 13.59).

Figure 55. Visible and infrared image of dark and light tile, with Iron Drainage Covers (19 June 2022, at 14.06).

More pictures have been taken to investigate the thermal behavior of different landscape materials using IR imaging: A Study Comparing Cement Tiles and Grass, Grass and Mulch, Stone Tiles and Asphalt, and Painted Asphalt. We found that the temperature measurement of the cement tiles revealed a range of 50°C to 60°C on the specified day, while the surrounding grass exhibited a temperature range of 32°C to 40°C. In comparison, the temperature range of the grass was observed to be 34°C to 40°C whereas, the temperature of the mulch reached 73°C, at the same location and time.

Figure 56. Visible and infrared image of dark tile, and grass (19 June 2022, at 15.10).

Figure 57. Visible and infrared image of painted grass and mulch (19 June 2022, at 15.09).

Doulos et al.(2004) found that among the material tiles tested, those with a black color had the highest surface temperatures. Moreover, in general, smooth-surfaced materials have lower surface temperatures than rough-surfaced materials. This is evident in Figures 50 and 51, where the temperature ranges of stone tiles (Gray color) were observed to be 41°C to 45°C, cobblestone tiles 55°C to 60°C, dark asphalt 60°C, and painted asphalt with white color 41°C to 45°C. As a result, the temperature of white materials is lower than that of darker materials.
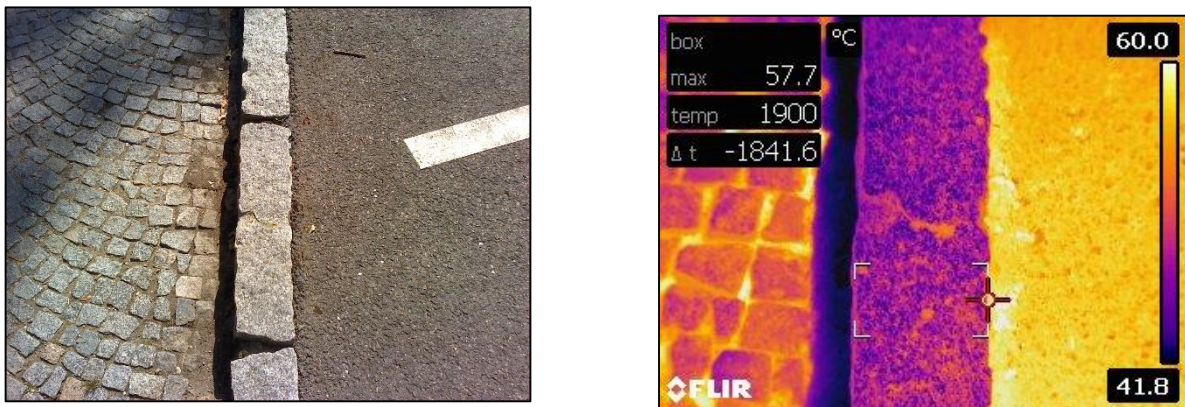
Figure 58. Visible and infrared image of stone tiles with cobblestone, stone, and asphalt (19 June 2022, at 15.22).

Figure 59. Visible and infrared image of white Paint on Asphalt Surfaces (19 June 2022, at 13.52).

Prior images were taken at a perpendicular angle to the object, so the sun's rays directly illuminated the object's surface, where the images below were obtained with a different orientation than the previous images. These images were captured to encompass the entire scene, which included multiple objects, rather than at a perpendicular angle to the object. The primary goal of capturing these images was to investigate the temperature distribution within a particular scene.
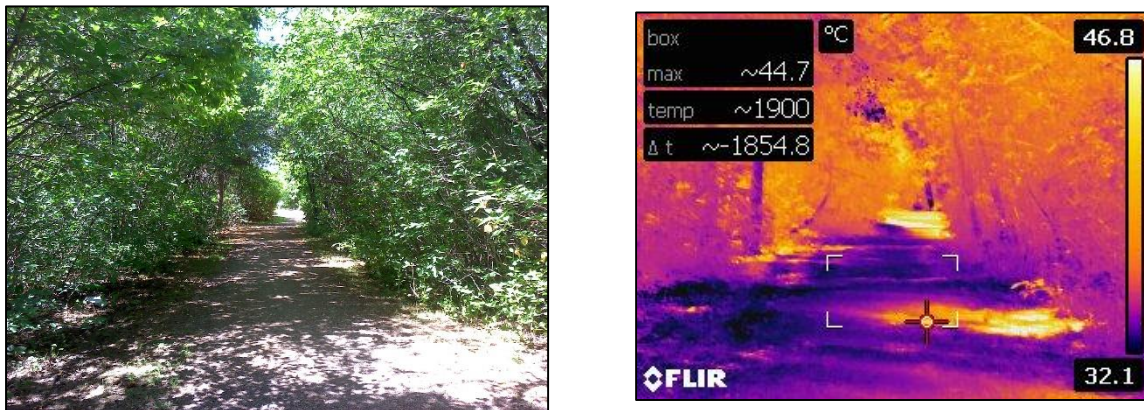
Figure 60. Visible and infrared image (19 June 2022, at 13.55).

Figure 61. Visible and infrared image (19 June 2022, at 13.40).

Figure 62. Visible and infrared image (19 June 2022, at 14.11).
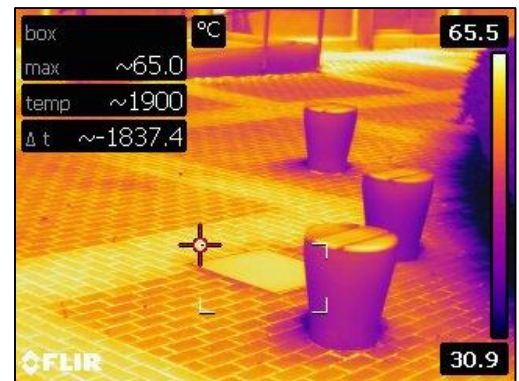
Figure 63. Visible and infrared image (19 June 2022, at 14.14).

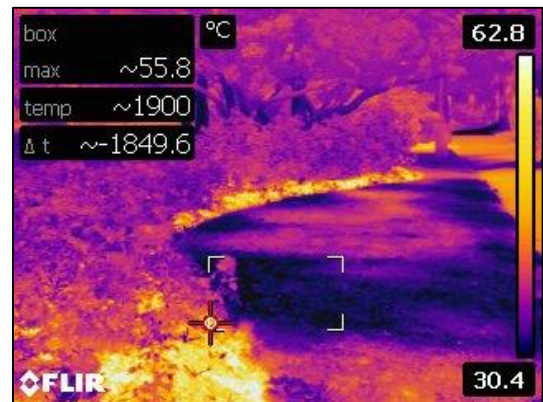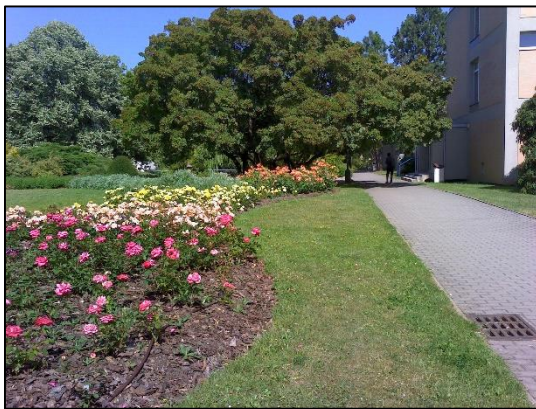**Figure 64. Visible and infrared image (19 June 2022, at 15.16).**

Figure 65. Visible and infrared image (19 June 2022, at 15.09).

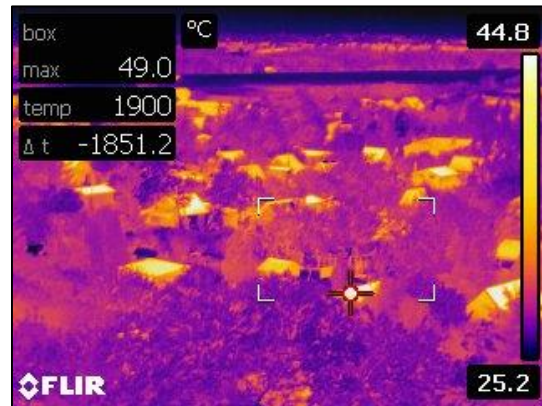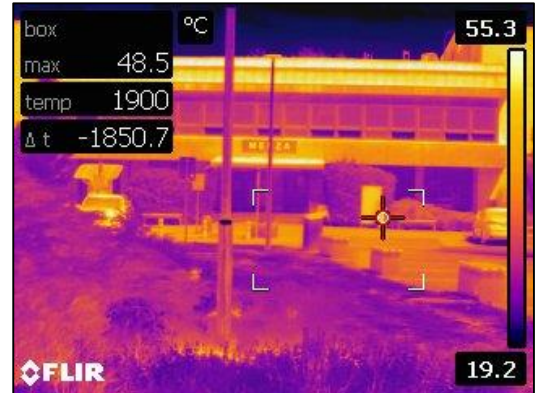**Figure 66. Visible and infrared image (19 June 2022, at 13.55).**

Figure 67. Visible and infrared image (20 May 2022, at 13.34).

Figure 68. Visible and infrared image (20 May 2022, at 14.01).

Figure 69. Visible and infrared image (20 May 2022, at 14.04).

Figure 70. Visible and infrared image (20 May 2022, at 14.13).

Figure 71. Visible and infrared image (20 May 2022, at 14.07).

The results depicted in the thermal images demonstrate the significant variations in temperature distribution, ranging from 12°C to a scorching 65°C. The coolest areas, with temperatures ranging from 12°C to 30°C, are found in areas shaded by trees. In stark contrast, the highest temperatures, reaching 65°C, are observed in non-shaded areas and specifically in those paved with highly absorbing materials, and 45 °C in the orange color roof houses.

Discussion 6

6.1 Development over the years in Suchdol

6.2 land surface temperature (LST) and land use / land cover

6.3 land surface temperature (LST) and elevation

6.4 Thermal behavior of various urban material

6.5 Suchdol welcomes new built-up zones.

6.6 Land Cover Change Prediction in 2050.

6. Discussion

6.1 Development over the years in Suchdol:

The development that occurred in the study area between 1938 and 2018 was analyzed using aerial photographs and maps. In 1938, the region was primarily rural with a sparse distribution of homes located in the eastern portion and open spaces in the western portion. This division of the area into two distinct segments made it easier to analyze the urban development that occurred in the study area. In 1945, a limited number of homes were constructed in the upper eastern region, and a few homes started to emerge, towards the open lands. By 1953, the growth of housing On the left side of Kamycka Road, which is the main road in Suchdol, had become more apparent, signifying the formation of a new residential area. The expansion of housing and construction of new roads continued until 1966 when two new zones of built-up areas started to appear. As a result, the study area underwent significant urban development from 1938 to 1989, developing from a predominantly rural area to a region with a distinct character, but after that, development became very slow and limited, and The study area had a distinct character in 2002, with five predominant residential zones, significant arable lands in the western sector, forests along the northern edge and in the eastern southern part, and a few scattered pastures. This scenario persisted until 2006, and the same landscape characteristics were observed in 2018.

Analysis of the changes in land use and land cover between 2006-2012 and 2012-2018, using data obtained from Copernicus.eu, shows only six changes significant enough to be identified. These changes were limited to specific areas and included the construction of new buildings and parking lots, as well as limited tree planting.

The temperature changes were not significant enough to affect the entire area. The result of land surface temperature retrieval from satellite data showed a 3 °C temperature decrease between 2002 and 2018. As a result, the identified changes were too localized to be considered a significant factor in the overall temperature of the area. Choosing one day per year is insufficient for explaining temperature fluctuations from 2002 to 2018. As a result, a more practical approach would be to compare the monthly average temperature of one year with that of another. Nonetheless, a significant relationship between land surface temperature (LST) and land use/land cover was found.

6.2 land surface temperature (LST) and land use/land cover:

The difference in land surface temperature (LST) was significant across various land use and land cover types, with the highest LST, observed in areas with continuous urban fabric (>80%) and areas with discontinuous urban fabric (50-80%). The temperature ranged from 24-27.7°C in 2018 and 31.6-27.7°C in 2002. In contrast, the lowest land surface temperatures (LST) were recorded in arable land, forests, pastures,

and natural grasslands, with a range of 20-23°C in 2002 and 15-24.4°C in 2018. Notably, the temperature differential between built-up areas and forested regions in 2018 was approximately 12°C, whereas the differential in 2002 was approximately 12.6°C. As a consequence, the present study emphasizes that land use and land cover categories have a significant influence on land surface temperature (LST), particularly in the presence of green spaces, which had lower land surface temperature (LST) values.

That has been emphasized by (Tran et al. 2017), the presence of vegetation and built-up areas influences the urban heat island (UHI) effect, with vegetation acting to mitigate the UHI effect whereas, built-up areas contribute to its intensity. When the building footprint and LST were mapped, the highest temperatures were concentrated in the built-up areas, while the coolest temperatures were found in the arable land and forest. Even in areas with low-intensity buildings, the temperature remained significantly lower than in the surrounding. Thus, the LST spatial pattern is directly related to zone transitions. From the hottest urban core to the open areas, LST decreases. This shows the important role of open areas such as parks, public spaces, and other non-built-up areas in reducing UHI effects (Tran et al. 2017). That explains why rural areas are always cooler than urban areas, where the imperviousness of the surfaces is very high. Because there is a strong positive correlation between imperviousness in urban areas and heat, since we have a lot of buildings, roads, and parking lots, these absorb and retain more heat than natural surfaces like vegetation and soil. In this study, the imperviousness range of between 0% and 100%, was mapped for the region, as illustrated by the imperviousness maps, the higher percent imperviousness values captured almost all of the developed land including density built-up areas, while the low imperviousness (10 - 30%) found in the vegetation landscapes in the urban structures. In the imperviousness map, Pixels were classified as urban at various levels of development when the percent imperviousness is equal to or greater than 10% and those pixels of less than 10% were classified as non-urban, and that was in the arable land and the forest.

The study's findings show a distinct correlation between imperviousness and two important variables, namely land surface temperature (LST) and the normalized differential vegetation index (NDVI). Particularly, regions with high degrees of imperviousness showed high temperatures and low NDVI values as a consequence. Land use and land cover categories have a significant influence on land surface temperature (LST), with a strong positive correlation between LST and imperviousness and a strong negative correlation between LST and NDVI. That has been emphasized by (Tran et al. 2017), the presence of vegetation and built-up areas influences the urban heat island (UHI) effect, with vegetation acting to mitigate the UHI effect whereas, built-up areas contribute to its intensity.

The negative correlation between LST and Normalized Difference Vegetation Index (NDVI) was analyzed using ArcMap GIS and R programming language to highlight the importance of vegetation and green space in urban areas, and as a result, a strong negative relationship between LST and NDVI was discovered. Figure 71 shows that the lighter the colors, the higher the NDVI values, indicating that the vegetation is healthier, and the lower the LST values. Showing how plants cover contributes to a cooling impact (Nguyen et al. 2022).
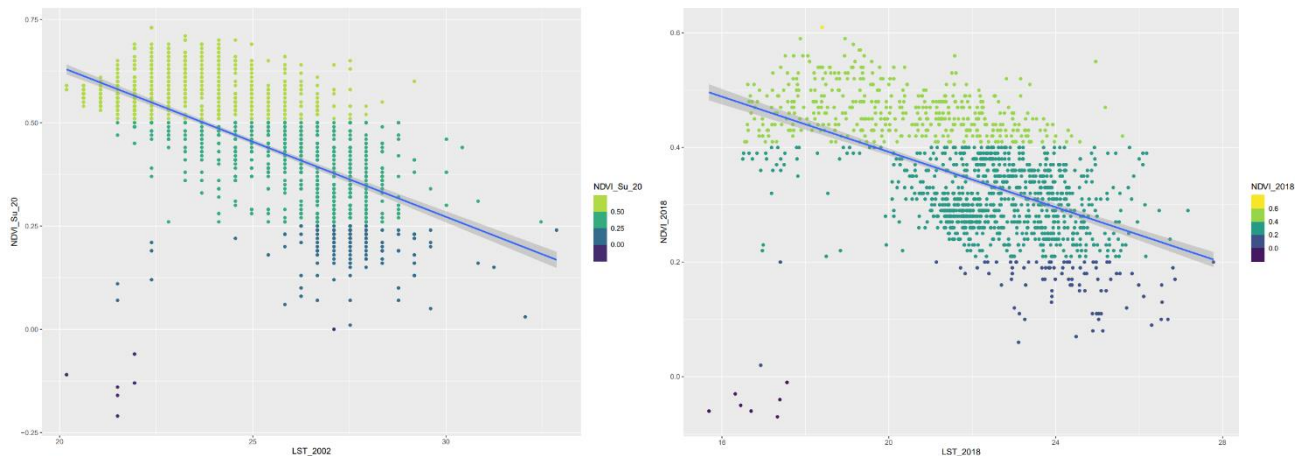
Figure 71. Relationship between LST and NDVI.

However, not all types of vegetation provide the same level of cooling. Many factors can influence vegetation's cooling abilities, such as its vertical structure and horizontal configuration; for example, the taller the vegetation, the cooler the LST. Furthermore, LST is also influenced by the size of vegetation patches and their connections (Nguyen et al. 2022)

6.3 land surface temperature (LST) and elevation:

Figure 72. LST and elevation.
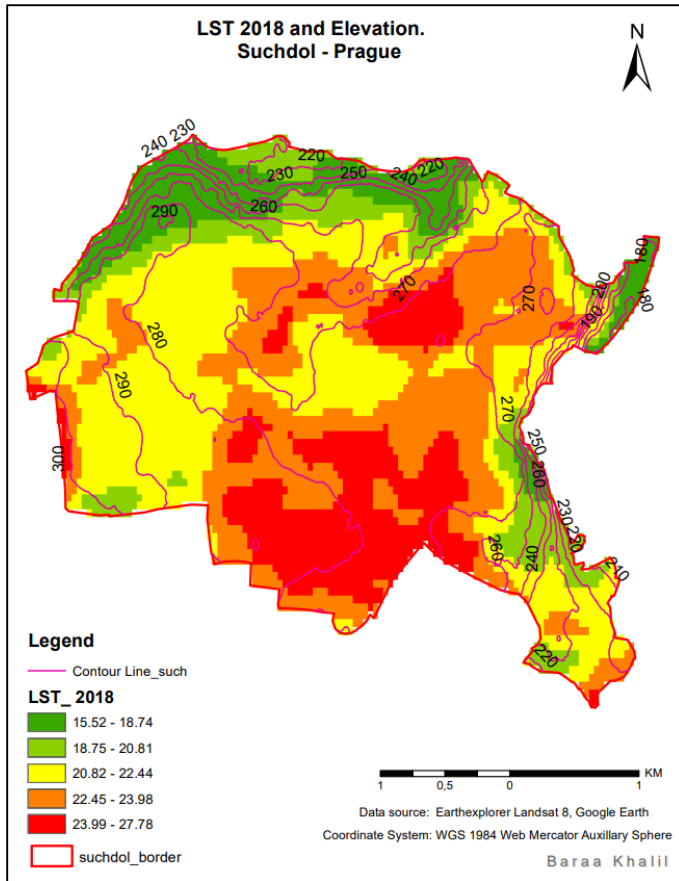
Normally, LST has a trend toward decreasing values as elevation increases, and a significant proportion of high temperatures occur within the urban boundary, resulting in a higher land surface temperature within the urban area when compared to regions outside the urban boundary (Mathew et al. 2016).

It is observable that a concentration of high temperatures occurs in the canter of the scene, whereas the northern western part exhibits cooler temperatures, which can be attributed to the differential elevation between the two regions. But,it is imperative to acknowledge that the impact of land use/land cover and elevation on land surface   temperature cannot be dissociated, particularly in the north-western region where the presence

of arable land or forests, Therefore, wind in the open area and tree canopy in the forest have a significant impact on mitigating land surface temperature.

A similar scenario can be found in the southeast, where, despite being at a lower elevation than the urban area, temperatures remain cooler due to the presence of forests. Furthermore, despite having similar elevations, the yellow portion of the area, which is classified as a Discontinuous medium-density urban fabric (30% - 50%), has cooler temperatures than its surroundings, demonstrating the importance of land use/land cover on land surface temperature. Solar incident radiation, angle of incidence, and surface properties such as roughness, moisture content, and vegetation coverage all have an impact on land surface temperature. As a result, scattering patterns differ according to the season. Therefore, elevation plays a significant role in determining land surface temperature dynamics, and any comprehensive study of the spatial distribution of land surface temperature over a large geographic area must account for the impact of elevation changes (Mathew et al. 2016). But not if the local elevation variations were relatively small. Suchdol can be considered as flat land, as shown in Figure 48. The difference between the high and low

elevation values is only 120 meters, which is not much considering the surface area is estimated at 19.5 km2 square kilometers.

6.4 Thermal behavior of various urban materials:

A thermal camera was used to investigate the thermal behavior of various materials used in the urban environment. This type of research can help to select more appropriate materials for outdoor urban applications, thereby helping to combat the heat island effect, reduce building electricity consumption, and improve outdoor thermal comfort conditions (Doulos et al. 2004b).

The selection criteria for building materials in urban environments do not always include consideration of surface color. Despite their widespread use, asphalt, concrete, pebble, and pave stone have been found to have insufficient thermal performance based on the outcomes of experimental studies. Moreover, the studies emphasized the significance of the physical characteristics of material tiles in determining their albedo. These characteristics include color, surface texture, and the material used in construction. Dark-colored and rough surfaces absorb more solar radiation than smooth, light-colored, and flat surfaces, leading to a greater temperature increase for dark surfaces (Doulos et al. 2004b).

 In this study, we found that concrete tiles had higher temperatures than stone tiles. The concrete tile pavement reached 60°C on a day when the average temperature was 35°C, whereas the stone tile pavement with cobblestone had a temperature range of 41°C to 45°C. The cobblestone also reached 60°C. This suggests that if the cobblestones were replaced with grass, the temperature values would be lower, helping in the mitigation of the urban heat island.

 Additionally, the color of the tiles was found to have a significant impact on temperature. The study revealed that the lighter color of concrete tiles resulted in lower surface temperatures when compared to the darker color. Specifically, the temperature of a light concrete tile was recorded to range between 53 and 55 degrees Celsius, while the temperature of a dark concrete tile reached 61 degrees Celsius. making a difference in the surface temperature around 7 C. Despite both colors being considered high temperature due to the nature of the material (concrete), it was found that even in comparison to other materials such as stone, the difference between dark and light colors remained evident. The texture and roughness of the surface were also found to play a role in the surface temperature, which explains the high temperature of the dark asphalt, which reached 60°C. While the white-painted asphalt had a temperature difference of at least 15 degrees Celsius, between 41 and 45 degrees Celsius. Consequently, the utilization of light-colored materials in urban settings proves to be an effective strategy for mitigating the surface temperature of the

urban material, therefore the temperature of the surrounding air. One example of such implementation would be painting asphalt surfaces, particularly in parking lots, with a light color (white) to achieve a comparable outcome, Furthermore, using a light-colored stone tile and seamless grass-paving instead of cobblestone can also contribute to mitigating the UHI. In addition to color, the texture and roughness of the surface were also found to impact surface temperature, as evidenced by the high temperature of the dark asphalt (dark and rough) (60°C). In contrast, the white-painted asphalt demonstrated a temperature difference of at least 15 degrees Celsius, ranging from 41 to 45 degrees Celsius. These findings highlight the importance of utilizing light-colored materials in urban settings as a means of mitigating surface temperature and, by extension, the temperature of the surrounding air.

One example of such an application would be using reflective coatings for buildings or parking lots, or benches, which can help lower surface temperatures and lead to a significant reduction in the surrounding temperature. It was demonstrated that the use of reflective coatings can reduce the surface temperature of white concrete tiles by 4 C in hot summer conditions and by 2 C at night. However, it's crucial to conduct a comprehensive study of the site's microclimate before applying these coatings, to prevent increased glare and unwanted solar gains. This way, the application of reflective materials can be optimized for optimal results. At a building scale, the use of reflective coatings can result in improved comfort and lower cooling requirements (Synnefa et al. 2006). According to the same research, 14 types of reflective coatings were studied, including Aluminum pigmented acrylic coating, acrylic ceramic coating, and acrylic elastomeric coating, among others. The colors of these coatings were white and silver-gray. The findings showed that while all the studied coatings have high solar reflectance, aluminum coatings retain more heat during the night due to their lower infrared emittance, meaning they radiate less of the solar energy they absorbed during the day as heat. In contrast, white coatings radiate more of their stored heat back to the sky. As a result, aluminum is not as effective as a white coating with similar solar reflectance (Synnefa et al. 2006).

In general, the thermal imaging study results clearly show the dramatic differences in temperature distribution across different areas of the specified location. We found, that the cool temperatures, ranging from 12°C to 30°C, are found in areas that are shaded by trees, while the hottest temperatures, reaching as high as 65°C, are found in unshaded areas and particularly in areas paved with highly absorbing materials, such as dark asphalt, therefore, incorporating green space in urban areas can help to reduce the urban heat island effect, which has been linked to increased energy consumption and negative health effects such as respiratory problems and heat-related illnesses. This emphasizes the importance of prioritizing green space in urban planning and design, not just for the aesthetic benefits, but also for the practical benefits it can bring to the local environment and residents' well-being. Furthermore, the availability of green spaces on campus can create a more conducive learning environment by reducing stress, increasing concentration,

and improving physical and mental health. It can also be used by students to unwind, exercise, and participate in recreational activities. Moreover, the orange color roof houses, with a temperature of 45°C, also demonstrate a significant increase in temperature compared to shaded areas. This result indicates that the selection of roofing materials in urban areas should not only consider the color of the material but also its thermal properties. The use of reflective roofing materials, for instance, can help to reduce the temperature of buildings and improve indoor comfort. It is well established that higher temperatures in urban areas can contribute to the urban heat island effect, which can cause increased air conditioning usage, decreased air quality, and increased stress on the electrical grid.

It would be highly advantageous to obtain measurements of the ambient air temperature of the selected materials. But, In another study, by (Doulos et al. 2004b), a comparative analysis of surface material temperatures and the ambient air temperature was conducted within an urban environment, they found;

A. The main materials studied, including concrete, pebble, pavers, and stone, exhibited higher average surface temperatures compared to the average ambient air temperature. Conversely, the white marble tiles were the sole exception, displaying lower temperatures than the surrounding air.

B. Among the light-colored materials studied, the white and green surfaced pebble tile was identified as the warmest. The maximum temperature difference between the light-colored materials and the ambient air was estimated to be 6.9°C.C. In regards to the dark-colored materials, the maximum temperature difference was observed in the asphalt material, with a value of 15.5°C. Additionally, the dark-colored stone material displayed the lowest temperature difference with the ambient air, at 10.2°C

The results depicted in the thermal images demonstrate the significance of green spaces in urban areas and their impact on temperature regulation. The blue or violet color in the thermal image is predominantly present in green spaces and shaded areas, as well as stone and paving stone surfaces, reflecting cooler areas. In contrast, hotter areas are represented by buildings, coated wood, asphalt roads, and dark paving materials. These findings highlight the crucial need for an increase in vegetation, the implementation of shading measures, and the utilization of materials with favorable thermal and optical properties in urban design, to effectively regulate temperature (Fintikakis et al. 2011).

6.5 Suchdol welcomes new built-up zones:

A new residential zone is proposed to be built north of the former village's historical core in Suchdol. This innovative development plan, proposed by the municipal district Praha-Suchdol, calls for the construction of new building blocks (with two floors above-ground floors) that will be separated from the historical part of the village by a non-building block that includes a green strip with lush greenery and a public area with a children's playground. The remaining building blocks will be solely for residential use. In addition, unpaved roads will be added to the zone, increasing its permeability and recreational potential. To ensure the area's sustainability, measures such as evaporation or retention, as well as the possibility of using rainwater for garden irrigation, will be implemented. Surfaces that allow for soaking, such as paving with wide joints or grass paving, will be used for paved areas (městská část Suchdol 2020).
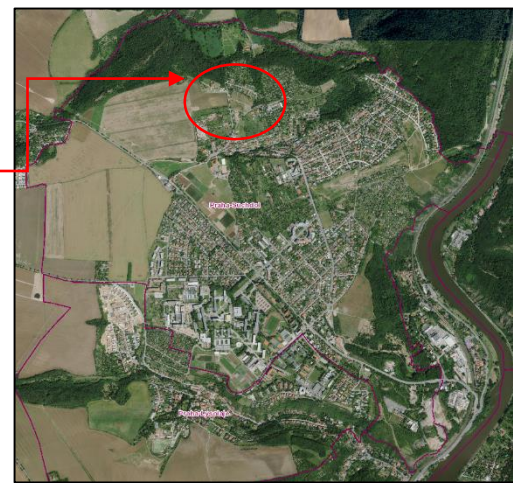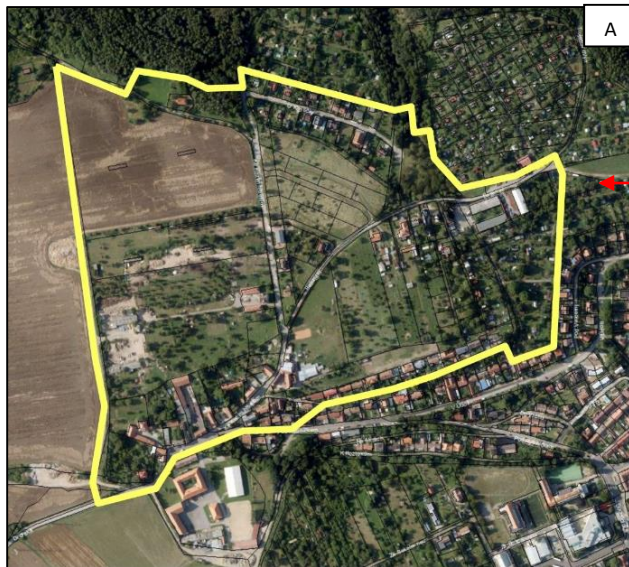
Figure 73. Suchdol 2022 (IPR Praha)
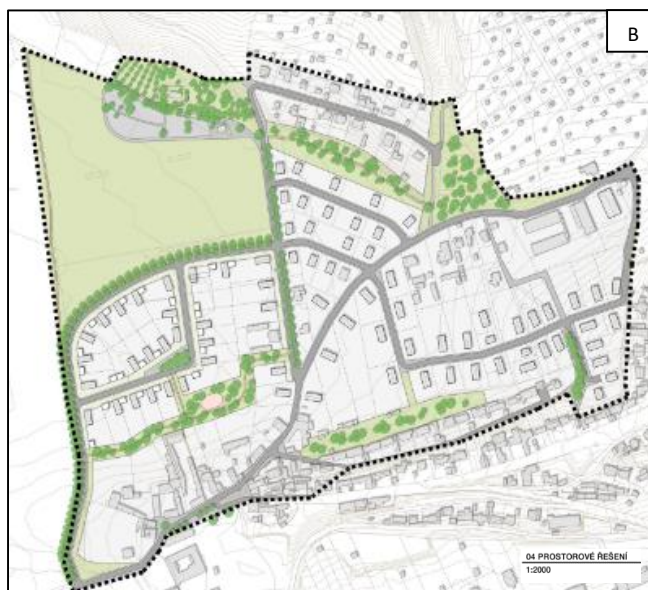
Figure 74. new built-up zone before (A) and after (B)(městská část suchdol 2020).

As part of the expansion of tram lines throughout Prague's capital city, it is planned to extend the tram line from the Podbaba – Vhledy station, which will lead through Podbabská, Roztocká, and Kamycká streets to the Výhledy area, where the construction of a transport terminal and the creation of an interchange between tram and suburban bus lines is expected in 2019-2029 (IPR Praha 2020).

Figure 75. Tram line from Podbaba to Suchdol

 (IPR Praha 2020).

6.6 Land Cover Change Prediction in 2050:

Understanding how our world has changed can help us build a more sustainable and prosperous future. We can make fundamental predictions and forecast future growth patterns by analyzing historical global land cover data and observing change over time. Clark Labs at Clark University and Esri are collaborating to predict land cover change in 2050. A new series of maps have been developed and released for public use using decades of satellite observation data from the European Space Agency (ESA) Climate Change Initiative (CCI). The resulting map series categorizes land cover by type and vulnerability to human development. So we can see the predicted land cover in 2050, as well as the vulnerability to changing from a natural to a human-modified class. According to Esri, Suchdol 2050 will have a significant reduction in forested land in the northwest, combined with a significant increase in built-up areas in the southeast, causing serious concern for the region's ecological diversity. The expected result of these developments appears to indicate an upcoming homogenization of the area's characteristics, requiring immediate intervention to avoid potentially irreversible environmental and social consequences (Esri 2020).
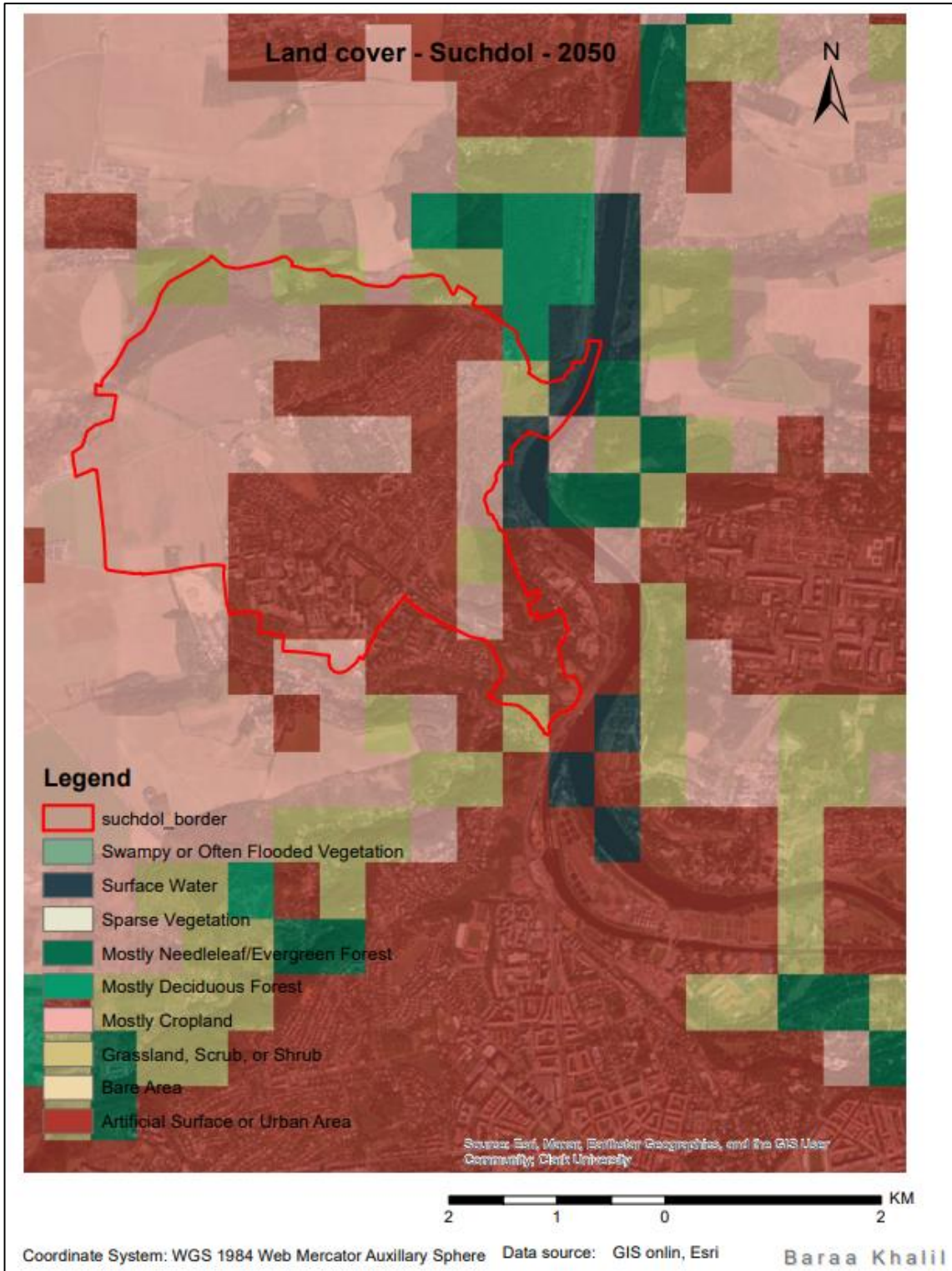
Figure 76. Land cover 2050 – Suchdol (Esri).

Conclusion 7

7. Conclusion

From 1938 to 1989, the study area experienced significant urban development, transitioning from a predominantly rural to an urbanized region. However, after 1989, development slowed down and became more restrained and landscape character remained mostly unchanged until 2018, with only a few localized changes identified between 2006 and 2018. However, this change was not enough to affect the temperature in of entire area, but a significant relationship between land surface temperature and land use/land cover was discovered, by means of UHI.

We discovered a strong positive correlation between imperviousness and LST, with built-up areas experiencing the highest temperatures due to their high percentage of impervious surfaces. Our analysis of the Normalized Difference Vegetation Index (NDVI) confirmed that green spaces and vegetation had a strong negative correlation with LST, with vegetation acting as a cooling factor and mitigating the UHI effect. In a conclusion, high surface imperviousness in urban areas with low NDVI leads to high temperatures. Furthermore, the study area was analyzed to investigate the relationship between land surface temperature (LST) and elevation. The results show that the local elevation varieties were too small to affect the overall temperature in the area. However, it is important to note that a comprehensive analysis of the influence of elevation on LST requires considering the land use and land cover characteristics within the study area.

Finally, the use of thermal cameras in this study highlights the importance of considering surface color, texture, and roughness when selecting building materials in urban environments. The utilization of materials with low thermal conductivity is crucial in urban settings, particularly in cities with hot climates. Such "cold" materials serve to lower air temperature through heat transfer processes. Unfortunately, "warm" materials such as asphalt, dark tiles, and cement are often used instead of "cold" materials like stones, light-colored marble, white granite, and white mosaic for reasons of economy and aesthetics or poor environmental planning. This practice leads to an increase in urban temperature, which exacerbates the need for cooling in buildings (Doulos et al. 2004b). This study reveals that light-colored and smooth materials, such as white-painted asphalt and light-colored stone tiles, have significant potential for lowering surface temperatures and mitigating the urban heat island effect. As a result, the study emphasizes the importance of reflective coatings in lowering surface temperature. Furthermore, the incorporation of trees and other shading elements can help to mitigate the negative effects of the urban heat island.

The study's findings suggest that incorporating these findings into urban planning and design could potentially improve outdoor thermal comfort and reduce energy consumption.

Finally, urban planners and policymakers must consider the impact of land use and land cover on LST and thus on UHI. A paradigm shift is required. We need to start thinking outside the box. We must prioritize the integration of green infrastructure and cool materials in our cities in order to create a sustainable and livable urban environment that benefits us all. It's not just an option, it's a necessity for a better future.

References

8
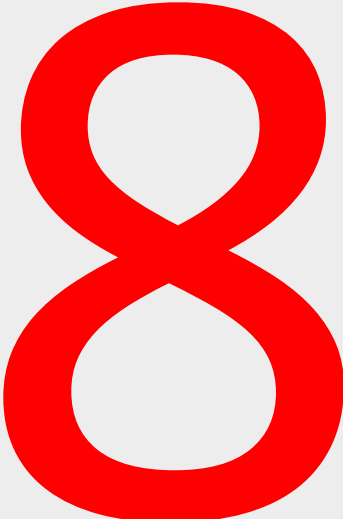
8. References

1. Akbari, H., Pomerantz, M. & Taha, H. (2001). Cool surfaces and shade trees to reduce energy use and improve air quality in urban areas. *Solar Energy*, 70 (3), 295–310. https://doi.org/10.1016/S0038-092X(00)00089-X

2. Alexander, C. (2021). Influence of the proportion, height and proximity of vegetation and buildings on urban land surface temperature. *International Journal of Applied Earth Observation and Geoinformation*, 95, 102265. https://doi.org/10.1016/j.jag.2020.102265

3. Amthor, J.S. (2010). From sunlight to phytomass: on the potential efficiency of converting solar radiation to phyto-energy. *New Phytologist*, 188 (4), 939–959. https://doi.org/10.1111/j.1469-8137.2010.03505.x

4. An, N., Hemmati, S. & Cui, Y.-J. (2017). Assessment of the methods for determining net radiation at different time-scales of meteorological variables. *Journal of Rock Mechanics and Geotechnical Engineering*, 9 (2), 239–246. https://doi.org/10.1016/j.jrmge.2016.10.004

5.Austin, E., Geisler, A.N., Nguyen, J., Kohli, I., Hamzavi, I., Lim, H.W. & Jagdeo, J. (2021). Visible light. Part I: Properties and cutaneous effects of visible light. *Journal of the American Academy of Dermatology*, 84 (5), 1219–1231. https://doi.org/10.1016/j.jaad.2021.02.048

6. Avdan, U. & Jovanovska, G. (2016). Algorithm for Automated Mapping of Land Surface Temperature Using LANDSAT 8 Satellite Data. *Journal of Sensors*, 2016, e1480307. https://doi.org/10.1155/2016/1480307

7. Avdelidis, N.P. & Moropoulou, A. (2003). Emissivity considerations in building thermography. *Energy and Buildings*, 35 (7), 663–667. https://doi.org/10.1016/S0378-7788(02)00210-4

8. Badaro-Saliba, N., Adjizian-Gerard, J., Zaarour, R. & Najjar, G. (2021). LCZ scheme for assessing Urban Heat Island intensity in a complex urban area (Beirut, Lebanon). *Urban Climate*, 37, 100846. https://doi.org/10.1016/j.uclim.2021.100846

9. Bala, R., Prasad, R. & Yadav, V.P. (2021). Quantification of urban heat intensity with land use/land cover changes using Landsat satellite data over urban landscapes. *Theoretical and Applied Climatology*, 145 (1), 1–12. https://doi.org/10.1007/s00704-021-03610-3

10. Butcher, G. (2016). *Tour of the Electromagnetic Spectrum*. Government Printing Office.

11. Büttner, G. (2014). CORINE Land Cover and Land Cover Change Products. In: Manakos, I. & Braun, M. (eds) *Land Use and Land Cover Mapping in Europe: Practices & Trends*. Dordrecht: Springer Netherlands. 55–74. https://doi.org/10.1007/978-94-007-7969-3_5

12. Campbell, I. to E.Spectrum.N.A. and S.A. (2018). *Introduction to Electromagnetic Spectrum*. *NASA*. [Text]. http://www.nasa.gov/directorates/heo/scan/spectrum/overview/index.html [2022-12-07]

13. Chaosheng, T., Bin, S.H.I. & Kai, G.U. (2011). EXPERIMENTAL INVESTIGATION ON EVAPORATION PROCESS OF WATER IN SOIL DURING DRYING. 工程地质学报, 19 (6), 875–881

14. Cheval, S., Dumitrescu, A. & Kveton, V. (2007). MODIS-BASED INVESTIGATIONS ON THE URBAN HEAT ISLANDS OF BUCHAREST (ROMANIA) AND PRAGUE (CZECH REPUBLIC).

15. Chudnovsky, A., Ben-Dor, E. & Saaroni, H. (2004). Diurnal thermal behavior of selected urban objects using remote sensing measurements. *Energy and Buildings*, 36 (11), 1063–1074. https://doi.org/10.1016/j.enbuild.2004.01.052

16. Coakley, J.A. (2003). REFLECTANCE AND ALBEDO, SURFACE. In: *Encyclopedia of Atmospheric Sciences*. Elsevier. 1914–1923. https://doi.org/10.1016/B0-12-227090-8/00069-5

17. Connor, N. (2019). *What is Emissivity - Emissivity of Materials - Definition. Thermal Engineering*. https://www.thermal-engineering.org/what-is-emissivity-emissivity-of-materials-definition/ [2022-12-08]

18. coops, N., Dury, S., Smith, M., Martin, M. & Ollingger, S. (2002). *Comparison of green leaf eucalypt spectra using spectral decomposition*. CRC Press.

19. **CZSO (2022).** *Population of municipalities in selected AD MEP (31 Dec)1*. *Czech Statistical Office*. https://vdb.czso.cz/vdbvo2/faces/en/index.jsf?page=vystup-objekt-vyhledavani&vyhltext=suchdol&bkvt=c3VjaGRvbA..&katalog=30829&pvo=RSO14&pvoch=2112&pvokc=65 [2023-01-17]

20. **De Vos, J.C. (1954)**. Evaluation of the quality of a blackbody. *Physica*, 20 (7), 669–689. https://doi.org/10.1016/S0031-8914(54)80181-9

21. **Di Sipio, E. & Bertermann, D. (2018).** Soil thermal behavior in different moisture condition: an overview of ITER project from laboratory to field test monitoring. *Environmental Earth Sciences*, 77 (7), 283. https://doi.org/10.1007/s12665-018-7454-y

22. **Ding, M., Yao, Y., Wei, L. & Cao, Y. (2018).** Visual tracking using Locality-constrained Linear Coding and saliency map for visible light and infrared image sequences. *Signal Processing: Image Communication*, 68, 13–25. https://doi.org/10.1016/j.image.2018.06.019

23. **Dirksen, M., Ronda, R.J., Theeuwes, N.E. & Pagani, G.A. (2019).** Sky view factor calculations and its application in urban heat island studies. *Urban Climate*, 30, 100498. https://doi.org/10.1016/j.uclim.2019.100498

24. **Doulos, L., Santamouris, M. & Livada, I. (2004a)**. Passive cooling of outdoor urban spaces. The role of materials. *Solar Energy*, 77 (2), 231–249. https://doi.org/10.1016/j.solener.2004.04.005

25. **Doulos, L., Santamouris, M. & Livada, I. (2004b)**. Passive cooling of outdoor urban spaces. The role of materials. *Solar Energy*, 77 (2), 231–249. https://doi.org/10.1016/j.solener.2004.04.005

26. **Du, H., Wang, D., Wang, Y., Zhao, X., Qin, F., Jiang, H. & Cai, Y. (2016).** Influences of land cover types, meteorological conditions, anthropogenic heat, and urban area on surface urban heat island in the Yangtze River Delta Urban Agglomeration. *Science of The Total Environment*, 571, 461–470. https://doi.org/10.1016/j.scitotenv.2016.07.012

27. **Eliška, L., Marie, H., Marjolijn, H. & David, V. (2014).** Exploring adaptation pathways: Case of Prague urban heat island. 1

28. **ESA (2008).** *Profile of Urban Heat Island*. https://www.esa.int/ESA_Multimedia/Images/2008/07/Profile_of_Urban_Heat_Island [2022-12-02]

29. **Esri (2020).** *Esri Land Cover 2050*. https://github.com/vannizhang/land-cover-2050#readme [2023-02-21]

30. **esri** Image Processing with ArcGIS {ArcMap 10.7}. esri.com. https://www.esri.com/training/Engine/defaultui/player/modern.html?configuration=ReturnUrl%7C&preventRightClick=False&cc=en-GB&cache=21.1.14.331&playerConfUrl=n&registration=InstanceId%7C0%21LearningObjectId%7C57630437851d31e02a43f25b-18090%21UserId%7Cbakd0001%40stud.slu.se_gis_slu&package=LearningObjectId%7C57630437851d31e02a43f25b-18090%21VersionId%7C6&tracking=True&forceReview=False [2023-01-20]

31. **Ferguson, G. & Woodbury, A.D. (2007).** Urban heat island in the subsurface. *Geophysical Research Letters*, 34 (23). https://doi.org/10.1029/2007GL032324

32. **Fintikakis, N., Gaitani, N., Santamouris, M., Assimakopoulos, M., Assimakopoulos, D.N., Fintikaki, M., Albanis, G., Papadimitriou, K., Chryssochoides, E., Katopodi, K. & Doumas, P. (2011).** Bioclimatic design of open public spaces in the historic centre of Tirana, Albania. *Sustainable Cities and Society*, 1 (1), 54–62. https://doi.org/10.1016/j.scs.2010.12.001

33. **Gade, R. & Moeslund, T.B. (2014).** Thermal cameras and applications: a survey. *Machine Vision and Applications*, 25 (1), 245–262. https://doi.org/10.1007/s00138-013-0570-5

34. **Georgakis, Ch., Zoras, S. & Santamouris, M. (2014).** Studying the effect of "cool" coatings in street urban canyons and its potential as a heat island mitigation technique. *Sustainable Cities and Society*, 13, 20–31. https://doi.org/10.1016/j.scs.2014.04.002

35. **Govender, M., Chetty, K. & Bulcock, H. (2007).** A review of hyperspectral remote sensing and its application in vegetation and water resource studies. *Water SA*, 33 (2), 145–151. https://doi.org/10.10520/EJC116430

36. **Gromicko, N. & Ward, E. (2006).** *IR Cameras: An Overview for Inspectors*. https://www.nachi.org/ir-camera-overview-inspectors.htm [2022-12-10]

37. **Grover, A. & Singh, R.B. (2015).** Analysis of Urban Heat Island (UHI) in Relation to Normalized Difference Vegetation Index (NDVI): A Comparative Study of Delhi and Mumbai. *Environments*, 2 (2), 125–138. https://doi.org/10.3390/environments2020125

38. **Gunawardena, K.R., Wells, M.J. & Kershaw, T. (2017).** Utilising green and blue space to mitigate urban heat island intensity. *Science of The Total Environment*, 584–585, 1040–1055. https://doi.org/10.1016/j.scitotenv.2017.01.158

39. **Hathway, E.A. & Sharples, S. (2012).** The interaction of rivers and urban form in mitigating the Urban Heat Island effect: A UK case study. *Building and Environment*, 58, 14–22. https://doi.org/10.1016/j.buildenv.2012.06.013

40. **Huang, L., Zhao, D., Wang, J., Zhu, J. & Li, J. (2008).** Scale impacts of land cover and vegetation corridors on urban thermal behavior in Nanjing, China. *Theoretical and Applied Climatology*, 94 (3), 241–257. https://doi.org/10.1007/s00704-007-0359-4

41. **Huete, A.R. (2004).** 11 - REMOTE SENSING FOR ENVIRONMENTAL MONITORING. In: Artiola, J.F., Pepper, I.L., & Brusseau, M.L. (eds) *Environmental Monitoring and Characterization*. Burlington: Academic Press. 183–206. https://doi.org/10.1016/B978-012064477-3/50013-8

42. **ICESS (1999).** *MODIS UCSB Emissivity Library*. https://icess.eri.ucsb.edu/modis/EMIS/html/em.html [2022-12-09]

43. **IPR Praha (2020).** *DETAIL Z3827*. https://app.iprpraha.cz/napp/zmeny/?cislotxt=Z3827&featureexist=1&action=view&presenter=Articlezmenyupravy [2023-02-20]

44. **Iznita Izhar, L. & Petrou, M. (2012).** Chapter 2 - Thermal Imaging in Medicine. In: Hawkes, P.W. (ed.) *Advances in Imaging and Electron Physics*. Elsevier. 41–114. https://doi.org/10.1016/B978-0-12-394297-5.00002-7

45. **Jain, S.K. & Singh, V.P. (2003).** Chapter 3 - Emerging Techniques for Data Acquisition and Systems Modeling. In: Jain, S.K. & Singh, V.P. (eds) *Developments in Water Science*. Elsevier. 123–205. https://doi.org/10.1016/S0167-5648(03)80057-6

46. **Jeanette, H.J. (2013).** *A practical guide to infra-red thermography for building surveys. AIVC*. [Text]. https://www.aivc.org/resource/practical-guide-infra-red-thermography-building-surveys [2022-12-13]

47. **Jiménez-Muñoz, J.C., Sobrino, J.A., Gillespie, A., Sabol, D. & Gustafson, W.T. (2006).** Improved land surface emissivities over agricultural areas using ASTER NDVI. *Remote Sensing of Environment*, 103 (4), 474–487. https://doi.org/10.1016/j.rse.2006.04.012

48. **Johnson, S.R., Rao, S., Hussey, S.B., Morley, P.S. & Traub-Dargatz, J.L. (2011).** Thermographic Eye Temperature as an Index to Body Temperature in Ponies. *Journal of Equine Veterinary Science*, 31 (2), 63–66. https://doi.org/10.1016/j.jevs.2010.12.004

49. **Kaplan, G., Avdan, U. & Avdan, Z.Y. (2018).** Urban Heat Island Analysis Using the Landsat 8 Satellite Data: A Case Study in Skopje, Macedonia. *Proceedings*, 2 (7), 358. https://doi.org/10.3390/ecrs-2-05171

50. **Ketterer, C. & Matzarakis, A. (2014).** Human-biometeorological assessment of the urban heat island in a city with complex topography – The case of Stuttgart, Germany. *Urban Climate*, 10, 573–584. https://doi.org/10.1016/j.uclim.2014.01.003

51. **Kotak, Y., Gul, M., Muneer, T. & Ivanova, S. (2015).** Investigating the Impact of Ground Albedo on the Performance of PV Systems., April 16, 2015.

52. **Lan, Y. & Zhan, Q. (2017).** How do urban buildings impact summer air temperature? The effects of building configurations in space and time. *Building and Environment*, 125, 88–98. https://doi.org/10.1016/j.buildenv.2017.08.046

53. **Landsberg, H.E. (1981).** *The Urban Climate*. Academic Press.

54. **Leal Filho, W., Echevarria Icaza, L., Neht, A., Klavins, M. & Morgan, E.A. (2018).** Coping with the impacts of urban heat islands. A literature based study on understanding urban heat vulnerability and the need for resilience in cities in a global climate change context. *Journal of Cleaner Production*, 171, 1140–1149. https://doi.org/10.1016/j.jclepro.2017.10.086

55. **Li, Z.-L., Wu, H., Wang, N., Qiu, S., Sobrino, J.A., Wan, Z., Tang, B.-H. & Yan, G. (2013).** Land surface emissivity retrieval from satellite data. *International Journal of Remote Sensing*, 34 (9–10), 3084–3127. https://doi.org/10.1080/01431161.2012.716540

56. **Lillesand, T., Kiefer, R.W. & Chipman, J. (2015).** *Remote Sensing and Image Interpretation*. John Wiley & Sons.

57. **Liou, K.N. (2002).** *An Introduction to Atmospheric Radiation*. Elsevier.

58. **Lu, D. & Weng, Q. (2006).** Use of impervious surface in urban land-use classification. *Remote Sensing of Environment*, 102 (1), 146–160. https://doi.org/10.1016/j.rse.2006.02.010

59. **Martin, M., Chong, A., Biljecki, F. & Miller, C. (2022).** Infrared thermography in the built environment: A multi-scale review. *Renewable and Sustainable Energy Reviews*, 165, 112540. https://doi.org/10.1016/j.rser.2022.112540

60. **Mathew, A., Khandelwal, S. & Kaul, N. (2016).** Spatial and temporal variations of urban heat island effect and the effect of percentage impervious surface area and elevation on land surface temperature: Study of Chandigarh city, India. *Sustainable Cities and Society*, 26, 264–277. https://doi.org/10.1016/j.scs.2016.06.018

61. **Mattson, B. & Newman, P. (2013).** *Electromagnetic Spectrum - Introduction*. *NASA.gov*. https://imagine.gsfc.nasa.gov/science/toolbox/emspectrum1.html [2022-12-07]

62. **McKenna, J. & Gromicko, N. (2006).** *The History of Infrared Thermography*. *Inter-national Association of Certified Home Inspectors*. https://www.nachi.org/history-ir.htm [2022-12-07]

63. **Meola, C. & Carlomagno, G.M. (2004).** Recent advances in the use of infrared thermography. *Measurement Science and Technology*, 15 (9), R27–R58. https://doi.org/10.1088/0957-0233/15/9/R01

64. **Meseguer, J., Pérez-Grande, I. & Sanz-Andrés, A. (2012).** *Spacecraft Thermal Control*. Elsevier.

65. **městská část suchdol (2020).** Územní studie Starý Suchdol. *Městská část Praha-Suchdol*. https://praha-suchdol.cz/mestska-cast-praha-suchdol/projekty-a-uzemni-rozvoj/uzemni-plan/uzemni-studie-stary-suchdol/ [2023-02-20]

66. **Middel, A., Brazel, A.J., Kaplan, S. & Myint, S.W. (2012).** Daytime cooling efficiency and diurnal energy balance in Phoenix, Arizona, USA. *Climate Research*, 54 (1), 21–34. https://doi.org/10.3354/cr01103

67. **Mira, M., Valor, E., Boluda, R., Caselles, V. & Coll, C. (2007).** Influence of soil water content on the thermal infrared emissivity of bare soils: Implication for land surface temperature determination. *Journal of Geophysical Research: Earth Surface*, 112 (F4). https://doi.org/10.1029/2007JF000749

68. **Mohammed, A., Khan, A. & Santamouris, M. (2021).** On the mitigation potential and climatic impact of modified urban albedo on a subtropical desert city. *Building and Environment*, 206, 108276. https://doi.org/10.1016/j.buildenv.2021.108276

69. **Mohan, M., Kikegawa, Y., Gurjar, B.R., Bhati, S. & Kolli, N.R. (2013).** Assessment of urban heat island effect for different land use–land cover from micrometeorological measurements and remote sensing data for megacity Delhi. *Theoretical and Applied Climatology*, 112 (3), 647–658. https://doi.org/10.1007/s00704-012-0758-z

70. **Monchau, J.-P., Ibos, L., Marchetti, M., Dumoulin, J., Feuillet, V., Candau, Y. & Ausset, P. (2013).** Infrared Emissivity Measurements for Mineral Materials and Materials Used for Infrastructure Building. EGU2013-10137

71. **Moropoulou, A., Koui, M., Avdelidis, N.P., Delegou, E.T. & Kouris, S. (2021).** CALCULATING THE EMISSIVITY OF BUILDING MATERIALS FOR INFRARED THERMOGRAPHIC APPLICATIONS.

72. **NASA (2000).** *Measuring Vegetation (NDVI & EVI).* [Text.Article]. https://earthobservatory.nasa.gov/features/MeasuringVegetation [2023-01-14]

73. **NASA (2010).** *Anatomy of an Electromagnetic Wave | Science Mission Directorate. NASA.gov.* https://science.nasa.gov/ems/02_anatomy [2022-12-07]

74. **NASA (2014).** *Spacecraft Maps Earth's Global Emissivity. NASA.gov.* https://photojournal.jpl.nasa.gov/catalog/PIA18833 [2022-12-09]

75. **National Geographic (2022).** *Visible Light | National Geographic Society.* https://education.nationalgeographic.org/resource/visible-light [2022-12-07]

76. **Nayak, A. (2018).** Infrared Radiation and its applications.

Nguyen, T.T., Eslick, H., Barber, P., Harper, R. & Dell, B. (2022). Cooling Effects of Urban Vegetation: The Role of Golf Courses. *Remote Sensing*, 14 (17), 4351. https://doi.org/10.3390/rs14174351

77. **Nitis, T. & Klai, Z.B. (2005).** EFFECTS OF TOPOGRAPHY ON URBAN HEAT ISLAND. 6

78. **Parente, C. & Pepe, M. (2019).** BENEFIT OF THE INTEGRATION OF VISIBLE AND THERMAL INFRARED IMAGES FOR THE SURVEY AND ENERGY EFFICIENCY ANALYSIS IN THE CONSTRUCTION FIELD. *Journal of Applied Engineering Science*, 17 (4). https://doi.org/10.5937/jaes17-22080

79. **Park, C.Y., Lee, D.K., Asawa, T., Murakami, A., Kim, H.G., Lee, M.K. & Lee, H.S. (2019).** Influence of urban form on the cooling effect of a small urban river. *Landscape and Urban Planning*, 183, 26–35. https://doi.org/10.1016/j.landurbplan.2018.10.022

80. **Peng, L.L.H. & Jim, C.Y. (2013).** Green-Roof Effects on Neighborhood Microclimate and Human Thermal Sensation. *Energies*, 6 (2), 598–618. https://doi.org/10.3390/en6020598

81. **Perini, K. & Magliocco, A. (2014).** Effects of vegetation, urban density, building height, and atmospheric conditions on local temperatures and thermal comfort. *Urban Forestry & Urban Greening*, 13 (3), 495–506. https://doi.org/10.1016/j.ufug.2014.03.003

81. **Pramanik, P., Bandyopadhyay, K.K., Bhaduri, D., Bhattacharyya, R. & Aggarwal, P. (2015).** Effect of mulch on soil thermal regimes - A review. *International Journal of Agriculture, Environment and Biotechnology*, 8 (3), 645. https://doi.org/10.5958/2230-732X.2015.00072.8

82. **Protherm (2013).** *INFRARED BASICS. openei.org.* https://openei.org/wiki/File:Infrared_Spectrum.PNG [2022-12-07]

83. **Qin, Y., He, Y., Hiller, J.E. & Mei, G. (2018).** A new water-retaining paver block for reducing runoff and cooling pavement. *Journal of Cleaner Production*, 199, 948–956. https://doi.org/10.1016/j.jclepro.2018.07.250

84. **Roman, A. & Ursu, T. (2016).** Multispectral satellite imagery and airborne laser scanning techniques for the detection of archaeological vegetation marks. 141–152.

85. **SAURAB, B. (2020).** Why is it cooler around trees? *Eco-intelligent™.* https://eco-intelligent.com/2020/05/23/why-is-it-cooler-around-trees/ [2022-12-13]

86. **Science Mission Directorate (2010).** *Infrared Waves. NASA Science.* https://science.nasa.gov/ems/07_infraredwaves [2022-12-08]

87. **Shashua-Bar, L. & Hoffman, M.E. (2000).** Vegetation as a climatic component in the design of an urban street: An empirical model for predicting the cooling effect of urban green areas with trees. *Energy and Buildings*, 31 (3), 221–235. https://doi.org/10.1016/S0378-7788(99)00018-3

88. **Shi, B., Tang, C.-S., Gao, L., Liu, C. & Wang, B.-J. (2012).** Observation and analysis of the urban heat island effect on soil in Nanjing, China. *Environmental Earth Sciences*, 67 (1), 215–229. https://doi.org/10.1007/s12665-011-1501-2

89. **Shimazaki, Y., Aoki, M., Nitta, J., Okajima, H. & Yoshida, A. (2021).** Experimental Determination of Pedestrian Thermal Comfort on Water-Retaining Pavement for UHI Adaptation Strategy. *Atmosphere*, 12 (2), 127. https://doi.org/10.3390/atmos12020127

90. **Singh, P., Kikon, N. & Verma, P. (2017).** Impact of land use change and urbanization on urban heat island in Lucknow city, Central India. A remote sensing based estimate. *Sustainable Cities and Society*, 32, 100–114. https://doi.org/10.1016/j.scs.2017.02.018

91. **Smith, N., Georgiou, M., King, A.C., Tieges, Z., Webb, S. & Chastin, S. (2021).** Urban blue spaces and human health: A systematic review and meta-analysis of quantitative studies. *Cities*, 119, 103413. https://doi.org/10.1016/j.cities.2021.103413

92. **Sobrino, J.A., Jiménez-Muñoz, J.C. & Paolini, L. (2004).** Land surface temperature retrieval from LANDSAT TM 5. *Remote Sensing of Environment*, 90 (4), 434–440. https://doi.org/10.1016/j.rse.2004.02.003

93. **Srivanit, M. & Hokao, K. (2013).** Evaluating the cooling effects of greening for improving the outdoor thermal environment at an institutional campus in the summer. *Building and Environment*, 66, 158–172. https://doi.org/10.1016/j.buildenv.2013.04.012

94. **Stathopoulou, M. & Cartalis, C. (2007).** Daytime urban heat islands from Landsat ETM+ and Corine land cover data: An application to major cities in Greece. *Solar Energy*, 81 (3), 358–368. https://doi.org/10.1016/j.solener.2006.06.014

95. **Steeneveld, G.J., Koopmans, S., Heusinkveld, B.G. & Theeuwes, N.E. (2014).** Refreshing the role of open water surfaces on mitigating the maximum urban heat island effect. *Landscape and Urban Planning*, 121, 92–96. https://doi.org/10.1016/j.landurbplan.2013.09.001

96. **Stephens, G.L., O'Brien, D., Webster, P.J., Pilewski, P., Kato, S. & Li, J. (2015).** The albedo of Earth: The Albedo of Earth. *Reviews of Geophysics*, 53 (1), 141–163. https://doi.org/10.1002/2014RG000449

97. **Stewart, I.D. & Oke, T.R. (2012).** Local Climate Zones for Urban Temperature Studies. *Bulletin of the American Meteorological Society*, 93 (12), 1879–1900. https://doi.org/10.1175/BAMS-D-11-00019.1

98. **Synnefa, A., Santamouris, M. & Livada, I. (2006).** A study of the thermal performance of reflective coatings for the urban environment. *Solar Energy*, 80 (8), 968–981. https://doi.org/10.1016/j.solener.2005.08.005

99. **Taha, H. (1997).** Urban climates and heat islands: albedo, evapotranspiration, and anthropogenic heat. *Energy and Buildings*, 25 (2), 99–103. https://doi.org/10.1016/S0378-7788(96)00999-1

100. **Teledyne FLIR (2021).** *How Does Emissivity Affect Thermal Imaging?* https://www.flir.com/discover/professional-tools/how-does-emissivity-affect-thermal-imaging/ [2022-12-09]

101. **Theeuwes, N.E., Steeneveld, G.-J., Ronda, R.J. & Holtslag, A.A.M. (2017).** A diagnostic equation for the daily maximum urban heat island effect for cities in northwestern Europe. *International Journal of Climatology*, 37 (1), 443–454. https://doi.org/10.1002/joc.4717

102. **Tran, D.X., Pla, F., Latorre-Carmona, P., Myint, S.W., Caetano, M. & Kieu, H.V. (2017).** Characterizing the relationship between land use land cover change and land surface temperature. *ISPRS Journal of Photogrammetry and Remote Sensing*, 124, 119–132. https://doi.org/10.1016/j.isprsjprs.2017.01.001

103. **Ulpiani, G. (2021).** On the linkage between urban heat island and urban pollution island: Three-decade literature review towards a conceptual framework. *Science of The Total Environment*, 751, 141727. https://doi.org/10.1016/j.scitotenv.2020.141727

104. **United Nations (2014).** *revision of the World Urbanization Prospects*. https://www.un.org/en/development/desa/publications/2014-revision-world-urbanization-prospects.html [2022-12-02]

105. **Wang, K., Wan, Z., Wang, P., Sparrow, M., Liu, J., Zhou, X. & Haginoya, S. (2005).** Estimation of surface long wave radiation and broadband emissivity using Moderate Resolution Imaging Spectroradiometer (MODIS) land surface temperature/emissivity products. *Journal of Geophysical Research: Atmospheres*, 110 (D11). https://doi.org/10.1029/2004JD005566

106. **Ward, S. & John, S. (1998).** Infrared thermography: principles and applications. *Zoology*, 101, 224–232

107. **Watson, I.D. & Johnson, G.T. (1987).** Graphical estimation of sky view-factors in urban environments. *Journal of Climatology*, 7 (2), 193–197. https://doi.org/10.1002/joc.3370070210

108. **weather and climate (2022).** *Suchdol, Prague, CZ Climate Zone, Monthly Averages, Historical Weather Data*. *weather and climate*. https://tcktcktck.org/czechia/prague/suchdol [2023-01-18]

109. **Williams, M.E. (2014).** 9 - Repair of deteriorated bridge substructures using carbon fiber-reinforced polymer (CFRP) composites. In: Kim, Y.J. (ed.) *Advanced Composites in Bridge Construction and Repair*. Woodhead Publishing. 265–286. https://doi.org/10.1533/9780857097019.2.265

110. **Wu, Y., Cheng, L., Wang, T. & Wu, H. (2022).** Infrared and visible light dual-camera super-resolution imaging with texture transfer network. *Signal Processing: Image Communication*, 108, 116825. https://doi.org/10.1016/j.image.2022.116825

111. **Xi, C., Ren, C., Wang, J., Feng, Z. & Cao, S.-J. (2021).** Impacts of urban-scale building height diversity on urban climates: A case study of Nanjing, China. *Energy and Buildings*, 251, 111350. https://doi.org/10.1016/j.enbuild.2021.111350

112. **Yang, L., Liu, X. & Qian, F. (2020).** Research on water thermal effect on surrounding environment in summer. *Energy and Buildings*, 207, 109613. https://doi.org/10.1016/j.enbuild.2019.109613

113. **Yang, X. & Li, Y. (2015).** The impact of building density and building height heterogeneity on average urban albedo and street surface temperature. *Building and Environment*, 90, 146–156. https://doi.org/10.1016/j.buildenv.2015.03.037

114. **Yang, X. & Zhao, L. (2016).** Diurnal Thermal Behavior of Pavements, Vegetation, and Water Pond in a Hot-Humid City. *Buildings*, 6 (1), 2. https://doi.org/10.3390/buildings6010002

115. **Yu, X., Guo, X. & Wu, Z. (2014)**. Land Surface Temperature Retrieval from Landsat 8 TIRS—Comparison between Radiative Transfer Equation-Based Method, Split Window Algorithm and Single Channel Method. *Remote Sensing*, 6 (10), 9829–9852. https://doi.org/10.3390/rs6109829

116. **Žák, M., Zahradníček, P., Skalák, P., Halenka, T., Aleš, D., Fuka, V., Kazmuková, M., Zemánek, O., Flegl, J., Kiesel, K., Jareš, R., Ressler, J. & Huszár, P. (2016).** Pilot Actions in European Cities – Prague. In: Musco, F. (ed.) *Counteracting Urban Heat Island Effects in a Global Climate Change Scenario*. Cham: Springer International Publishing. 373–400. https://doi.org/10.1007/978-3-319-10425-6_14

117. **Zeng, L., Lu, J., Li, W. & Li, Y. (2018).** A fast approach for large-scale Sky View Factor estimation using street view images. *Building and Environment*, 135, 74–84. https://doi.org/10.1016/j.buildenv.2018.03.009

118. **Zhao, Q. & Wentz, E.A. (2016).** A MODIS/ASTER Airborne Simulator (MASTER) Imagery for Urban Heat Island Research. *Data*, 1 (1), 7. https://doi.org/10.3390/data1010007

119. **Zhao, Z.-Q., He, B.-J., Li, L.-G., Wang, H.-B. & Darko, A. (2017).** Profile and concentric zonal analysis of relationships between land use/land cover and land surface temperature: Case study of Shenyang, China. *Energy and Buildings*, 155, 282–295. https://doi.org/10.1016/j.enbuild.2017.09.046

120. **Zhou, X. & Wang, Y.-C. (2011).** Spatial–temporal dynamics of urban green space in response to rapid urbanization and greening policies. *Landscape and Urban Planning*, 100 (3), 268–277. https://doi.org/10.1016/j.landurbplan.2010.12.013

List of Figures

9

9. List of Figures